

Cite this: *Lab Chip*, 2012, **12**, 515

www.rsc.org/loc

**CRITICAL REVIEW****Design of pressure-driven microfluidic networks using electric circuit analogy****Kwang W. Oh,<sup>\*a</sup> Kangsun Lee,<sup>a</sup> Byungwook Ahn<sup>a</sup> and Edward P. Furlani<sup>b</sup>***Received 23rd August 2011, Accepted 22nd November 2011*

DOI: 10.1039/c2lc20799k

This article reviews the application of electric circuit methods for the analysis of pressure-driven microfluidic networks with an emphasis on concentration- and flow-dependent systems. The application of circuit methods to microfluidics is based on the analogous behaviour of hydraulic and electric circuits with correlations of pressure to voltage, volumetric flow rate to current, and hydraulic to electric resistance. Circuit analysis enables rapid predictions of pressure-driven laminar flow in microchannels and is very useful for designing complex microfluidic networks in advance of fabrication. This article provides a comprehensive overview of the physics of pressure-driven laminar flow, the formal analogy between electric and hydraulic circuits, applications of circuit theory to microfluidic network-based devices, recent development and applications of concentration- and flow-dependent microfluidic networks, and promising future applications. The lab-on-a-chip (LOC) and microfluidics community will gain insightful ideas and practical design strategies for developing unique microfluidic network-based devices to address a broad range of biological, chemical, pharmaceutical, and other scientific and technical challenges.

<sup>a</sup>SMALL (Sensors and MicroActuators Learning Lab), Department of Electrical Engineering, University at Buffalo, The State University of New York at Buffalo (SUNY-Buffalo), New York, 14260, USA.  
E-mail: kwangoh@buffalo.edu

<sup>b</sup>Department of Biological/Chemical and Department of Electrical Engineering, University at Buffalo, The State University of New York at Buffalo (SUNY-Buffalo), New York, 14260, USA



Kwang W. Oh

Kwang W. Oh is an Assistant Professor at University at Buffalo, State University of New York (SUNY at Buffalo) where he leads Sensors and MicroActuators Learning Lab—SMALL ([small.buffalo.edu](http://small.buffalo.edu) or [MicroTAS.org](http://MicroTAS.org)). He received his bachelor's degree in physics from Chonbuk National University, Korea, in 1995. He earned his MS and PhD degrees in electrical and computer engineering from University of Cincinnati in 1997 and 2001, respectively. Prior to joining

SUNY at Buffalo, he worked at Samsung Advanced Institute of Technology (SAIT), Korea, where he developed micro-PCR and LOC platforms for clinical diagnostics. His current research focuses on microfluidic networks, droplet-based microfluidics, 3D cell culture platforms, microvalves and actuators, and microfluidic applications for terahertz spectroscopy, platelet aggregation, and metamaterials.



Kangsun Lee

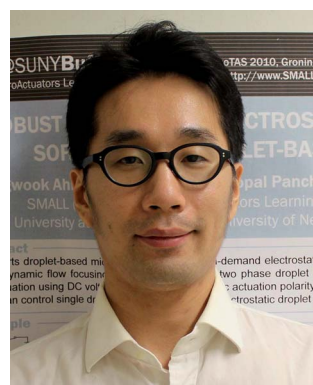
Kangsun Lee received his bachelor's and master's degrees in electrical engineering from Dankook University, Korea in 2004 and 2006, respectively. He worked at Nano-Bio System Laboratory, Microsystem Research Center, Korea Institute of Science and Technology (KIST), Korea. Recently, he earned his PhD degree in electrical engineering at University at Buffalo, State University of New York (SUNY at Buffalo) in 2011 in Kwang W. Oh's SMALL lab. He is currently at

LG Electronics Advanced Institute of Technology, Korea. His current research interests are MEMS/NEMS design, pressure-driven microfluidic devices and networks, two-phase microfluidic devices, 3D cell culture platforms, and cell sorting.

## 1. Introduction

Microfluidics deals with precise manipulation of small volumes of fluid mostly in pressure-driven microfluidic networks for complex biological, chemical or pharmaceutical processes.<sup>1–9</sup> Systematic networking of microchannels from inlet to outlet ports can readily establish relatively simple to very complex microfluidic network-based devices. Broadly speaking, as the number of processes to be performed in a device increases, the configuration of the microfluidic network becomes more complex. In turn, the precise control of fluid flow in each segment of a complex microfluidic network becomes more challenging. A rigorous analysis of flow through such networks can be achieved using computational fluid dynamic (CFD) analysis. However, CFD-based microfluidic design typically requires specialized and costly software and highly trained users with considerable expertise in theoretical fluid dynamics and associated numerical methods. Moreover, CFD analysis tends to be computationally intensive and awkward for the kind of parametric analysis that is often needed for the optimization of practical large-scale microfluidic networks. Thus, a need exists for an efficient strategy for designing such systems, *i.e.* predicting pressure drop, fluidic resistance, and flow rate through microchannel networks.

The use of a physical analogy to transfer the concept and solution from one branch of science and technology to another is very powerful in understanding problematic physical phenomena with deeper insights.<sup>10–12</sup> In fluid mechanics, the Hagen–Poiseuille equation is a physical law that explains the hydraulic behaviour of pressure-driven flow through a circular channel.<sup>13</sup> Analogously, Ohm's law in electric circuit analysis describes the voltage drop and the electric current in a resistive conductor.<sup>14</sup> To a first approximation, electricity was understood to be a kind of fluid (*e.g.*, drain-pipe theory)<sup>15–17</sup> and *vice versa*.<sup>18–20</sup> This well-known hydraulic–electric circuit analogy is still conceptually useful for understanding both hydraulic and electric circuits, and can be found in many textbooks.<sup>21–26</sup>



**Byungwook Ahn**

research interests include design and analysis of microfluidic systems with applications in BioMEMS, active and passive manipulation of microdroplets, particle encapsulation and sorting, and microfabrication technology.

Hagen–Poiseuille's law corresponds to Ohm's law, where the pressure drop is analogous to the voltage drop, the volumetric flow rate to the current, and the hydraulic resistance to the electric resistance (Fig. 1).<sup>27</sup> The key assumption of the analogy is that the flow is laminar, viscous, and incompressible. This analogy enables a sound engineering estimate of steady-state pressure drops, flow rates, and hydraulic resistance of one-dimensional (1D) long and straight microchannels, and is still effective even for channels with non-circular cross-sections that are neither perfectly straight nor infinite in extent. Analytical solutions prescribing fluid flow in microfluidic networks can be derived from equivalent electric circuit equations, which typically reduce to a system of linear algebraic equations. However, while electric circuit methods can be used to predict the average steady-state volumetric flow and corresponding pressure drop across 1D microchannels, such methods are limited in that they do not account for transient flow, nor do they provide information on the spatial distribution of flow velocity even within the 1D channel. Rigorous numerically based CFD simulations are typically used to obtain such detailed information, especially in 2D and 3D systems. Nevertheless, the use of a hydraulic–electric circuit analogy is extremely advantageous in designing complex microfluidic networks with large numbers of 1D-like microchannels.

In this paper, we critically review practical aspects of designing microfluidic networks using the electric circuit analogy. The first section introduces the governing equations for pressure-driven laminar flows in long cylindrical channels and rectangular microchannels (Section 2). This is followed by a description of the electric circuit analogy and basic fluidic circuit models (Section 3). Assumptions, practical design rules and strategies are discussed (Section 4). The electric circuit analogy is demonstrated *via* application to systems that involve concentration- and flow-dependent microfluidic networks. Applications of concentration-dependent networks include proportional, pyramidal, serial, combinatorial, and T-type network-based dilutions

*Byungwook Ahn graduated from Ajou University, Korea in 2004 with bachelor's degree in electrical engineering before pursuing his MS in electrical engineering at University at Buffalo, State University of New York (SUNY at Buffalo) in 2007. He subsequently received his PhD in electrical engineering at SUNY at Buffalo in 2011 in Kwang W. Oh's SMALL lab. He is currently a post-doc at Emory University School of Medicine and Georgia Institute of Technology. His research interests include design and analysis of microfluidic systems with applications in BioMEMS, active and passive manipulation of microdroplets, particle encapsulation and sorting, and microfabrication technology.*



**Edward P. Furlani**

*Edward P. Furlani is a Professor at University at Buffalo, State University of New York (SUNY at Buffalo). Currently he holds joint appointments in Chemical Biological and Electrical Engineering departments. He earned dual undergraduate degrees in physics and electrical engineering in 1977, and a PhD degree in theoretical physics from SUNY at Buffalo in 1982. Upon completing his graduate studies, he joined Eastman Kodak Research Laboratories, Rochester, NY, USA, working in the field of multidisciplinary modeling for the development of novel devices and materials. His research experience spans applications in the fields of microfluidics, magnetics, and photonics.*

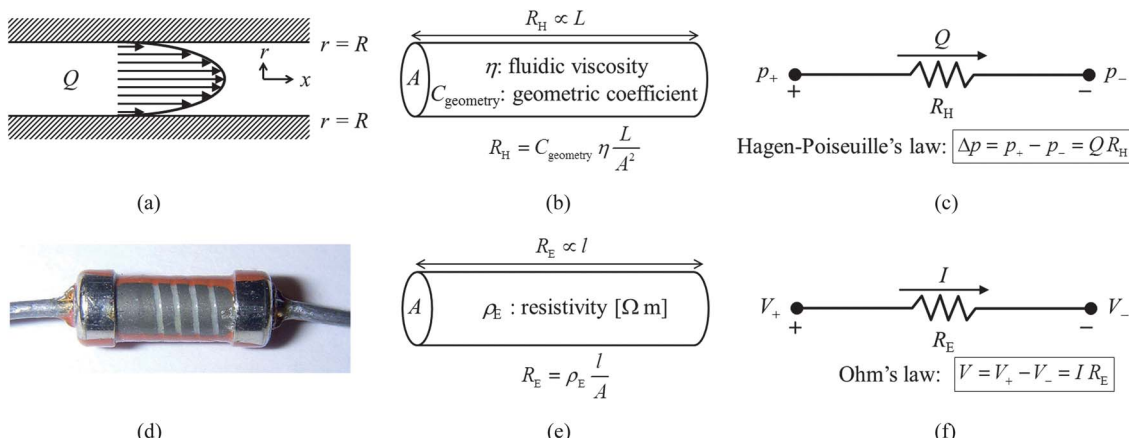


**Fig. 1** The physical similarities between the flow of a fluid and the flow of electricity: (a) Poiseuille flow in a circular channel, (b) the hydraulic resistance of the circular channel ( $C_{\text{geometry}} = 8\pi$  for the circular channel), (c) equivalent circuit symbol of a fluidic resistor for the hydraulic resistance and Hagen–Poiseuille's law analogous to a resistor for the electric resistance and Ohm's law, (d) a partially exposed Tesla TR-212 1 kΩ carbon film resistor, (e) the electric resistance of a conductive wire, and (f) circuit symbol of the resistor for the electric resistance and Ohm's law.

(Section 5). Applications of flow-dependent networks include flow division networks for distribution and shear stress generation; flow fraction networks for hydrodynamic filtering; and dynamic flow change networks for hydrodynamic trapping (Section 6). Finally, limitations and an outlook of future trends in this field are discussed (Section 7). This review article will provide insightful, efficient, and convenient design strategies for developing microfluidic network-based devices without a significant level of expertise in CFD simulation.

## 2. Physics of pressure-driven lamina flow in microfluidic channels

In order to understand and work with the pressure-driven microfluidic networks, we must first understand the hydrodynamic behaviour of fluids. Other microfluidic reviews have been published,<sup>28–31</sup> but none contain a comprehensive look at the physics of the pressure-driven laminar flow and how it makes certain microfluidic network-based devices possible. This section focuses on the physical phenomena of such flows through channels. In particular, steady-state pressure-driven laminar flow through circular and rectangular microchannels is discussed.

### 2.1 Navier–Stokes equation

For flows in microfluidic devices, fluids (primarily water and aqueous solutions) are well approximated as incompressible.<sup>22</sup> Consider the incompressible Navier–Stokes equation for uniform-viscous Newtonian fluids with no body forces:

$$\rho \frac{\partial \vec{u}}{\partial t} = -\rho \vec{u} \nabla \vec{u} - \nabla p + \eta \nabla^2 \vec{u}$$

(Rate of change of momentum) = (convective force)  
+ (pressure force) + (viscous force) (1)

where  $\vec{u}$  is the velocity field [ $\text{m s}^{-1}$ ], which is a description of the velocity of the fluid at a given point in space and time, and is

denoted by  $\vec{u} = \vec{u}(\vec{r}, t)$ , where  $\vec{r}$  is a position vector specifying a location in space [m] and  $t$  is time [s];  $\rho$  is the fluid density [ $\text{kg m}^{-3}$ ];  $\eta$  is the viscosity [Pa s] ( $\mu$  is often used); and  $p$  is the pressure [Pa]. It should be noted that the viscosity is a function of temperature; fluid becomes less viscous as temperature increases. In this review, we assume the temperature is constant during the operation of microfluidic devices. The Navier–Stokes equation dictates velocity rather than position.<sup>22</sup> Once the velocity field is solved for, other quantities of interest (e.g., flow rate, pressure drop, hydraulic resistance) can be found.

### 2.2 Poiseuille flow

Consider a long cylindrical channel with the  $x$ -direction along the axis of the channel (Fig. 1a). In the steady-state of fully developed fluid flow in the channel, its velocity field is unidirectional and laminar and there is no acceleration of the fluid. Thus, the unsteady and convection terms are all zero, and eqn (1) becomes

$$\nabla p = \eta \nabla^2 \vec{u}. \quad (2)$$

Eqn (2) highlights the balance between the net pressure force and the net viscous force. Due to the geometric simplifications and the boundary condition ( $u = 0$  at  $r = R$ ), the pressure-driven motion, termed Poiseuille flow, in the circular channel of radius  $R$  [m] is parabolic across a diameter:

$$u = \frac{R^2 - r^2}{4\eta} \left( -\frac{dp}{dx} \right) = u_{\max} \left( 1 - \frac{r^2}{R^2} \right) \quad (3)$$

where  $u_{\max}$  is the maximum velocity:  $u_{\max} = R^2/4\eta (-dp/dx)$  at  $r = 0$ .

The Poiseuille flow is characterized by a parabolic velocity profile; the velocity of flow in the center of the channel is greater than that toward the outer walls. In contrast, electrically driven flow that is a useful alternative to pressure-driven flow of water, known as electroosmotic flow (EOF), offers a flat velocity profile across the channel.<sup>31,32</sup>

### 2.3 Hagen–Poiseuille's law

To get the total volumetric flow rate  $Q$  [ $\text{m}^3 \text{s}^{-1}$ ] in the circular channel, we need to spatially integrate the velocity contributions (eqn (3)) from each lamina. Accordingly, the volumetric flow rate for the steady-state pressure-driven fluid flow in the channel, described by Hagen–Poiseuille's law, becomes

$$Q = \frac{\pi R^4}{8\eta} \left( -\frac{dp}{dx} \right). \quad (4)$$

And we can normalize eqn (4) by the cross-sectional area to generate the area-averaged velocity  $U$  [ $\text{m s}^{-1}$ ]:

$$U = \frac{Q}{\pi R^2} = \frac{R^2}{8\eta} \left( -\frac{dp}{dx} \right). \quad (5)$$

To be precise, the Hagen–Poiseuille's law applies only for a channel that is perfectly straight and infinitely long. However, we can reasonably apply eqn (4) even to a channel with finite length  $L$  [m]. The laminar flow in a long narrow channel can be assumed fully developed if  $L/R \gg 1$  and  $L/R \gg Re$ , where  $Re$  is the Reynolds number (see Section 2.4).<sup>22</sup> For most pressure-driven microfluidic devices, we can assume that the pressure gradient along the channel length is uniform. Then, we can approximate the term  $-dp/dx$  to  $\Delta p/L$ , where  $\Delta p$  is the pressure difference [Pa] through a finite channel length  $L$ . With this approximation, eqn (4) becomes simply

$$Q = \frac{\pi R^4 \Delta p}{8\eta L} \quad (6)$$

where  $Q$  is defined as positive for flow from inlet to outlet. This formula will be used to define the hydraulic resistance later (see Section 2.5).

### 2.4 Reynolds number

As discussed in Section 2.2, Poiseuille flow is laminar and parabolic across the channel diameter. To characterize the fluidic behaviour in channels, such as laminar or turbulent flow, the Reynolds number is conventionally defined as the ratio of inertial forces to viscous forces. It is well known that laminar flow occurs at low Reynolds numbers ( $Re < 2300$  for the straight and smooth channels<sup>33</sup>), where viscous forces are dominant. To describe the Reynolds number, we need a characteristic velocity  $V$  [ $\text{m s}^{-1}$ ] (or the area-averaged velocity  $U$  [ $\text{m s}^{-1}$ ]) and a characteristic length  $D$  [m] (or a hydraulic diameter  $D_H$  of the channel [m]). The hydraulic diameter is a computed value that depends on the channel's cross-sectional geometry (see Section 2.5). The Reynolds number is

$$Re = \frac{(\text{inertia force})}{(\text{viscous force})} = \frac{\rho V D}{\eta} \approx \frac{\rho U D_H}{\eta}. \quad (7)$$

For Poiseuille flow in a circular channel, we typically state  $D_H \approx 2R$  and  $U = Q/\pi R^2$ , then the Reynolds number becomes  $Re = 2\rho U R / \eta = 2\rho Q / \pi \eta R$ . For a square channel with the width  $w$  [m], we typically state  $D_H = w$  and  $U = Q/w^2$ , then the Reynolds number becomes  $Re = \rho U w / \eta = \rho Q / \eta w$ . Fluid flows in microchannels are almost always at low Reynolds number ( $Re < \sim 1$ ) due to small hydraulic diameters and relatively slow volumetric flow rates, and the inertial effects<sup>34</sup> (e.g., gravity-based

separation,<sup>35</sup> secondary flow,<sup>36</sup> and turbulence) are negligible. Typical values are  $Q = 1 \mu\text{l min}^{-1}$ ,  $\rho = 10^3 \text{ kg m}^{-3}$ ,  $\eta = 10^{-3} \text{ Pa s}$ , and  $w = 100 \mu\text{m}$ , giving  $Re = 0.17$ . Laminar flow and the absence of turbulence are essential to minimize unsteady-state flows at bending and branching points in microfluidic networks.<sup>37</sup>

### 2.5 Hydraulic resistance

Eqn (6) gives the flow–pressure relation in pressure-driven channels, and Hagen–Poiseuille's law can be simplified as

$$\begin{aligned} Q &= \frac{\Delta p}{R_H} \\ \Delta p &= QR_H \end{aligned} \quad (8)$$

where the hydraulic resistance  $R_H$  [ $\text{Pa s}^3 \text{ m}^{-1}$ ] is defined as

$$R_H = \frac{8\eta L}{\pi R^4} \approx \frac{8\eta L}{\pi r_H^4}. \quad (9)$$

In general, eqn (9) can be applied for non-circular channels, by replacing the channel radius  $R$  with the hydraulic radius  $r_H$  or diameter  $D_H = 2r_H$ . The hydraulic radius of the channel  $r_H$  [m] is a geometric constant and defined as  $r_H = 2A/P$ , where  $A$  is the cross-sectional area of the channel [ $\text{m}^2$ ] and  $P$  is the wetted perimeter [m]. If the channel cross-section is circular, the hydraulic radius is equal to the channel radius:  $r_H = R$ .

In microfluidic networks, most channel geometries are rectangular. For a rectangular microchannel with a low aspect ratio (e.g.,  $w \approx h$ ), the reciprocal of the hydraulic radius becomes the sum of the reciprocals of the channel width  $w$  [m] and the channel height  $h$  [m]:  $1/r_H = 1/w + 1/h$  or  $r_H = (w \times h)/(w + h)$ . This estimate gives about 20% error for a square cross-section (e.g.,  $w = h$ ).<sup>38</sup> In fact, the solution to eqn (2) for a rectangular channel is quite complicated to derive, and it can be only calculated as the summation of a Fourier series. The hydraulic resistance for the rectangular microchannel is well known.<sup>39</sup>

$$R_H = \frac{12\eta L}{wh^3 \left( 1 - \frac{h}{w} \left( \frac{192}{\pi^5} \sum_{n=1,3,5}^{\infty} \frac{1}{n^5} \tan h \left( \frac{n\pi w}{2h} \right) \right) \right)}. \quad (10)$$

Note that when the aspect ratio is high (e.g.,  $h/w \ll 1$ ), the hydraulic resistance of a rectangular microchannel can be approximated as  $R_H = 12\eta L/wh^3$ .

Combining eqn (8)–(10) and incorporating a geometric coefficient  $C_{\text{geometry}}$ , Hagen–Poiseuille's equation can be generalized as<sup>27</sup>

$$\begin{aligned} \Delta p &= QR_H \\ R_H &= C_{\text{geometry}} \eta \frac{L}{A^2} \end{aligned} \quad (11)$$

where  $C_{\text{geometry}} = 8\pi$  for the circular channel and  $C_{\text{geometry}} = 12 \times (w/h) / (1 - (h/w) \times ((192/\pi^5) \times \Sigma(\dots)))$  for the rectangular channel. Other channel geometries and their hydraulic resistances can be found elsewhere in ref. 23,40 and 41.

Eqn (11) leads to the following important observations: (i) the pressure drop through a channel is proportional to the volumetric flow rate and the hydraulic resistance:  $\Delta p \propto Q$  and  $\Delta p \propto R_H$ .<sup>42</sup> Notice that it is the *difference* in pressure between the two ends of the channel, not the absolute pressure in the channel, that determines the volumetric flow rate. (ii) The hydraulic resistance

is normally constant for the fixed fluidic and geometric condition, such as homogeneous fluidic viscosity and the same cross-sectional area and its geometry. (iii) Under such a condition, the hydraulic resistance is purely proportional to the channel length:  $R_H \propto L$  (Fig. 1b). These facts are central to design microfluidic networks that need to precisely control the volumetric flow rates and the pressure drops only in terms of the channel length variable (see Box 1).

### 3. Electric circuit analogy

It is quite intuitive to consider the flow of a fluid like the flow of electricity; the molecules of fluid in a hydraulic circuit behave much like the electrons in an electrical circuit. Table 1 summarizes the analogy between fluidics and electronics, or microfluidic/hydraulic circuits and electric circuits. This section highlights the physical similarities between microfluidic circuits and electric circuits. The mapping of electric circuit elements and theory onto corresponding microfluidic circuit elements (*e.g.*, fluidic resistor, independent fluid flow and pressure sources, ground, node, loop, and common channel) and models (*e.g.*, fluidic equivalent resistor, mass conservation, energy conservation, pressure division, flow division, and computer-aided analysis) will be discussed. This well-known hydraulic–electric circuit analogy can be straightforwardly used to prescribe the flow/pressure relation in complex microfluidic networks based on conventional electric circuit theory.

From a different point of view, during the 1960–70 time frame, serious consideration was given to the development of no-moving-part fluidic logic devices that perform analog or digital

operations similar to those performed by electronic components.<sup>26,43</sup> The physical basis of such fluidic devices was the hydraulic–electric circuit analogy.

#### 3.1 Fluidic resistor and Hagen–Poiseuille's law: electric resistor and Ohm's law

In electronics, linear resistors are the simplest circuit element (Fig. 1d) and their resistance  $R_E [\Omega]$  is predetermined by physical parameters (Fig. 1e):  $R_E = \rho_E l/A$ , where  $\rho_E$  is the resistivity of a conductor [ $\Omega \text{ m}$ ],  $l$  is the length of the conductor [m], and  $A$  is the cross-sectional area [ $\text{m}^2$ ]. The resistance of the resistors can be prescribed by Ohm's law:  $V = IR_E$ , where  $V$  is the voltage [V] across a conducting material and  $I$  is the current [A] flowing through the conductor. The circuit symbol of the resistor for the electric resistance and Ohm's law is shown in Fig. 1f.

The formulae and relations between voltage, current, resistance, and conductor length are physically similar to those between pressure, flow, hydraulic resistance, and channel length. Fig. 1c represents the equivalent circuit symbol of a fluidic resistor for the hydraulic resistance and Hagen–Poiseuille's law, analogous to those of a resistor for the electric resistance and Ohm's law. The fluidic resistor is a two-terminal (*e.g.*, input and output terminals) passive fluidic element that implements hydraulic resistance as a fluidic circuit element.

If  $N$  fluidic resistors are collectively arranged in series, an equivalent single fluidic resistor has a hydraulic resistance equal to the sum of the  $N$  hydraulic resistances:

$$R_{H,\text{eq}} = R_{H,1} + R_{H,2} + \dots + R_{H,N}. \quad (12)$$

**Table 1** The physical similarities between microfluidics and electronics: the electric circuit analogy

Microfluidics	Electronics	Related sections, figures, equations
Molecules	Electrons	
Flow of fluid	Flow of electricity	Fig. 1
Volumetric flow rate $Q/\text{m}^3 \text{ s}^{-1}$	Electric current $I/\text{Amp}$	2.3, Fig. 1, and 2
Pressure drop $\Delta p/\text{Pa}$	Voltage drop $\Delta V/\text{Volt}$	2.3, Fig. 1, and 2
Hydraulic resistance $R_H/\text{Pa s}^3 \text{ m}^{-1}$ : $R_H \propto L/A^2$	Electric resistance $R_E/\Omega$ : $R_E \propto L/A$	2.5, Fig. 1, 2 and eqn (11)
Hagen–Poiseuille's law: $\Delta p = QR_H$	Ohm's law: $V = IR_E$	2.5, Fig. 1, 2, eqn (4), (6), (8), and (11)
Hydraulic circuit or microfluidic network	Electric circuit	Fig. 2
Microchannel segment (fluidic resistor)	Conductive wire (electric resistor)	3.1, Fig. 1, and 2
Source-inlet and drain-outlet port	Input and output terminal	3.1, 3.2, and Fig. 2
Equivalent series-connected fluidic resistors: $R_{H,\text{eq}} = R_{H,1} + R_{H,2}$	Equivalent series-connected resistors: $R_{E,\text{eq}} = R_{E,1} + R_{E,2}$	3.1, Fig. 2 and eqn (12)
Equivalent parallel-connected fluidic resistors: $R_{H,\text{eq}} = R_{H,1} \parallel R_{H,2} = (R_{H,1} \times R_{H,2})/(R_{H,1} + R_{H,2})$	Equivalent parallel-connected fluidic resistors: $R_{E,\text{eq}} = R_{E,1} \parallel R_{E,2} = (R_{E,1} \times R_{E,2})/(R_{E,1} + R_{E,2})$	3.1, Fig. 2 and eqn (13)
Independent, constant fluid flow source	Independent, constant current source	3.2, Fig. 3
Independent, constant pressure source	Independent, constant voltage source	3.2, Fig. 3
External pump ( <i>e.g.</i> , syringe and peristaltic pump)	Power supply or battery	3.2, Fig. 3
Atmospheric pressure $p_{\text{atm}}$	Earth or floating ground (GND)	3.2, Fig. 3
Law of mass conservation: $\sum Q_n = 0$ at a node	Kirchhoff's current law (KCL): $\sum I_n = 0$ at a node	3.3, Fig. 4 and eqn (15)
Law of energy conservation: $\sum \Delta p_n = 0$ in a closed path (or mesh)	Kirchhoff's voltage law (KCL): $\sum V_n = 0$ in a closed path (or mesh)	3.3, Fig. 4 and eqn (16)
Pressure division (or pressure fraction)	Voltage division	3.4, Fig. 4 and eqn (17)
Flow division (or flow fraction)	Current division	3.4, 4.3, Fig. 4, 8, eqn (18) and (22)
Hydraulic compliance (or capacitance) $C_H [\text{m}^3 \text{ Pa}^{-1}]$ : $\Delta Q(t) = C_H \Delta p/dt$ ( $\Delta Q$ : stored volumetric flow rate change)	Capacitance $C [\text{F}]$ : $I(t) = C dV/dt$	4.7, 7.2 <sup>a</sup>
Inertia (which is negligible in microfluidic systems)	Inductance $L [\text{H}]$	7.2 <sup>a</sup>
Maximum velocity = speed of sound	Maximum velocity = speed of light	<sup>a</sup>

<sup>a</sup> These are not covered in this review article. However, it is worth mentioning in this table.

This is due to series-connected fluidic resistors carrying the same volumetric flow from one terminal to the other.

Similar simplification can be applied to parallel-connected fluidic resistors. In a circuit containing  $N$  fluidic resistors in parallel, the reciprocal of an equivalent single fluidic resistor has a hydraulic resistance equal to the sum of reciprocals of each hydraulic resistance:

$$R_{H,\text{eq}} = R_{H,1} \parallel R_{H,2} \parallel \dots \parallel R_{H,N}$$

$$\frac{1}{R_{H,\text{eq}}} = \frac{1}{R_{H,1}} + \frac{1}{R_{H,2}} + \dots + \frac{1}{R_{H,N}}. \quad (13)$$

For instance, consider a simple microfluidic network connected with different channel lengths, but with the same cross-sectional area and shape (Fig. 2a):  $L_1 = L_5$ ,  $L_3 = 2L_1$ , and  $L_2 = L_4 = 4L_1$ . Following eqn (11), each channel segment in the microfluidic network can be treated like a fluidic resistor linearly proportional to the channel length, thus the microfluidic network can be converted to an equivalent circuit networked with fluidic resistors (Fig. 2b):  $R_{H,1} = R_{H,5}$ ,  $R_{H,3} = 2R_{H,1}$ , and  $R_{H,2} = R_{H,4} = 4R_{H,1}$ . And the total equivalent fluidic resistor becomes

$$R_{H,\text{eq}} = R_{H,1} + (R_{H,2} \parallel R_{H,3} \parallel R_{H,4}) + R_{H,5}$$

$$= (1 + (4 \parallel 2 \parallel 4) + 1) \times R_{H,1}$$

$$= \left(1 + \left(\frac{4 \times 2}{4+2} \parallel 4\right) + 1\right) \times R_{H,1} = 3R_{H,1}. \quad (14)$$

Therefore, the equivalent channel length would be  $L_{\text{eq}} = 3L_1$  because of  $R_{H,\text{eq}} = 3R_{H,1}$  and  $R_H \propto L$ . Notice that in the parallel connection the hydraulic resistance of the equivalent fluidic resistor is always smaller than the hydraulic resistance of the smallest resistor:  $(4 \parallel 2 \parallel 4) = 1 < 2$ .

### 3.2 Independent fluid flow and pressure sources: independent current and voltage sources

Most pressure-driven microfluidic devices need to be operated using external pressure sources, if they are not integrated with

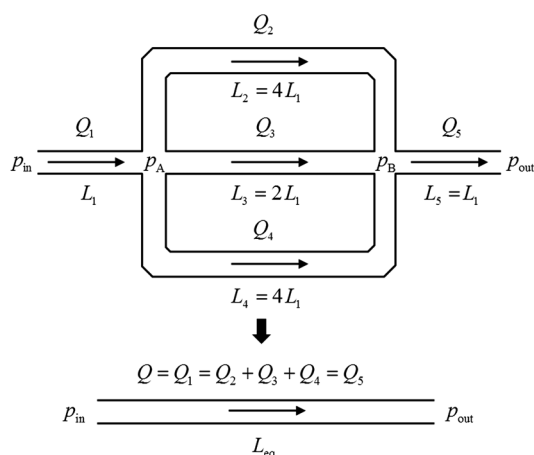


**Fig. 2** A simple microfluidic network: (a) a simple microfluidic network connected with different channel lengths but with the same cross-sectional area and shape and (b) its equivalent fluidic circuit with fluidic resistors and an equivalent single fluidic resistor. “ $\parallel$ ” indicates a shorthand notation for a parallel combination of electric elements. A point at which two or more circuit elements have a common connection is called a node (e.g., node A and node B). If no node was encountered more than once, then the set of nodes and elements that we have passed through is defined as a path; a dotted box in the equivalent fluid circuit indicates a closed path.

on-chip pumping components.<sup>44</sup> Conventionally, external pumps such as syringe and peristaltic pumps are widely used to supply constant fluid flow to devices (Fig. 3a). The volumetric flow supplied by the pumps is completely independent of the pressure drop across the inlet and outlet ports of a device. We do not know *a priori* what the pressure drop across an independent fluid flow source (e.g., syringe pump) will be, because it depends entirely on the equivalent hydraulic resistance of the circuit to which it is connected. In this case, an independent constant fluid flow source  $Q_S$  is analogous to an independent DC current source (Fig. 3b).

An alternative method is to connect an independent pressure source to inlet ports. Basically, the flow is controlled by the gravity-driven flow induced by the hydraulic-head difference,  $\Delta h$  [m], between the vertical source-inlet and drain-outlet reservoirs of microfluidic devices.<sup>45,46</sup> For an independent and constant pressure source,  $\Delta h$  has to be held constant all the time.<sup>45,47,48</sup> Alternatively, pressurized reservoirs connected with external pneumatic sources are used to provide independent, constant, and controllable pressure to a device (Fig. 3c).<sup>49–51</sup>

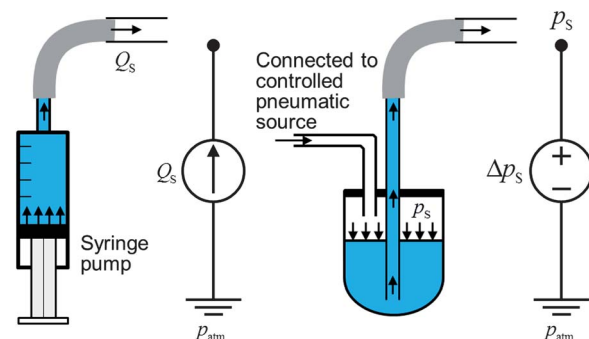
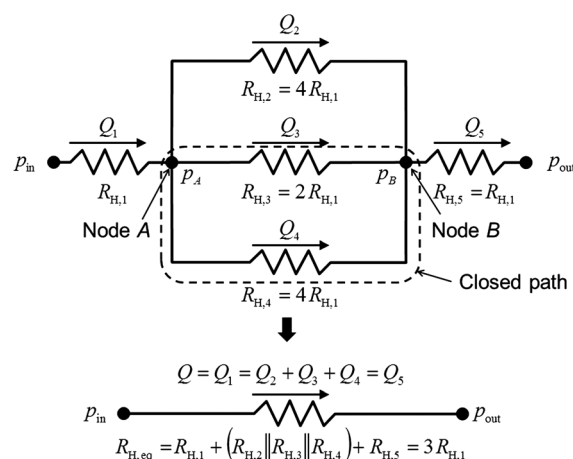


**Fig. 3** Independent pumping sources: (a) an independent constant fluid flow source with a syringe pump, (b) its equivalent circuit symbol, (c) an independent constant pressure source connected with a controlled pneumatic source, and (d) its equivalent circuit symbol.



The independent constant pressure source  $p_S$  is analogous to the independent DC voltage source (Fig. 3d).

Most microfluidic network-based devices are connected with two or more pumping sources for the source-inlet ports and several drain-outlet ports normally open to atmosphere. But the pumping sources are physically disconnected from the drain-outlet ports. In electric circuit analogy, the drain-outlet port can be treated as earth or floating ground (GND) since the output port is open to atmospheric pressure  $p_{\text{atm}}$ .

### 3.3 Conservation of mass and energy: Kirchhoff's current law (KCL) and Kirchhoff's voltage law (KVL)

One of the most fundamental concepts in electric circuit theory is charge conservation; the algebraic sum of the currents entering any node is zero:  $I_1 + I_2 + \dots + I_N = 0$ . This law is called Kirchhoff's current law (KCL).<sup>14</sup> Similarly, the conservation of mass in fluidic circuits implies that the sum of the flows into a node should be equal to the sum of the flows leaving the node. Therefore, the flow relation for the mass conservation at a node, analogous to KCL, is

$$\sum_{n=1}^N Q_n = 0. \quad (15)$$

If we consider the same microfluidic network as shown in Fig. 2, we can express eqn (15) as  $Q_1 - Q_2 - Q_3 - Q_4 = 0$  at the node A and  $Q_2 + Q_3 + Q_4 - Q_5 = 0$  at the node B:  $Q_1 = Q_2 + Q_3 + Q_4 = Q_5$ .

The second fundamental concept in electric circuit theory is energy conservation; the energy required to move a unit charge from point X to point Y in a circuit must have a value independent of the path chosen to get from X to Y. Any route must lead to the same value for the energy or the voltage. We may assert this fact through Kirchhoff's voltage law (KVL); the algebraic sum of the voltages around any closed path is zero:  $V_1 + V_2 + \dots + V_N = 0$ .<sup>14</sup> Similarly, conservation of energy in fluidic circuits implies that the sum of each pressure drop around the closed path is zero. Thus, the pressure drop relation for energy conservation in a closed path, analogous to KVL, is

$$\sum_{n=1}^N \Delta p_n = 0. \quad (16)$$

If we consider the same microfluidic network as shown in Fig. 2, we can express eqn (16) as  $\Delta p_3 + \Delta p_4 = 0$  around the closed path in a clockwise direction (indicated with a dotted box in Fig. 2b), where  $\Delta p_3 = p_A - p_B$  and  $\Delta p_4 = p_B - p_A$ . By using the parameters indicated in Fig. 2b, eqn (16) results in the following:  $\Delta p_3 = -\Delta p_4 \rightarrow Q_3 R_{H,3} = Q_4 R_{H,4} \rightarrow 2Q_3 R_{H,1} = 4Q_4 R_{H,1} \rightarrow Q_3 = 2Q_4$ . The mass conservation law, analogous to KCL (eqn (15)), and energy conservation law, analogous to KVL (eqn (16)), combined with Hagen–Poiseuille's law, analogous to Ohm's law (eqn (11)), can prescribe the approximate flow solution with the linear algebraic equations derived from the equivalent fluidic circuit.

### 3.4 Pressure and flow division: voltage and current division

In electric circuit theory, the application of concepts such as voltage and current division can also greatly simplify the

analysis. Voltage division is used to express the voltage across one of several series resistors in terms of the voltage across the series combination. If a microfluidic network includes series fluidic resistors of  $R_{H,1}, R_{H,2}, \dots, R_{H,N}$ , then we have the general result for pressure division across a channel network of N series fluidic resistors:

$$\Delta p_n = \frac{R_{H,n}}{R_{H,1} + R_{H,2} + \dots + R_{H,N}} \Delta p_S = \frac{R_{H,n}}{R_{H,\text{eq}}} \Delta p_S \quad (17)$$

where the pressure drop across the independent pressure source is  $\Delta p_S = p_S - p_{\text{atm}}$ . Eqn (17) allows us to compute the pressure drop that appears across an arbitrary  $n^{\text{th}}$  fluidic resistor of the series. In Fig. 4a, the pressure drop will be  $\Delta p_1 = (R_{H,1}/(R_{H,1} + R_{H,2})) \times \Delta p_S$  across the first fluidic resistor and  $\Delta p_2 = (R_{H,2}/(R_{H,1} + R_{H,2})) \times \Delta p_S$  across the second fluidic resistor based on the pressure division.

The dual of voltage division is current division in electric circuit theory. Current division is used to describe the current across one of several parallel resistors in terms of the current across the parallel combination. If a total flow of  $Q_S$  is supplied to  $N$  parallel fluidic resistors, then the volumetric flow rate  $Q_n$  through the fluidic resistor  $R_{H,n}$  is given by

$$Q_n = \frac{(1/R_{H,n})}{(1/R_{H,1}) + (1/R_{H,2}) + \dots + (1/R_{H,N})} Q_S = \frac{R_{H,\text{eq}}}{R_{H,n}} Q_S. \quad (18)$$

In Fig. 4b, the volumetric flow rate will be  $Q_1 = (R_{H,2}/(R_{H,1} + R_{H,2})) \times Q_S$  across the first fluidic resistor and  $Q_2 = (R_{H,1}/(R_{H,1} + R_{H,2})) \times Q_S$  across the second fluidic resistor based on the flow division. For the flow division, the expression appears to be inversely different from that for the pressure division.

Let us find out the volumetric flow rate ratio of  $Q_2 : Q_3 : Q_4$  in the microfluidic network shown in Fig. 2. By the flow division (eqn (18)), the flow ratio becomes  $Q_2 : Q_3 : Q_4 = 1 : 2 : 1$  because the ratio of three parallel fluidic resistors is  $R_{H,2} : R_{H,3} : R_{H,4} = 2 : 1 : 2$ . Notice that smaller fluidic resistors in a parallel network carry proportionally larger flows, thus providing shortcut pathways through microfluidic networks.

Interesting microfluidic networks solving maze-like problems were studied by the Whitesides group.<sup>37</sup> Pressure-driven flow in the networks could be used to identify global pathways of least fluidic resistance (Fig. 5). At each node, fluids follow flow division analogous to electric current division by taking the path of least resistance. Roughly speaking, fluids cannot enter dead-end channels due to their infinite hydraulic resistance. Thus, fluids

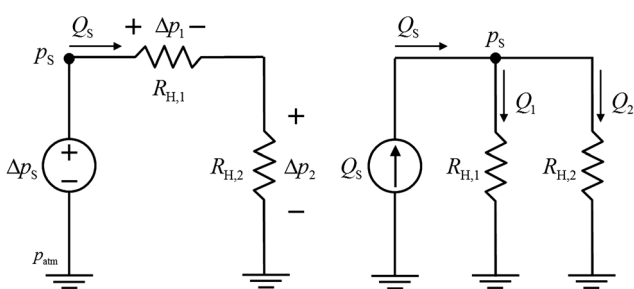


**Fig. 4** Illustrations of (a) pressure division and (b) flow division in fluidic circuits, analogous to voltage and current division in electric circuit theory.

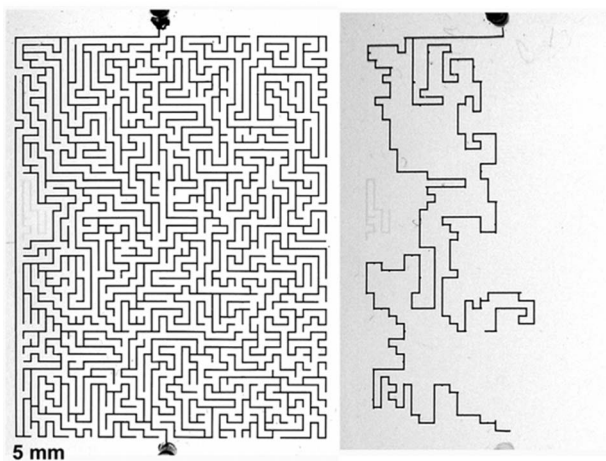


**Fig. 5** A maze-like microfluidic network filled completely with an aqueous ink solution (left) and the real-time solution of the same maze (right). At each node, fluids flow through the shortest pathway faster than the others, based on the flow division, analogous to the electric current division (reprinted with permission from ref. 37, copyright 2003 American Chemical Society).

can find the best solution to a maze-like problem by taking the flow path of least fluidic resistance between the inlet and the outlet of the corresponding microfluidic network. The use of pressure and flow division methods provides intuitive and practical ideas for configuring segments of channel networks in the design of complex microfluidic systems.

### 3.5 Computer-aided analysis: PSpice and CFD

By applying mass and energy conservation laws in combination with Hagen–Poiseuille's law, we can analyze relatively simple purely resistive microfluidic networks. We can use this approach for all microfluidic networks, but as we continue to add more resistive channel networks, it will become time-consuming to verify solutions by hand. A powerful graphical user interface (GUI)-driven computer software package known as PSpice (an acronym for Personal Simulation Program with Integrated Circuit Emphasis; Cadence Design, NY, USA) is commonly used for the rapid analysis of electric circuits. Complex microfluidic circuits can also be easily analysed using the PSpice tool once they have been converted to equivalent electrical circuits.<sup>27,52–57</sup> Obviously, the finite element method by CFD simulation is the preferred method of modelling microfluidic networks. Particularly, if complex microfluidic mixers are included in microfluidic networks, CFD-aided analysis is unavoidable.<sup>58</sup> However, for most microfluidic networks with simple mixers, the PSpice-aided analysis is a relatively quick means of determining flows and pressures in microfluidic circuits.

### 3.6 General procedure of using the electric circuit analogy

Suppose we have a typical microfluidic network consisting of  $N_S$  channel segments,  $N_M$  meshes,  $N_N$  nodes,  $N_F$  flow sources, and  $N_O$  drain-outlet ports. A mesh is defined as a loop that does not contain any other loops within it. A node is defined as a point at

which two or more fluidic resistors have a common connection. Here is a general procedure to analyse the microfluidic network.

(i) Convert the microfluidic network into an equivalent purely resistive circuit using the analogy.

(ii) Label each of the volumetric flow rates and the hydraulic resistances in each channel segment. Pay close attention to flow directions in each channel. This gives a number of  $N_S$  flow rates and a number of  $N_S$  hydraulic resistances.

(iii) Write a mass conservation equation (eqn (15)), analogous to KCL, at each node. This gives a number of  $N_N$  equations.

(iv) Express any additional unknowns associated with flow sources in each source-terminal in terms of appropriate volumetric flow rates. This may give a number of  $N_F$  equations, but you may have already done this in step (iii).

(v) Write an energy conservation equation (eqn (16)), analogous to KVL, around each mesh in terms of flow rates and hydraulic resistances. This gives a number of  $N_M$  equations.

(vi) Determine the total number of unknowns and equations to solve. Organize these into a system of linear equations, and solve the system using standard methods.

(vii) Optionally, verify your solutions using the PSpice simulation tool. This check will help identify mistakes made during step (vi).

## 4. Practical design of microfluidic networks

The generalized Hagen–Poiseuille's equation (eqn (11)) can be straightforwardly used to estimate the laminar flow in circular or non-circular channels that are either infinite or finite in length. The validity of this approach is based on the following assumptions: (i) incompressible, homogeneously viscous, and no convective mixing flow, (ii) steady-state, parabolic, and laminar flow, and (iii) uniform pressure gradient along the channel length. Additionally, inertial effects (analogous to inductance) and hydraulic compliance (analogous to capacitance) can be ignored if (i) the operating frequency is well below the resonance frequency of the flow and (ii) rigid tubes and channels are used with an incompressible fluid.<sup>59</sup> Then, the converted equivalent electric circuit contains purely resistive components, which are easy to analyze.

For a better understanding of microfluidic network design and analysis using the electric circuit analogy, a tutorial example of a simple serial dilution microfluidic network (Fig. 6) is discussed in **Box 1**. This section focuses on practical aspects, often encountered during microfluidic network design, such as volume concentration, mixing channel, flow fraction, shear stress, channel geometry, layout design, device fabrication, and device operation.

### 4.1 Volume concentration

The networks of microchannels permit precise and predictable volumetric mixing ratios of two mixing solutions (*e.g.*, buffer and sample). Therefore, they can generate a set of well-defined volume concentrations (also referred to as volume fractions), where the volume concentration is defined as the volumetric flow rate of a sample divided by the total volumetric flow rate of the mixture prior to mixing. If the initial concentration of a buffer is

**Box 1—Tutorial example: design of a simple microfluidic network.**

This tutorial problem demonstrates the use of the electric circuit analogy for the analysis and design of a microfluidic network.

**Problem.** Suppose we want to design a microfluidic network producing a particular output response (*e.g.*, a set of concentrations and/or flow rates) at drain-outlet ports. Consider a typical serial dilution microfluidic network generating a 10-fold log profile of sample concentration (Fig. 6a). For simplicity, the width and height of all channels in the device will be the same. Design a serial dilution microfluidic network such that equivalent electric circuit analysis can be used to model the microfluidic network and such that the desired set of output concentrations and flow rates is given:  $C_1 = 0\%$ ,  $C_2 = 1\%$ ,  $C_3 = 10\%$ , and  $C_4 = 100\%$  and  $Q_1 = Q_2 = Q_3 = Q_4 = 1 \mu\text{l min}^{-1}$  at drain-outlet ports O1, O2, O3, and O4, respectively. This device consists of: 11 channel segments ( $N_S = 11$ ), 4 meshes ( $N_M = 4$ ), 5 nodes ( $N_N = 5$ ), 2 flow sources ( $N_F = 2$ ), and 4 drain-outlet ports ( $N_O = 4$ ). Determine geometrical parameters (*e.g.*, length, width, and height) of all channel segments and required input conditions (*e.g.*, flow rate or pressure from pumping sources) at source-inlet ports.

**Solution.** First we must determine the length of mixing channels at the given flow rate condition. From eqn (20), the minimum length of the mixing channels (segments S2 and S7) will be  $L_D = 1.7 \text{ mm}$  with  $w = h = 100 \mu\text{m}$  when  $Q = 1 \mu\text{l min}^{-1}$ . To cover higher flow rate ranges, let  $L_D = 10 \text{ mm}$ ;  $L_2 = L_7 = L_D = 10 \text{ mm}$  for mixing channel segments S2 and S7. We can arbitrarily tailor the length of other channel segments that are not critical to output responses for efficient experimental accessibility and/or better appearance; let  $L_6 = L_8 = L_{10} = L_{11} = 2 \text{ mm}$  for segments S6, S8, S10, and S11, respectively, and  $L_9 = 4 \text{ mm}$  for segment S9. Then,  $L_1$ ,  $L_3$ ,  $L_4$ , and  $L_5$  for segments S1, S3, S4, and S5, respectively, are still unknown values that need to be determined by the analysis.

To achieve the 10-fold log concentration profile, the volumetric flow rate ratios should be  $Q_5 : Q_6 = 9 : 1$  and  $Q_9 : Q_{10} = 9 : 1$  (see eqn (19)). Next, we use a mass conservation equation in each node, analogous to KCL (eqn (15)). This gives five equations because of  $N_N = 5$ :

$$Q_8 = Q_1 + Q_5 + Q_9 \text{ in node N1}$$

$$Q_5 + Q_6 = Q_2 \text{ in node N2}$$

$$Q_7 = Q_3 + Q_6 \text{ in node N3}$$

$$Q_9 + Q_{10} = Q_7 \text{ in node N4}$$

$$Q_{11} = Q_4 + Q_{10} \text{ in node N5}$$

These equations combined with the given output condition ( $Q_1 = Q_2 = Q_3 = Q_4 = 1 \mu\text{l min}^{-1}$ ) will give all flow rates in each channel segment:  $Q_5 = 0.9$ ,  $Q_6 = 0.1$ ,  $Q_7 = 1.1$ ,  $Q_8 = 2.89$ ,  $Q_9 = 0.99$ ,  $Q_{10} = 0.11$ , and  $Q_{11} = 1.11 \mu\text{l min}^{-1}$ . From these results, we can determine the required input conditions at two source-inlet ports, volumetric flow rates to be supplied from external syringe pumps to the source-inlet ports:  $Q_{F1} = Q_8 = 2.89 \mu\text{l min}^{-1}$  for flow source F1, and  $Q_{F2} = Q_{11} = 1.11 \mu\text{l min}^{-1}$  for flow source F2.

In this device design, the cross-sectional area of all channels will be the same. Therefore, the Hagen–Poiseuille's equation (eqn (11)) can be rewritten as

$$\Delta p \equiv QL$$

Instead of stating the hydraulic resistance, we can use the channel length because  $R_H \propto L$ . This makes our analysis straightforward; *i.e.* we do not need to calculate the hydraulic resistance in each channel segment.

Now, we can write an energy conservation equation around each mesh in terms of flow rates and channel lengths, analogous to KVL (eqn (16)). This gives four equations because of  $N_M = 4$ :

$$Q_1 L_1 = Q_5 L_5 + Q_2 L_2 \rightarrow 1 \times L_1 = 0.9 \times L_5 + 1 \times 10 \text{ around mesh M1}$$

$$Q_3 L_3 = Q_6 L_6 + Q_2 L_2 \rightarrow 1 \times L_3 = 0.1 \times 2 + 1 \times 10 \text{ around mesh M2}$$

$$Q_4 L_4 = Q_{10} L_{10} + Q_7 L_7 + Q_3 L_3 \rightarrow 1 \times L_4 = 0.11 \times 2 + 1.1 \times 10 + 1 \times L_3 \text{ around mesh M3}$$

$$Q_5 L_5 = Q_9 L_9 + Q_7 L_7 + Q_6 L_6 \rightarrow 0.9 \times L_5 = 0.99 \times 4 + 1.1 \times 10 + 0.1 \times 2 \text{ around mesh M4}$$

If we organize the four equations with known values, the four unknown channel lengths can be analytically solved:  $L_1 = 25.16$ ,  $L_3 = 10.20$ ,  $L_4 = 21.42$ , and  $L_5 = 16.84 \text{ mm}$  for channel segments S1, S3, S4, and S5, respectively. Finally, we verify the solutions by PSpice simulation tool (Fig. 6b). Now we can layout a mask of the microfluidic network corresponding to the equivalent circuit (Fig. 6c) and fabricate a real serial dilution microfluidic network producing the 10-fold log concentration profile.

This simple tutorial example shows in detail how to use the electric circuit analogy to design a specific pressure-driven microfluidic network. Notice that in fact we can generate not only any arbitrary monotonic concentration profile but also arbitrary flow rate profiles at the outlet ports, and even increase the number of outlet ports. A more generalized model and method has been previously reported by the Oh group.<sup>27</sup> The model enables the development of universal microfluidic concentration and/or shear flow rate gradient generators using a serial dilution-based microfluidic network module.

not zero ( $C_B \neq 0$ ), the concentration value ( $0 \leq C \leq 1$ ) of the mixture after full mixing will be (Fig. 7)

$$C = \frac{Q_B}{Q_B + Q_S} C_B + \frac{Q_S}{Q_B + Q_S} C_S \quad (19)$$

where  $Q_B$  is the volumetric flow rate of the buffer with the initial concentration  $C_B$  ( $0 \leq C_B \leq 1$ ) prior to mixing and  $Q_S$  is the volumetric flow rate of the sample with the initial concentration  $C_S$  ( $0 \leq C_S \leq 1$ ) prior to mixing.

## 4.2 Mixing channel

If the full mixing of two or multiple flows is necessary, the length of mixing channels  $L$  [m] should be sufficient to allow their full mixing:  $L > L_D$ , where  $L_D$  [m] is the minimum length of the mixing channels required to achieve the full diffusional mixing (Fig. 7). In laminar flows through straight microchannels, the only native mixing mechanism is by molecular diffusion. The diffusion distance  $d$  [m] of molecules in a liquid for a time  $t$  [s] depends on the diffusion coefficient of molecules  $D_D$  [ $\text{m}^2 \text{ s}^{-1}$ ]:  $d \approx \sqrt{2D_D t}$ .<sup>60</sup> A rough estimate of the mixing time required for purely diffusive mixing can be obtained by examining the diffusion time  $t_D$  across the cross-section of channels when the diffusion distance is about the same as the channel width  $w$  [m] ( $d \approx w$ ). We conventionally use  $t_D \approx w^2/D_D$ , called the characteristic diffusion time.<sup>61–63</sup> Thus, the minimum length  $L_D$  [m] of the mixing channels required to achieve the full diffusional mixing can be estimated as

$$L_D = U t_D = U \frac{d^2}{D_D} \approx U \frac{w^2}{D_D} \quad (20)$$

where  $U$  [ $\text{m s}^{-1}$ ] is the area-averaged velocity in the mixing channels. In particular, for a straight square channel, the minimum channel length required for full mixing becomes  $L_D = Ud^2/D_D \approx (Q/w^2)(w^2/D_D) \approx Q/D_D$ . For water ( $D_D = \sim 10^{-9} \text{ m}^2 \text{ s}^{-1}$ ,  $\rho = 10^3 \text{ kg m}^{-3}$ , and  $\eta = 10^{-3} \text{ Pa s}$ ) typical values are  $L_D = 1.7 \text{ mm}$ , when  $Q = 1 \mu\text{l min}^{-1}$ ,  $w = h = 100 \mu\text{m}$ , and  $Re = 0.17$ . If we need to deal with biological molecules, we have to design much longer mixing channels due to their lower diffusion coefficients; for example, the minimum mixing channel length becomes  $L_D = 17 \text{ mm}$  for glucose solution ( $D_D = \sim 10^{-10} \text{ m}^2 \text{ s}^{-1}$ ).<sup>64</sup>

To allow short mixing channel length and/or higher operation flow rates and Reynolds numbers ( $Re > 1$ ), we need to include micromixer designs in the flow path to enhance diffusive or convective mixing effects. For this purpose, a variety of micro-mixers have been exploited, such as passive and active micro-mixers.<sup>65</sup> However, it is known that their hydraulic resistances across the complicated micromixing structures are generally non-linear to flow rates or Reynolds numbers. Thus, their hydraulic behaviour cannot be analytically estimated according to Hagen–Poiseuille's law. Additionally, CFD-assisted analysis may be required for the complete design of the microfluidic networks in order to determine precise values of hydraulic resistances of micromixers and adjust each channel length in the microfluidic circuits.<sup>58</sup> An alternative strategy is to make fluidic channels thin and diffusion-mixing channels thick.<sup>66</sup> This approach allows sufficiently long residence times even with short mixing channel length.

In general, however, a symmetric configuration of micromixers in parallel-connected flow paths will allow us to use the flow

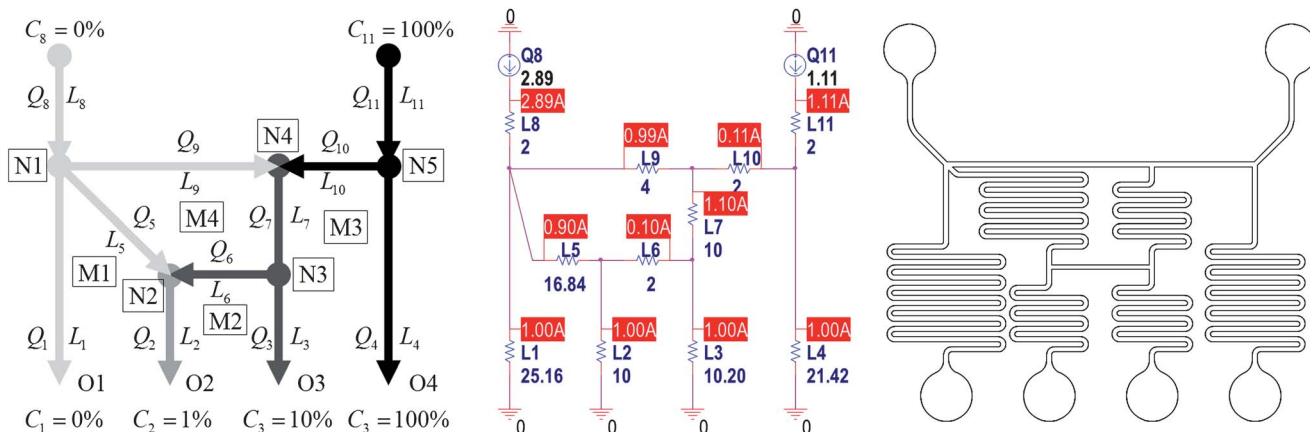


**Fig. 6** (a) Illustration of a typical serial dilution microfluidic network generating a 10-fold log profile of a sample concentration, (b) PSpice simulation results, and (c) resulting mask layout of the network. See Box 1 for more detailed information.  $C$ : concentration,  $Q$ : volumetric flow rate,  $L$ : channel length,  $M$ : mesh,  $N$ : node,  $O$ : drain-outlet port,  $F$ : flow source,  $S$ : channel segment.

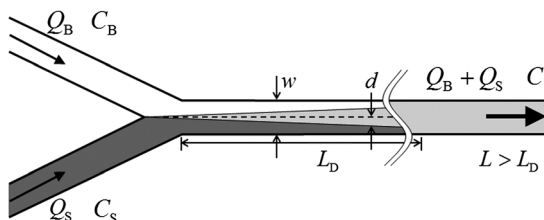


**Fig. 7** Illustration of diffusive mixing in a long channel with the length  $L$  and the width  $w$ .  $Q_B$  and  $Q_S$  are the volumetric flow rates of incoming buffer and sample solutions, respectively.  $C_B$  and  $C_S$  are the initial concentrations of the buffer and sample solutions. The outcome of the full mixing is diluted sample with the volumetric concentration value  $C$ .

division method for design (see Section 3.4). In this specific configuration, our interest is in the relative ratio between the hydraulic resistances of the channels with the same micromixing structures, not in their absolute numerical values. Suppose micromixers with the same length and structure are connected in parallel from one node<sup>61,67</sup> (or common channel<sup>68</sup>) to the other. Then, their hydraulic resistances and the pressure drops between the two nodes will be equal to each other. Therefore, the ratio of flow rates divided into each micromixing channel will be equal to ‘one’ and invariable to a wide range of operation flow rates or Reynolds numbers.

#### 4.3 Flow fraction

If the mixing between two incoming streams is very slow, then there will be a clear boundary between the two streams. This phenomenon happens if less diffusive particles or molecules are flowing within the streams; the Peclet number ( $Pe$ ) will be relatively large in this system because the diffusivities of particles, cells, or macromolecules can be quite small.<sup>69</sup> The Peclet number is defined as

$$Pe = \frac{VD}{D_D} \approx \frac{UD_H}{D_P} \quad (21)$$

where  $V$  [ $\text{m s}^{-1}$ ] is the characteristic velocity transverse to the diffusion (or the area-averaged velocity  $U$  [ $\text{m s}^{-1}$ ]),  $D$  [m] is the characteristic length (or the hydraulic diameter  $D_H$  of the channel [m]), and  $D_D$  [ $\text{m}^2 \text{s}^{-1}$ ] is the diffusion coefficient of molecules (or the diffusion coefficient of the particles within the liquid stream  $D_P$  [ $\text{m}^2 \text{s}^{-1}$ ]). It is known that the diffusivity  $D_P$  depends inversely on the particle size according to the Stokes–Einstein equation.<sup>22</sup>

The boundary width can be predicted given the flow ratio between the incoming streams. It is known that, for fully developed laminar flows far from the channel node, the channel length has to be substantially longer than the channel hydraulic diameter:  $L \gg D_H$ ,  $L/D_H \gg Re$ , and  $Re < 2300$ .<sup>22</sup> Therefore, steady-state flow fraction starts to occur at the distance  $l$  [m] from the channel node that is roughly  $l \approx w \times Re$  (assuming  $D_H \approx w$ ), and its velocity profile becomes the parabolic shape. From this 2D model, the partial areas of the parabola will be proportional to the volumetric flow rates of each stream:  $S_1 : S_2 = Q_1 : Q_2$  (Fig. 8a). Similarly, there will be a virtual boundary fractioned by each outgoing stream:  $S_3 : S_4 = Q_3 : Q_4$ .<sup>70,71</sup>

Assuming pressure-driven flows and no-slip boundary conditions in a high aspect ratio channel (e.g., Hele-Shaw limit:

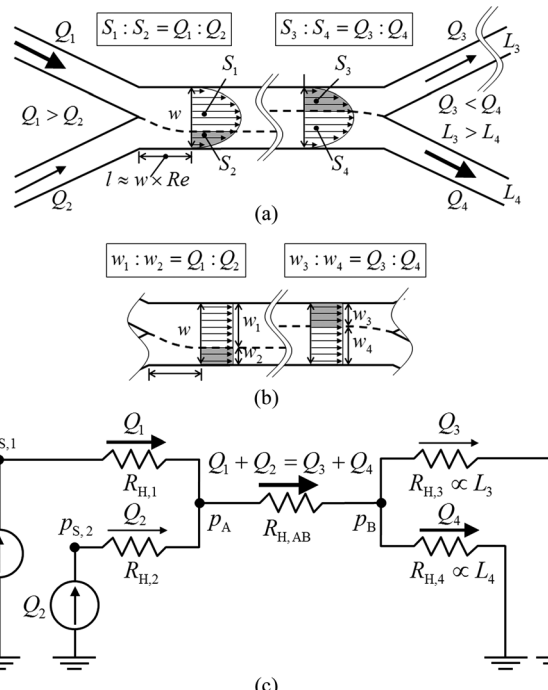


**Fig. 8** Schematic of a typical flow fraction-dependent microfluidic network when  $Q_1 > Q_2$  and  $Q_3 < Q_4$ . There exists a boundary (dotted lines) between the two incoming streams or the two outgoing streams. (a) 2D model (e.g., parabolic flow profile) to estimate the boundary width. The partial areas of the parabola ( $S_1$  and  $S_2$ , or  $S_3$  and  $S_4$ ) are proportional to the volumetric flow rates of each stream ( $Q_1$  and  $Q_2$ , or  $Q_3$  and  $Q_4$ ). (b) 1D model (e.g., flat flow profile) to estimate the boundary width. With this rough approximation, the ratio of the boundary widths of the two incoming streams ( $w_1 : w_2$ ) or that of the two outgoing streams ( $w_3 : w_4$ ) can be estimated with the volumetric flow rate ratio of the input streams ( $Q_1 : Q_2$ ) or that of the output streams ( $Q_3 : Q_4$ ), respectively. (c) Equivalent electric circuit.

$h/w \ll 1$ ), the flow velocity is independent of the position across the channel width. From this rough 1D model, the boundary width is accurately approximated by the ratio of the incoming or outgoing flow rates with (Fig. 8b):<sup>72–74</sup>

$$\frac{w_1}{w_2} = \frac{Q_1}{Q_2} \text{ or } \frac{w_3}{w_4} = \frac{Q_3}{Q_4} \quad (22)$$

However, in order to make a more precise prediction, we must take the actual 3D flow profile at the rectangular cross-section into account and use the flow rates for each incoming or outgoing stream to determine the fractionated boundary width.<sup>75,76</sup>

Fig. 8c illustrates an equivalent electric circuit. By supplying input flows from external pumps with different ratios, each incoming stream can be actively divided into fractions with different boundary widths. Similarly, the fractions of each outgoing stream can be controlled by different ratios of the output volumetric flow rates that depend on hydraulic resistances or simply channel lengths of the output channels with the same cross-section.

#### 4.4 Shear stress

Channel surface plays an important role in microfluidic networks, especially for cell-based studies, such as adhesion, cell

seeding, and shear-dependent response.<sup>77</sup> The amount of shear experience by a microchannel wall in laminar flow can be originally calculated from Newton's law of viscosity:  $\tau_w = -\eta(du/dz)_{\text{at wall}}$ , where  $\tau_w$  [dyn cm<sup>-2</sup>] is the shear stress at the wall,  $u$  is the flow velocity, and  $z$  is the position within the height of the microchannel.<sup>78</sup> If we design channels or chambers with a high aspect ratio (*e.g.*,  $h < w$ ), the shear stress at the wall between two parallel plates under parabolic flow can be reasonably approximated, depending on the channel height and the pressure drop across the channels with a length  $L$ . By combining eqn (10) and (11), the wall shear stress in a microchannel with the high aspect ratio can be expressed as a function of the volumetric flow rate and the channel geometry:<sup>79,80</sup>

$$\tau_w \approx \frac{h \Delta p}{2 L} = \frac{6\eta Q}{wh^2}. \quad (23)$$

Notice that this 2D approximation assumes an ideal case of infinite flat plate. A more precise prediction in a rectangular cross-section can be derived by using the 3D velocity profile *via* Fourier series expansions.<sup>78</sup>

#### 4.5 Channel geometry

For the successful design and stable operation of microfluidic networks, it is important that any non-linear and turbulence effects be circumvented over the flow rates of interest. We can adopt similar geometric configurations to highway ramp systems for smooth traffic flow. Specifically, a curved turn in a channel is better than a right-angle turn, and a slanted junction at a node is better than a right-angle junction. In particular, the behaviour at the microfluidic nodes (junctions) should be independent of the flow rate up to moderate Reynolds number ( $Re \ll 2300$ ) for high-speed or high-throughput applications.<sup>54</sup>

Thoughtful consideration is needed to determine the cross-sectional dimension and length of microchannels. The pressure drop is inversely proportional to the fourth power of the hydraulic radius (see eqn (9)). Thus, for smaller channel sizes, the pressure drop increases rapidly. The small cross-sectional area means that a significant pressure is needed to achieve a certain flow rate. Pressure build-up in microchannels can lead to the deformation or delamination of microchannels. On the other hand, small cross-sectional dimensions give rise to shorter mixing distances (see eqn (20)). Therefore, clearly defined operational ranges of flow rate and throughput are a prerequisite for designing microfluidic networks.

We may arbitrarily tailor the length or geometry of channel segments that are not critical to functions in microfluidic networks for efficient experimental accessibility or even better appearance. Then, the inlet and outlet ports can be carefully partitioned and placed in line with fluidic interconnection and external detection schemes. Most of the designers of microfluidic networks use AutoCAD to manually layout the devices. During the layout design, computer-aided analysis using PSpice or CFD can be used to validate the network layout design.

#### 4.6 Device fabrication

Current microfluidic devices are mostly made out of PDMS (polydimethylsiloxane), a commonly used silicone material that

is transparent, biocompatible, deformable, and gas permeable, and seals easily on contact with glass slides.<sup>81–84</sup> Standard fabrication methods depend on photolithography and associated clean-room processes. Soft lithography is a widespread method in which PDMS is cast on a master mold fabricated from thick photoresists, typically SU-8. Alternative rapid prototyping technology that is cost-efficient for general laboratories has been reported from several groups: xurography using desktop cutting plotters<sup>85–87</sup> and microscale plasma-activated templating technology ( $\mu$ PLAT).<sup>88</sup> Their typical resolution of channel cross-sections was  $\sim 50$   $\mu$ m. In addition, hot embossing and microinjection molding has been used to mass produce microfluidic devices using COC (cyclic olefin copolymer), PC (polycarbonate), or PMMA (polymethyl methacrylate) polymers that are biocompatible, optically transparent, and rigid.<sup>89–91</sup> Silicon and glass may still be the preferred materials due to their mechanical rigidity, chemical resistance, low permeability, and optical properties (*e.g.* transparency of glass).<sup>92,93</sup>

During device fabrication, care is needed to minimize potential mismatch between the electric circuit analogy-based design and experimental results. If the cross-sectional geometry, *i.e.* height and width, is fixed across a network, then the only critical design parameter is the channel length as it defines the relative hydraulic resistance of the channels (see eqn (11)).<sup>27</sup> This approach offers easy fabrication and flexibility in defining channel height, but may need a relatively large footprint. To minimize the device size, multiple height, multiple width<sup>66,94</sup> or multiple layer<sup>55–57</sup> configurations can be incorporated. However, special fabrication consideration is needed to achieve precise and uniform channel heights or widths.

Pressure-induced deformation of PDMS<sup>95</sup> is the essential material property enabling pneumatic valves developed by the Quake group.<sup>82</sup> However, deformability under very high pressure can be problematic in pressure-driven microfluidic networks fabricated using standard 10 : 1 ratio PDMS materials (*e.g.*, Sylgard 184 silicone elastomer kit from Dow Corning and RTV615 from Momentive Performance Materials).<sup>96</sup> Hydraulic resistances in each channel may dynamically fluctuate depending on the applied pressure.<sup>95</sup> This hydraulic compliance, which gives rise to a change in the volumetric flow rate through a channel, is due to pressure-induced elastic deformation of its walls. This behaviour corresponds to capacitance in the electric circuit analogy (see Table 1).<sup>22,59,97,98</sup> Circuits with capacitive effects can provide less reliable predictions of hydraulic behaviour. If this problem is critical to device functions, more rigid materials, such as plastic, glass, or silicon, need to be used. The use of highly cross-linked PDMS (*e.g.*, 5 : 1 ratio,<sup>99</sup> hard PDMS<sup>96,100</sup>) may reduce the issue on the deformability by increasing its elastic modulus. An alternative method using a thin PDMS channel layer sandwiched between two glass slides will significantly reduce the total volume of the deformable bulky PDMS layer, thus lessening its deformability.<sup>96,101</sup>

#### 4.7 Device operation

One of the practical issues in operating pressure-driven microfluidic networks is reliable world-to-chip interfaces, which allow easy coupling between the macroscale in the real world and the microscale in the microfluidic devices. If the microfluidic

Published on 16 December 2011. Downloaded by University of California - Riverside on 14/09/2015 19:19:59.

networks are fabricated in PDMS, interfacing is straightforward. A common method is to punch access holes 20–50% smaller than the diameter of fittings such as polyethylene tubing, glass or metal capillaries, sippers, and even micropipette tips to be tightly fit by press fitting.<sup>102</sup> Additional useful information for general ideas of the reliable microfluidic interfacing technology can be found in the literature.<sup>92,103–110</sup> Also, the *Chips & Tips* forum in the *Lab on a Chip* journal includes many useful tips for the microfluidic interfaces, as well as practical problems and solutions encountered in the laboratories, which are seldom reported in the literature.<sup>111</sup>

If air bubbles are trapped in microfluidic networks, converted equivalent electric circuits cannot be treated as purely resistive circuits due to additional contribution of hydraulic compliances from the compressible air bubbles. Several methods have been used to prime microfluidic devices without air traps. Flushing channels with isopropyl alcohol will make trapped air bubbles to flow through more easily than water.<sup>50</sup> Pressurizing channels with fluid from inlet ports while all other open ports are blocked will make air bubbles to diffuse through gas-permeable PDMS.<sup>112,113</sup> Another popular method is to submerge entire devices in a large reservoir of buffer solution and place it inside a vacuum chamber.<sup>114,115</sup> This will make the air bubbles move out of the device through PDMS or open channels. Recent work introduced geometry-assisted meniscus priming by placing phaseguiding structures on the surface of channels to control priming and emptying in a step-wise manner between phaseguides.<sup>116</sup>

Once free of air bubbles the devices are ready for testing. In general, we can simplify microfluidic network analysis by avoiding dynamic fluctuation and response. The use of rigid and short tubing connection from external pumping sources to inlet ports significantly reduces dynamic fluctuation of hydraulic resistances. Also, the use of steady-state constant pumping sources, analogous to DC current or voltage sources, will diminish dynamic response. Of course, microfluidic networks can be operated using frequency-dependent pumping sources, analogous to AC current or voltage sources.<sup>117–119</sup> Dynamic frequency modulation from the pumping sources could create continuous-flow temporal concentration variations in frequency-dependent microfluidic networks.

Fluorescence-based quantification using aqueous fluorescein solutions<sup>27,120,121</sup> or colour-based pH indicating solutions<sup>122</sup> is conventionally used to verify performance of microfluidic networks. In practice, a calibration curve (or a look-up table) should be obtained in order to correlate the intensity of fluorescence signals with a range of fluorescence concentrations of interest.<sup>55,59,123</sup> When capturing fluorescence images *via* microscopes, the region of interest should be scanned in the same location of each image as the fluorescence intensity is not uniform across the entire field of view. Saturation of fluorescence signals may also occur if fluorescein solutions are exposed to the excitation light source for a long time.<sup>59</sup> This often happens at very low volumetric flow rates due to the photo-bleaching effect.<sup>124</sup>

## 5. Application: concentration-dependent microfluidic networks

Pressure-driven microfluidic networks are widely used for the generation of concentration gradients. This section focuses on

various concentration-dependent continuous-flow microfluidic networks, such as proportional, pyramidal, serial, and combinatorial networks. These networks need complete mixing in each round to achieve the desired concentration profiles. Another concentration-dependent microfluidic network that needs well-controlled partial mixing (*e.g.*, T-type network) will also be discussed.

### 5.1 Proportional network

A proportional network that brings a series of volumetric proportions of two solutions together is a straightforward network configuration (see Fig. 7). The volumetric proportions of the two solutions can be controlled by adjusting the hydraulic resistance ratios of the distribution channels for the solutions. For example, Fig. 9a shows a working principle to generate a linear concentration profile using proportional networks.<sup>125</sup> When the ratio of the distribution channel lengths for liquids A and B is  $a : b$ , the mixing ratio will be  $b : a$  according to the flow division, analogous to the electric current division (eqn (18)). The proportional networks can be built on either single (Fig. 9b)<sup>126–128</sup> or multiple layers<sup>125,129</sup> depending on the network configuration. A series of linear volumetric proportions can give stepwise linear concentration profiles.<sup>125–127,129</sup> If a series of non-linear volumetric proportions is included in the network, non-linear concentration profiles can also be created as shown in Fig. 9c.<sup>128</sup>

This method is not sensitive to the flow rate because only one round of diffusional mixing occurs for each dilution. Typically, the proportional network can generate a dilution range with a single order of magnitude. It will be difficult to create high orders of logarithmic concentrations using the proportional networks due to a condition of extremely high hydraulic resistance difference between the distribution channels; for example it needs 10 000 times difference in distribution channel lengths for 4-log scale.

### 5.2 Pyramidal network

A pyramidal network of microchannels, originally suggested by the Whitesides group, is the most popular type to generate concentration gradients (Fig. 10a).<sup>121,130–132</sup> The generation of the gradients is based on the complete diffusive mixing of fluids by repeated splitting, mixing, and recombination of fluid streams through pyramidal networks. The hydraulic resistances, thus the volumetric flow rates, were maintained to be the same for all vertical mixing channels within each branch. For simple analysis, the approximation was that the resistance of the horizontal channels was negligible in comparison with the resistance of vertical channels because the length of the horizontal channels was 20 times shorter than that of the vertical ones.

The static or dynamic variation of input flow rates and initial concentrations of buffer and sample solutions and/or numbers and configurations of input ports could result in concentration gradients of complex shapes (*e.g.*, linear,<sup>133</sup> polynomial,<sup>121</sup> and periodic<sup>130</sup>) in the outlet channel of the pyramidal networks (Fig. 10b). Various mathematical models have been reported to study the fluid transport for the original design including the same lengths for all vertical mixing channels.<sup>134–137</sup> Recent approaches are more general and predictable to create desired

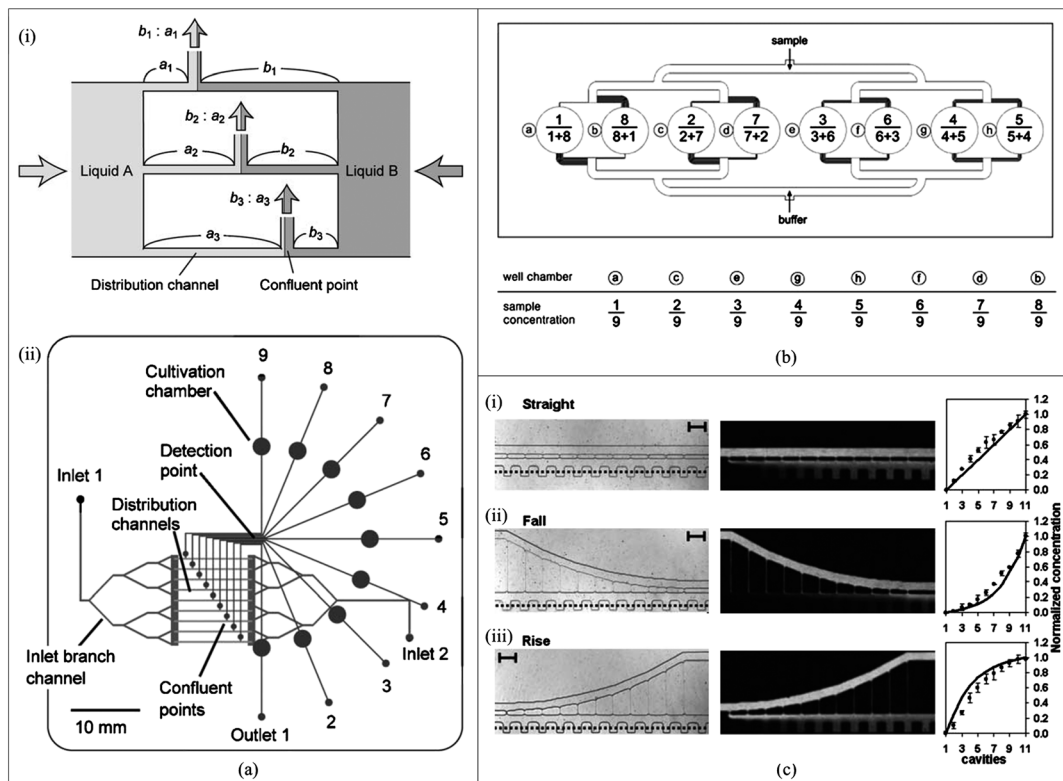


**Fig. 9** Selected examples of proportional networks to generate concentration gradients. (a) Device to generate a linear concentration gradient: (i) principle of proportional flow division with different volumetric flow rate ratios of two solutions and (ii) schematic diagram of the two-layer microfluidic network (reprinted with permission from ref. 125, copyright 2004 Institute of Physics Publishing). (b) Single-layer device to generate a linear concentration gradient (from ref. 126, copyright 2006 Royal Society of Chemistry). (c) Devices to generate linear and non-linear concentration gradients (from ref. 128, copyright 2007 Royal Society of Chemistry).

concentration profiles, especially a very precise linear concentration gradient that was a challenge with the original pyramidal design. The main idea was to make well-controlled volumetric mixing ratios at each branch, by modifying the channel lengths, thus the hydraulic resistances, for vertical mixing channels (Fig. 10c).<sup>62,138–140</sup> Another interesting approach is to alter the number, length, and spacing between asymmetric pyramidal dividers across a long single channel, generating custom shaped profiles (Fig. 10d).<sup>141</sup>

The use of the pyramidal networks is widespread ranging from cellular studies (*e.g.*, adhesion,<sup>142</sup> axon guidance,<sup>143</sup> chemotaxis,<sup>80,139,144–146</sup> differentiation,<sup>147</sup> drug screening,<sup>67,148,149</sup> gene expression,<sup>150</sup> and growth and migration<sup>151–154</sup>) to on-chip sensors (*e.g.*, amperometric quantification,<sup>155</sup> surface-enhanced Raman scattering (SERS)-based immunoassays,<sup>156</sup> and optofluidics<sup>157,158</sup>). Although the design and fabrication of the pyramidal networks is relatively simple, the majority of applications that use such networks are limited to linear or polynomial concentration gradients or to a dilution range with few orders of magnitude. In general, it is very difficult to achieve different but controllable output flow rates using the pyramidal networks.

### 5.3 Serial network

A serial network of microchannels mimics a serial dilution comprising a series of stepwise dilutions to reduce the

concentration of sample into a broad range. In conventional manual serial dilutions, a sample solution is serially diluted wherein the sample diluted from a previous step is processed sequentially through successive dilution steps. A 10-fold logarithmic gradient is obtained by the same 9 : 1 volumetric mixing ratio of the buffer and the sample diluted from the previous step in each step. A 2-fold logarithmic gradient can be obtained by the same 1 : 1 volumetric mixing in each step. Unconventional serial dilutions are possible using different volumetric mixing ratios in each step. For example, a linear gradient with 4 serial dilution steps can be accomplished with a 1 : 4 volumetric mixing ratio of the buffer and the sample in the first step, 1 : 3 in the second step, 1 : 2 in the third step, and 1 : 1 in the last step. If the factor of dilution at each step is arbitrarily different from the previous step, we can create stepwise, monotonic, universal concentration gradients.

Fig. 11a shows a generalized serial network including  $N$  cascaded-mixing stages that can generate universal concentration profiles by successive serial dilution steps as reported by the Oh group.<sup>27</sup> Using the generalized mathematical modelling based on the electric circuit analogy, stepwise linear, 2-fold log, and Gaussian concentration profiles have been demonstrated. In the design, the only variable parameter was the channel length because the cross-sectional area of all channels was the same. This approach may increase proportionally the occupancy area of the serial networks with the number of mixing

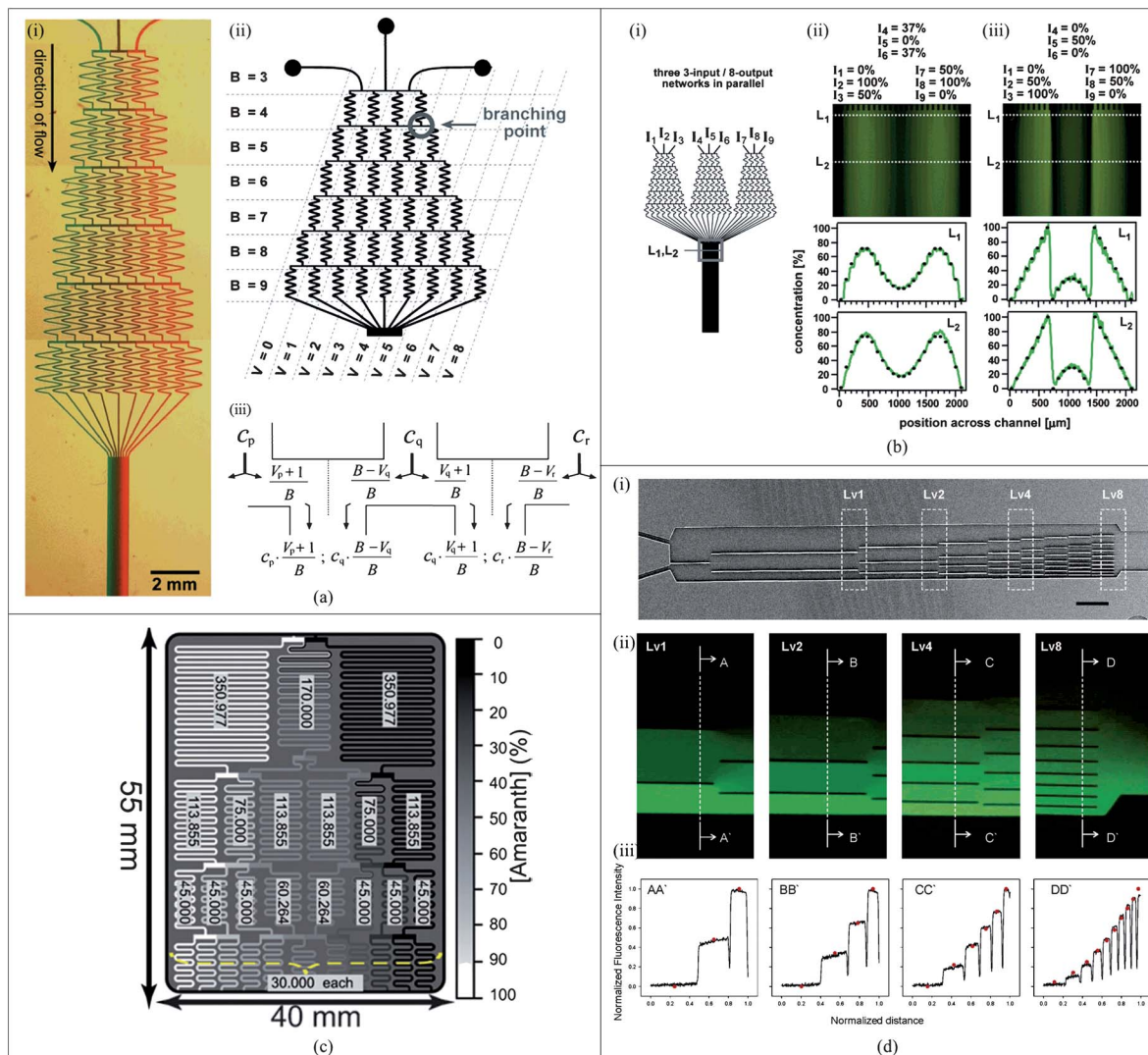


**Fig. 10** Selected examples of pyramidal networks to generate concentration gradients. (a) Pyramidal network of microchannels suggested by the Whitesides group: (i) a device with 3-input/9-output; (ii) equivalent electric circuit of the network; and (iii) working principle showing the splitting ratios at the branching points.  $B$  is the order of the branched system and  $V$  is the vertical channel within the branched system. The concentrations at the end of the vertical mixing channels can be calculated by multiplying the concentration of the incoming streams ( $C_p, C_q, C_r$ ) with the corresponding numbers of the splitting ratio ( $(V_p + 1)/B, (B - V_q)/B, (V_q + 1)/B$ , and  $(B - V_r)/B$ ) (reprinted with permission from ref. 130, copyright 2001 American Chemical Society). (b) Generation of gradients having complex shapes: (i) pyramidal networks with multiple inputs; (ii) fluorescence image of two parabolic periodic gradients; and (iii) fluorescence image of a mixture of parabolic and linear parts (from ref. 130, copyright 2001 American Chemical Society). (c) Generation of gradients having linear shapes in a 2-input/11-output network design with the modified channel lengths (indicated in mm scale) (from ref. 138, copyright 2009 Royal Society of Chemistry). (d) Universal gradient generator: (i) micrograph of the main channel and asymmetric pyramidal dividers (scale bar is 500  $\mu\text{m}$ ); (ii) fluorescence images of the concentration distribution of FITC at various points; and (iii) normalized fluorescence intensity profiles (from ref. 141, copyright 2006 American Chemical Society).

stages. The network design was not geometrically compact due to the requirement of long diffusive mixing channels for complete mixing in each stage within limited flow rates less than 1  $\mu\text{l min}^{-1}$ . Nevertheless, the proposed strategy enabled very straightforward analysis and design of the serial networks (see **Box 1**). The method was capable of generating universal monotonic gradients with a single module or arbitrary gradients with multiple modules ranging from linear to complex non-linear shapes of concentration gradients. As well, the method could generate arbitrary output flow rate gradients, which are useful in studying shear stress-dependent phenomena.

Instead of using the long diffusion microchannels,<sup>27,159,160</sup> herringbone patterns (Fig. 11b)<sup>161</sup> or serpentine Tesla micromixers (Fig. 11c)<sup>58</sup> were embedded in the mixing channels. For example, the latter device could be operated at relatively high flow rates ( $<\sim 100 \mu\text{l min}^{-1}$ ) and Reynolds numbers ( $<15$ ).<sup>58</sup> However, CFD-assisted analysis may be required for the complete design of the serial networks to estimate precise values of the hydraulic resistance of the micromixers.

Another design strategy for compact serial networks is to make fluidic channels thin and diffusion-mixing channels thick to allow sufficiently long residence times during the diffusive mixing (Fig. 11d).<sup>66,94</sup> This method could be used for analyzing drug

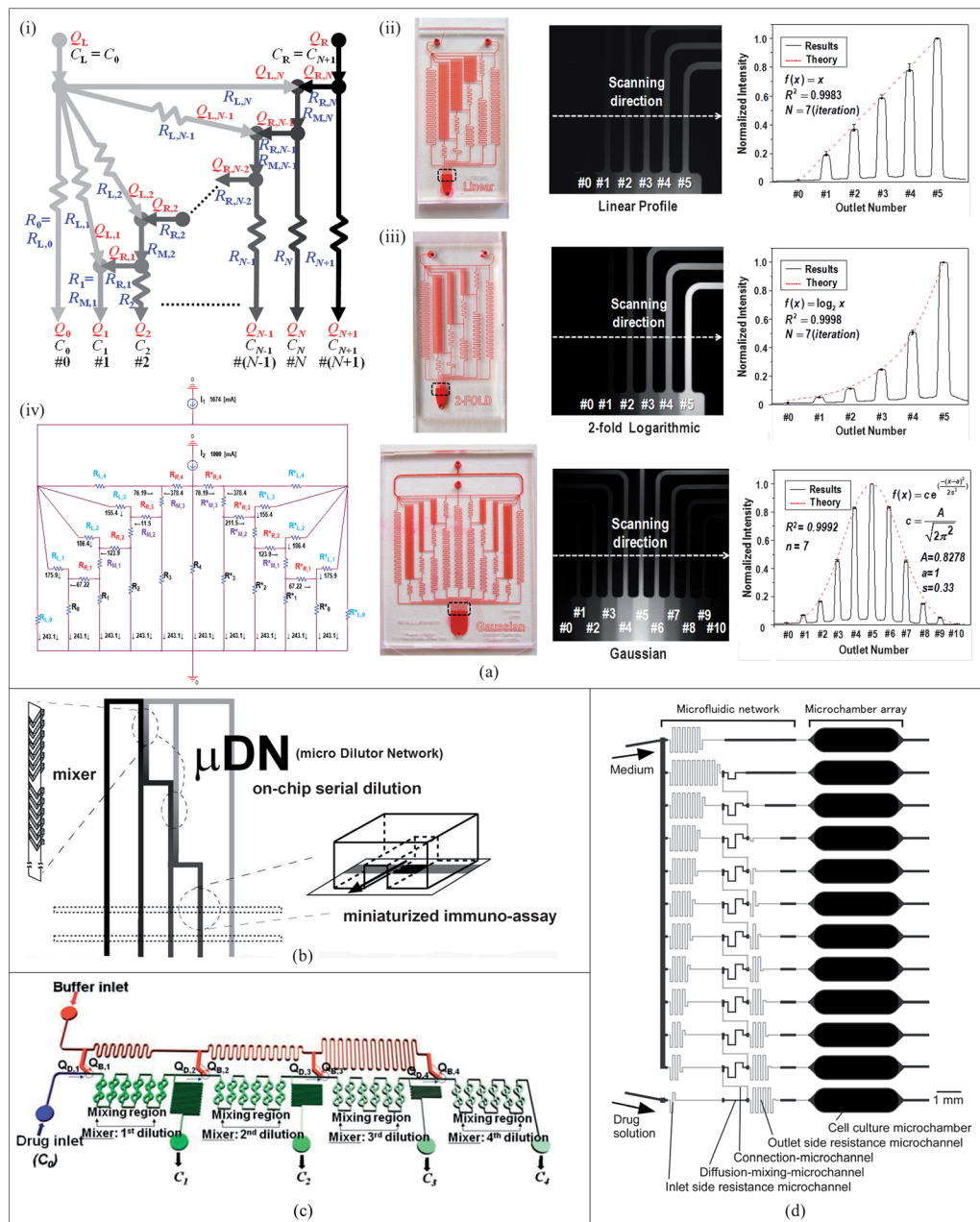


**Fig. 11** Selected examples of serial networks to generate concentration gradients. (a) Generalized serial dilution module for monotonic and arbitrary microfluidic gradient generators: (i) generalized microfluidic serial network, including  $N$  cascaded-mixing stages that mix two solutions to each output port with the desired output concentration  $C_i$  and output flow rate  $Q_i$ ; (ii) devices, fluorescence images, and intensity profiles for the linear concentration profile; (iii) devices, fluorescence images, and intensity profiles for the 2-fold log profile; and (iv) PSpice electrical analysis, devices, fluorescence images, and intensity profiles for the Gaussian profile (reprinted with permission from ref. 27, copyright 2009 Royal Society of Chemistry). (b) Serial network integrated with herringbone patterned micromixers (from ref. 161, copyright 2003 American Chemical Society). (c) Serial network integrated with serpentine Tesla micromixers (from ref. 58, copyright 2008 Royal Society of Chemistry). (d) Serial network with different cross-sectional channel areas (from ref. 94, copyright 2010 American Chemical Society).

dose-response over a concentration range spanning 6 orders of magnitude. An alternative compact design was obtained by a hybrid 2-layer configuration of the serial and the proportional networks.<sup>56</sup> This approach could significantly reduce the total number of cascaded serial dilution stages for 14 doses with a combination of 4-order logarithmic and 4-point linear concentrations. The Voldman group designed a serial network that simultaneously generated a logarithmic concentration

gradient and logarithmic flow rate (or shear stress) gradient across a  $4 \times 4$  cell perfusion array.<sup>162</sup>

The serial networks can easily generate high orders of logarithmic concentrations, which is useful for dose-response experiments and high-throughput drug screening and optimization. However, a large number of serial dilution steps can result in a large occupancy area of the device and a large dilution error accumulated from previous dilution steps. For operation with

Published on 16 December 2011. Downloaded by University of California - Riverside on 14/09/2015 19:19:59.

relatively high flow rates, it is recommended that the networks be integrated with micromixers for the complete mixing in each serial dilution stage. The performance of the serial networks is very sensitive to the volumetric flow rate ratio of buffer and sample solutions at input ports that is mostly not ‘one’; thus it requires precise flow control from external pumps. Nevertheless, the use of the serial networks is a powerful method to generate universal concentration and flow rate profiles with broad ranges.

#### 5.4 Combinatorial network

Combinatorial science is widely used to screen and optimize complex components in the areas of biotechnology, chemistry, material science, and pharmaceuticals.<sup>163–165</sup> Combinatorial drug therapy allows reduced dosage of each drug in the combination of two or more drugs that can increase synergistic effects and reduce toxicity and side effects caused by high dose of a single drug on biological targets.<sup>166,167</sup> Studies have shown that stem cell differentiation is governed by the combinatorial effects of several extracellular factors due to the nature of biological complexity.<sup>168–170</sup> The study of combinatorial effects in complex

biological or chemical systems requires numerous specific and accurate combinatorial dilutions of the sample candidate. The commonly used methods for a large number of samples with various kinds of conditions (e.g., drug combinations and their diluted concentrations) are limited to using multiple well plates or robotics that use relatively large reaction volumes and require expensive and complicated systems.

Combinatorial binary blends can be formed at the cross-intersection of two layers of channel networks. A combinatorial network designed by the Whiteside group generated  $5 \times 5$  binary blends in a microfluidic array consisting of two layers of channels that are separated by a polycarbonate membrane or a microwell (Fig. 12a).<sup>171</sup> Assays for inorganic ions, bacteria, and enzymatic activity were demonstrated in the pores of the membrane or the microwell as species diffuse from both layers of channels into the cross-intersection. An alternative approach is to use a ‘microfluidic patterning network’ that can be provisionally attached to a substrate of interest to immobilize components of interest supplied from the microfluidic patterning network on the substrate by means of physical adsorption.<sup>172–175</sup> Then, the patterning network is detached and a second microfluidic

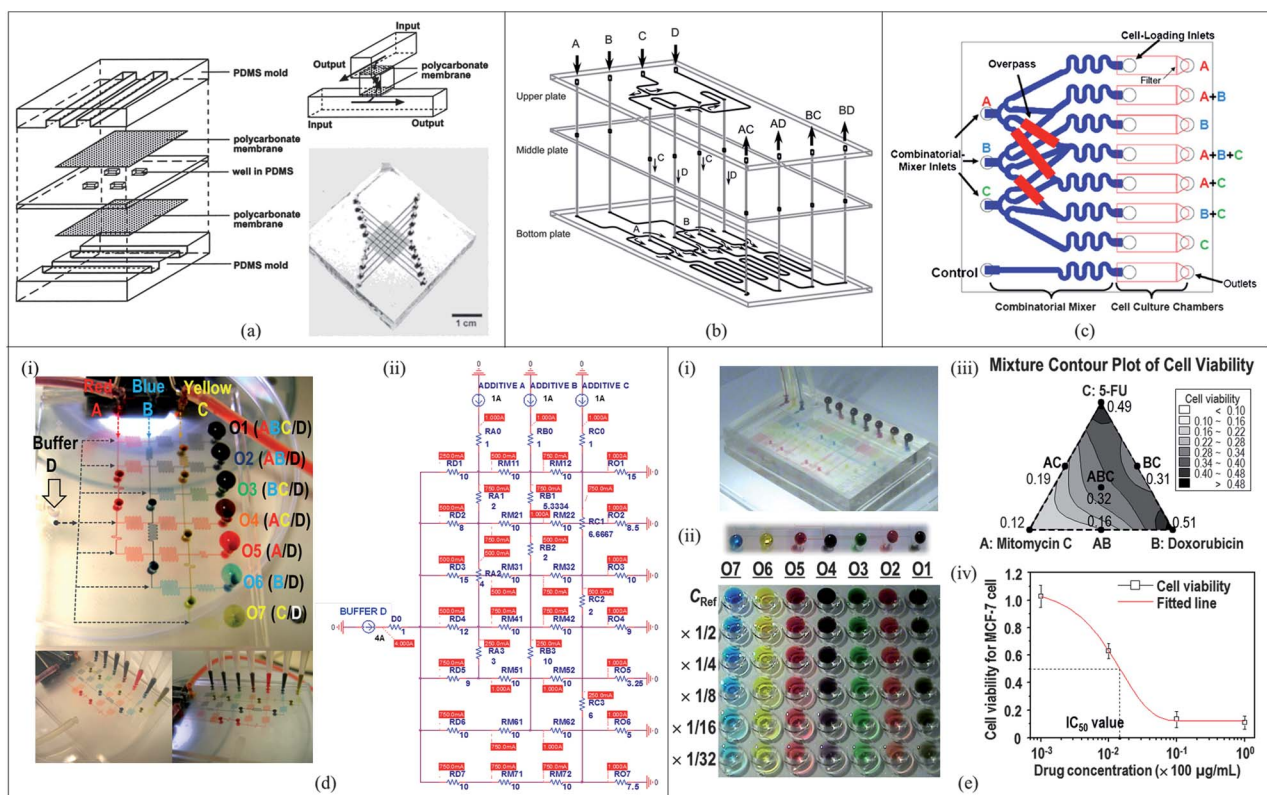


**Fig. 12** Selected examples of combinatorial networks. (a) Combinatorial network generating binary combinations in a microfluidic array consisting of two layers of channels that are separated by a polycarbonate membrane or a microwell (reprinted with permission from ref. 171, copyright 2001 American Chemical Society). (b) Continuous-flow combinatorial network with multiple glass layers creating combinatorial parallel synthesis of  $2 \times 2$  binary blends (from ref. 178, copyright 2002 Royal Society of Chemistry). (c) Monolithically fabricated parylene-C combinatorial microfluidic network (from ref. 180, copyright 2008 Elsevier). (d) Combinatorial network providing a simplex centroid configuration consisting of points at the center (ABC/D), the midpoints of the sides (AB/D, BC/D, and AC/D), and corners (A/D, B/D, and C/D): (i) the combinatorial network device filled with color dyes and (ii) its electric PSpice analysis (from ref. 55, copyright 2010 Springer). (e) Combinatorial network capable of concentration-on-demand combinatorial dilutions of all input samples in the range of a 3D simplex centroid configuration: (i) the device filled with color dyes; (ii) 2-fold logarithmically diluted samples in the combinatorial manner using the device; (iii) mixture contour plot of a cell viability test with 3-drug combinations (Mitomycin C, Doxorubicin, and 5-FU); and (iv) a dose–response experiment with the effect of 4-order logarithmic doses of Mitomycin C for MCF-7 cancer cells (from ref. 57, copyright 2011 Springer).

network is aligned and bonded to the substrate, facilitating binary combinations at the cross-intersection on the substrate. Integration of the Quake pneumatic valves is another method to replace the detachable microfluidic patterning, and allows an isolated chamber array for cell culture or assays.<sup>176,177</sup>

On the other hand, continuously flowing combinatorial networks can be designed for the generation of high-throughput combinatorial mixtures. The Kitamori group fabricated a combinatorial network with multiple glass layers that was used for combinatorial parallel synthesis of  $2 \times 2$  binary blends (Fig. 12b).<sup>178,179</sup> In another design, a monolithic fabrication process was used to generate 7 combinations (A, B, C, AB, BC, AC, and ABC) of 3 components (A, B, and C) in a polyethylene-C microchannel network (Fig. 12c).<sup>180,181</sup>

A more desirable but more difficult function is to generate systematic concentration variations of all the solutions in a combinatorial fashion.<sup>182</sup> For such combinatorial experiments, design of experiments (DOE) is a useful technique that minimizes experimental effort at maximal information output with systematic variations of large-scale multiple components.<sup>165,183–186</sup> In particular, a mixture DOE is an effective method to screen and optimize combinations and mixtures of all the multiple components.<sup>55,57,187–189</sup> A simple combinatorial network was designed and modelled by the Oh group that could produce systematic variations of buffer and additive solutions in a combinatorial fashion for high-throughput screening and optimization.<sup>55,57</sup> Fig. 12d shows the combinatorial network device and its electric PSpice analysis providing a simplex centroid configuration consisting of points at the corners (A/D, B/D, and C/D), the midpoints of the sides (AB/D, BC/D, and AC/D), and the center (ABC/D).<sup>55</sup> Also, a combinatorial network capable of concentration-on-demand combinatorial dilutions of all input samples in the range of a 3D simplex-centroid configuration was introduced (Fig. 12e).<sup>57</sup> The device was used to perform a simple combinatorial cytotoxicity test with 3 drugs (Mitomycin C, Doxorubicin, and 5-FU) as well as a dose-response experiment with the effect of 4-order logarithmic doses of Mitomycin C for MCF-7 cancer cells.

Due to the nature of combinatorial mixing of multiple components, most combinatorial network devices have been fabricated in complicated 3D formats with multiple layers. For example, an algorithm showed that it required 15 layers containing reservoirs and splitting channels, one filter membrane, and one bottom layer connecting vertical channels and the

membrane for the 6-vertex maximal clique problem.<sup>189</sup> The Folch group also reported a combinatorial network capable of combinatorial dilutions (*e.g.*, different concentration levels of 2 components) made by stacking 9 laser-cut Mylar laminates together.<sup>190</sup> Nevertheless, combinatorial networks of microchannels are significantly advantageous for screening and optimization of multiple combinations of components, especially in the fields of systems biology, drug discovery, and stem cell research, in an automated, miniaturized, and high-throughput manner.

## 5.5 T-type network

Although complete mixing is preferable in most applications, partial mixing in T-type networks can be used to generate simple parallel-flow concentration gradients. The T-type networks consist of multiple input and output microchannels that join into a single mixing channel in a T-shaped configuration. The mixing channel length  $L$  needs to be shorter than the minimum length  $L_D$  required for the complete diffusional mixing:  $L < L_D$  (see eqn (20)). After the fixed distance, output channels are split into a linear array of independent parallel channels (Fig. 13a).<sup>191</sup> The degree of diffusion is a function of residence time between the streams. With short diffusion times, the gradient profile is steep sigmoid-shaped. Thus, controlling input flow rates and initial concentration of solutions can define the steepness of the sigmoid.

T-type dilution-based microfluidic networks have been used to combine dissimilar fluid streams to create mixtures of two different chemicals,<sup>191</sup> perform biological assays,<sup>192–194</sup> and study bacterial tactic responses (Fig. 13b)<sup>195</sup> and cell infection *via* virus gradients (Fig. 13c).<sup>196</sup> Although the design and fabrication of the T-type networks is relatively simple, the majority is limited to sigmoidal or to dilution range with few orders of magnitude. Furthermore, the diffusional method using the T-type networks requires precise flow rate control to achieve the desired degree of diffusion. If a particular range of flow rates is needed, then the network must be redesigned with the appropriate channel dimension.

## 6 Application: flow-dependent microfluidic networks

In addition to controlling concentration, another important use of microfluidic networks is for applications involving the control of

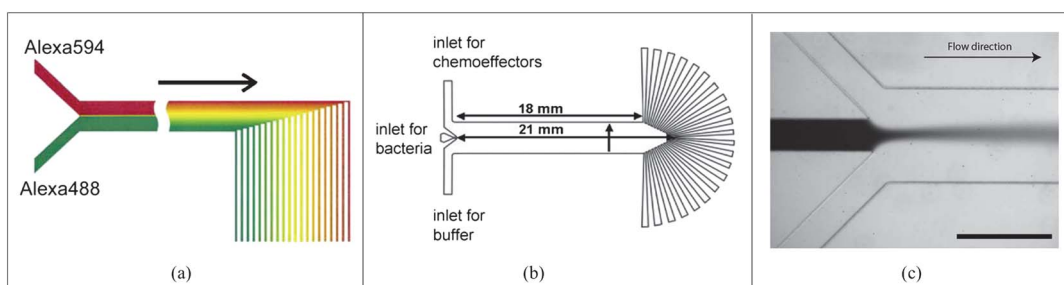


**Fig. 13** Selected examples of T-type networks to generate concentration gradients. (a) T-type network of two analytes split into a linear array of independent parallel channels (reprinted with permission from ref. 191, copyright 2003 Elsevier). (b) Device used to study bacterial tactic responses with 3-input/22-output (from ref. 195, copyright 2003 National Academy of Sciences, USA). (c) Device used to study cell infection *via* virus gradients (from ref. 196, copyright 2004 Elsevier).

flow. Applications of flow-dependent microfluidic networks include (i) flow division (see Section 3.4), (ii) flow fraction (see Section 4.3), and (iii) dynamic flow change networks (see Section 6.5).

This section focuses on various flow-dependent continuous-flow microfluidic networks. Microfluidic networks based on the flow division (Fig. 4b) will be discussed. Uniform or fractional distribution of fluids for cell seeding, microvessel study, or bifurcation can be performed using flow division-dependent microfluidic networks. Also, linear or non-linear shear stress gradient profiles can be created in the flow division-dependent microfluidic networks. In addition, flow fraction-based microfluidic networks (Fig. 8) have been used for hydrodynamic filtering of particles or cells. Finally, the use of autonomous, dynamic change of hydraulic resistances for trapping cells, droplets, and particles will be discussed.

### 6.1 Flow division network: distribution

In the flow-dependent microfluidic networks, the use of the flow division is essential to distribute the fluid stream containing species of interest. For high-throughput parallel reaction, the main stream can be evenly divided into multiple daughter channels arranged in hierarchical structures. Therefore massive parallel assays or reactions can be done in the network at the same time. The hierarchical networks have been used for studying morphology of large numbers of live *C. elegans*

(Fig. 14a),<sup>197</sup> the interactions (e.g., adhesion and cellular response to flow-induced shear stress) between the endothelial and underlying extracellular matrix,<sup>198</sup> or membrane viscoelasticity of red blood cells<sup>199</sup> in a high-throughput manner. In a circular arrayed flow division-based microfluidic network, a total of 108 reactions could be prepared with nine sample injections, which significantly improves the throughput.<sup>200</sup>

Flow division-based microfluidic networks can also be used to seed cells, perfuse cell culture, and perform on-chip cell-based assays.<sup>51,201,202</sup> Carefully designed microfluidic networks are required to deliver a cell suspension from an external source to an array of each cell culture chamber uniformly. The common strategy is to use the electric circuit analogy in order to design the channel networks with the same hydraulic resistance from the inlet to each chamber (Fig. 14b).<sup>201</sup> Therefore, a series of cell seeding, perfusion, and cell-based assays can be homogeneously performed in the large number of chambers.

Recently, an interesting flow-dependent microfluidic network was suggested by the Viovy group, for uniform distribution of flow across a whole wide microfluidic chamber (Fig. 14c).<sup>203</sup> In their design, the geometry and dimension of the distribution channels were optimized to equalize the hydraulic resistance of each path. Conventional configurations without the optimized distribution channels would result in the parabolic flow profile across the wide chamber due to uneven flow paths along the center and the sidewalls through the chamber.<sup>203,204</sup>

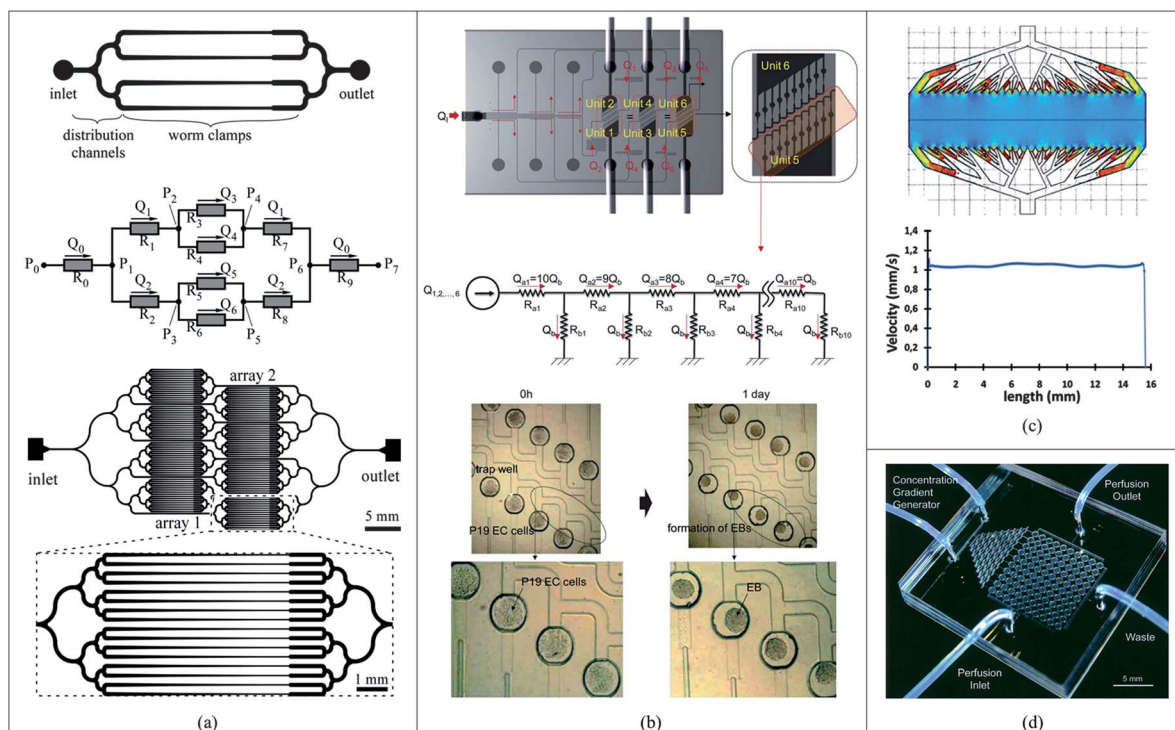


**Fig. 14** Selected examples of flow division network for flow distribution. (a) Hierarchical network to clamp live *C. elegans* in a high-throughput parallel channel network (reprinted with permission from ref. 197, copyright 2007 Royal Society of Chemistry). (b) Flow division-based microfluidic network to distribute cells for uniform 3D spheroid formation, which was designed based on the electric circuit analogy (from ref. 201, copyright 2011 Royal Society of Chemistry). (c) Flow distribution network allowing uniform distribution of flow across the whole wide chamber, in which geometry and dimension of the distribution channels were optimized to equalize the hydraulic resistance of each path (from ref. 203, copyright 2011 Royal Society of Chemistry). (d) Flow division cell perfusion network integrated with the pyramidal network generating concentration gradients for high-throughput cell-based assays (from ref. 205, copyright 2004 Wiley Periodicals).

Pressure-driven distribution networks can be combined with the concentration-dependent microfluidic networks. The Luke Lee group reported a flow division-based cell perfusion network integrated with a pyramidal network (Fig. 14d).<sup>205</sup> Such hybrid functions can be integrated in complex microfluidic networks by manipulating flow directions (*e.g.*, forward, backward, or side flows)<sup>94,147,149,159,205,206</sup> or employing the Quake pneumatic valves.<sup>182,206,207</sup>

## 6.2 Flow division network: shear stress generation

The use of the electric circuit analogy allows precise control of not only the volumetric flow rate but also the flow-induced shear stress in flow division-based microfluidic networks (see Section 4.4). Microfluidic networks generating shear stress gradients have been an important tool to study mechano-physiological effects on mammalian cells.<sup>77,202,208</sup> A simple approach to generate different shear stress is to vary the width of the channel.<sup>209</sup> If flow distribution channels that are hierarchically arranged are connected to a wide chamber, cells can be selectively deposited only in the chamber not in the distribution channels (Fig. 15a).<sup>204,210</sup> In the narrow distribution channels, cells experience a wall shear stress from the fast-moving flow that overcomes the initial adhesion of the cells to the surface of the channels. In the wide chamber, cells can adhere to the surface due to the reduced flow velocity and corresponding shear stress.

Another network design having cell culture chambers with different widths, and having resistance correction channels compensated for the overall resistance to allow equal flow

distribution towards the chambers, was used to study shear-dependent calcium dynamics in osteoblasts (Fig. 15b).<sup>211</sup> Shear-dependent protein transcription and membrane expression of cell adhesion molecules were performed by applying a 10-fold range of shear stress to endothelium in a tapered channel network.<sup>212</sup> A flow division-based microfluidic network was used to investigate shear-dependent platelet adhesion (Fig. 15c).<sup>79</sup> In this design, 250  $\mu\text{m}$  deep feeder and collector channels were used to reduce the shear stress through the channels, while a 100-fold range of shear stress was set through 24  $\mu\text{m}$  test chambers connected in series to the resistance channels. Another design was used to demonstrate a scratch wound healing assay under a 128-fold range of shear stress in steady and pulsatile flows with endothelial cells.<sup>213</sup>

Flow division-based microfluidic networks have also been used to study the human vascular system, which is made up of various vessels (*e.g.*, veins, arteries, capillaries). By mimicking the structure of vascular trees according to Murray's law, each channel dimension can be optimized to generate constant shear stress at the wall in the channel throughout the network.<sup>214–217</sup> Murray's law states the relationship between the diameter of the parent vessel and the optimum diameters of the daughter vessels based on the principle of minimum work (Fig. 15d);<sup>214</sup> the cube of the diameter of a parent vessel equals the sum of the cubes of the diameter of the daughter vessels:  $r_0^3 = r_1^3 + r_2^3$ , where  $r_0$  is the radius of the parent vessel and  $r_1$  and  $r_2$  are the radii of the daughter vessels. This principle enabled the study of artificial blood vessels<sup>217,218</sup> and respiratory systems (Fig. 15e)<sup>219–221</sup> using flow division-based microfluidic networks.

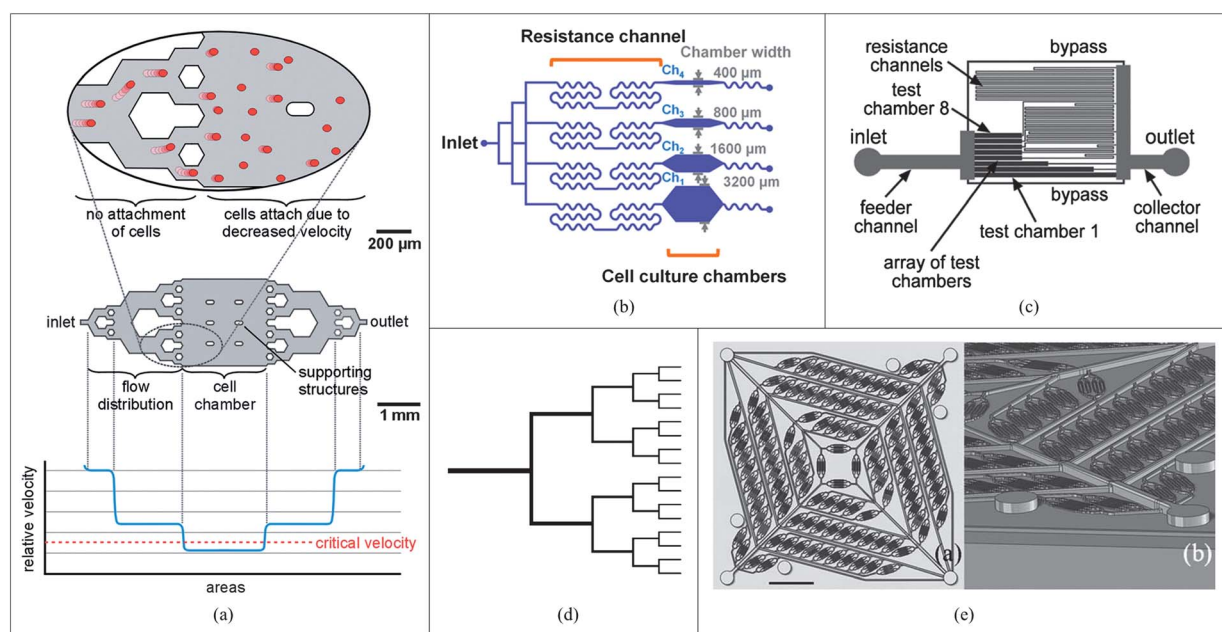


**Fig. 15** Selected examples of flow division network for shear stress generation. (a) Flow division network for controlled deposition of cells, where they can adhere to the surface of the cell chamber, not the flow distribution, due to reduced shear stress (reprinted with permission from ref. 204, copyright 2009 Royal Society of Chemistry). (b) Shear stress generation network with different widths connected in series to long resistance correction channels to allow equal flow distribution towards the chambers (from ref. 211, copyright 2011 Elsevier). (c) Flow division-based microfluidic network generating a 100-fold range of shear stress for a shear-dependent platelet adhesion study (from ref. 79, copyright 2008 Royal Society of Chemistry). (d) Biomimetic network designed according to Murray's law to generate constant shear stress at the wall in the channel throughout the network (from ref. 214, copyright 2006 Royal Society of Chemistry). (e) High density microfluidic vascular network developed for blood inflow from the pulmonary artery and blood return to the left atrium (from ref. 219, copyright 2011 Royal Society of Chemistry).

Hybrid networks generating both concentration and shear stress gradients have been designed. The Voldman group proposed a flow division-based microfluidic network generating both logarithmic concentration and shear stress profiles for perfused embryonic stem cell culture.<sup>59</sup> Another hybrid network was used for uniform distribution of cell seeding or other species to a large array of chambers and for providing concentration gradients, combinatorial mixtures, or even shear stress gradients of various soluble factors affecting cell or chemical assays in a high-throughput manner.<sup>206</sup> It is possible to design microfluidic networks such that both flow-induced shear stresses and concentrations are orders of magnitude higher or lower—those at which chemical and mechanical gradient effects of interest can be observed.

### 6.3 Flow fraction network: hydrodynamic filtering

Flow fraction-based hydrodynamic filtering networks can replace conventional cross-flow filtration devices that include physical barriers (*e.g.*, micropillars, microdams).<sup>222</sup> Hydrodynamic filtration, developed by the Seki group, is based on the selective extraction of streamlines controlled by the flow fraction at each branch for particle concentration, alignment, and separation (Fig. 16a).<sup>71,76</sup> A continuous flow with randomly spread

particles enters a main channel networked with multiple side branches. Only the stream near the sidewall enters the side branches, with the amount of fluid leaving the main channel being dictated by the relative flow rate ratio between the main and side channels, which are in turn determined by the hydraulic resistances in the various channel networks. If the strength of the flow fraction is very weak, the particles with radii larger than the width of the stream will not enter the side branches, rather they will be carried past the channel opening. During this process, the particles are gradually shifted and aligned against both sidewalls and particles of certain size can escape from the main channel at a specific branch where its ratio of the flow fraction is optimized for the right particle size. Different routing schemes of the side channels (*e.g.*, flow splitting and recombining) were used to concentrate and align the particles not only against one sidewall<sup>223,224</sup> but also in the center of the main channel.<sup>225</sup>

Hydrodynamic filtering networks have been used for a variety of applications. White blood cells (WBCs) in a blood sample<sup>53,76</sup> and liver cells<sup>224</sup> could be filtered. Blood plasma could be separated from whole blood based on the similar principle of the flow fraction and flow division, called the Zweifach–Fung effect.<sup>52,226–231</sup> The effect is basically that at branching points of capillary blood vessels, RBCs have a tendency to enter the capillary with a higher

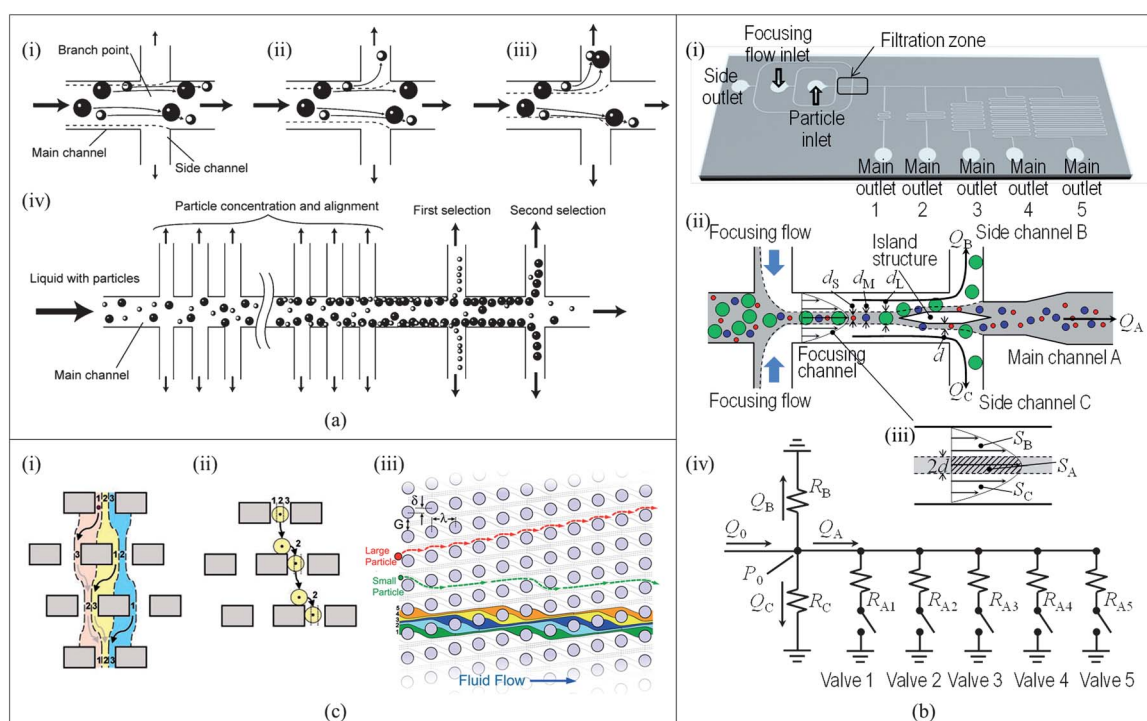


**Fig. 16** Selected examples of flow fraction network for hydrodynamic filtering. (a) Principle of hydrodynamic filtration: (i) the relatively low flow fraction, (ii) the medium flow fraction, and (iii) high flow fraction at a branch point. (iv) Schematic diagram showing particle concentration and separation in a hydrodynamic filtering network with multiple branch points and side channels (reprinted with permission from ref. 71, copyright 2005 Royal Society of Chemistry). (b) Principle of hydrodynamically focused particle filtration: (i) layout of the hydrodynamic filtering network; (ii) schematic of the streamlines containing different-sized particles in the focusing channel and the filtration zone; (iii) the virtual width of the stream entering the main channel A according to the flow fraction; and (iv) an equivalent electric circuit. By valving each main outlet, the boundary width can be tuned (from ref. 70, copyright 2009 Korean BioChip Society). (c) Principle of deterministic lateral displacement: (i) three streams (red, yellow, and blue) in a gap flow through a post-array. Lane 1 at the first post-row becomes lane 3 at the second row, lane 3 becomes lane 2 at the third row, and so on. Small particles following streamlines will thus stay in the same lane; (ii) particles larger than the width of lane 1 are displaced laterally at each row by the post; (iii) larger particles move along the asymmetric axis at an angle to the flow, while smaller particles move along streamline paths (from ref. 237, copyright 2008 National Academy of Sciences and ref. 238, copyright 2004 American Association for the Advancement of Science).

flow rate when the branching flow rate ratio is more than 2.5 and the cell-to-vessel diameter ratio is of the order of 1. Also, rapid medium exchange or chemical treatment of beads,<sup>232</sup> cells,<sup>233,234</sup> or droplets<sup>235</sup> was performed based on the particle-cross-over mechanism in carefully designed flow fraction-based hydrodynamic filtering networks. Furthermore, a network without suspended particles was applied to extract depleted boundary layers due to electrochemical reaction to side channels.<sup>236</sup>

Another flow fraction-based hydrodynamic filtration was introduced by the Oh group (Fig. 16b).<sup>70</sup> An island structure was placed in the middle of the filtration zone connected with three channels. This approach combined (i) 2D hydrodynamic focusing to align particles in the center of the channel and against the sidewalls of the island structure and (ii) hydrodynamic filtering to continuously separate particles according to the flow fraction. By valving each main outlet, the ratio of hydraulic resistances of the three channels was controlled, thereby tuning the width of the boundary layer. Unlike the design shown in Fig. 16a, this configuration made larger particles to first be extracted from the main channel. Therefore, the device is very efficient for filtering large particles from inhomogeneous mixtures. For instance, by connecting filtration stages in series, multiplexed microparticles can be filtered in series. The largest particles can be filtered at the first stage. Then the second largest particles can be filtered at the second stage, and so on. The alignment of the particles in the middle rather than near the sidewalls could have the following advantages: less particle adhesion to the sidewalls or clogging, faster separation due to the maximum velocity in the middle of the channel, and precise control of the boundary width to separate particles by size due to easy control of the volumetric flow rates in the middle of the channel.

A different approach worth mentioning is the concept of deterministic lateral displacement in an asymmetric array of hydrodynamic filtering microposts (not networks of microfluidic channels), as suggested by the Sturm group (Fig. 16c).<sup>237–240</sup> This approach is also based on the flow fraction of streamlines near the sidewalls in each post. Particles larger than a critical size are displaced laterally at each row by the post and move along the asymmetric axis at an angle to the flow, while smaller particles move along streamline paths. This method has been applied for particles, cells, or biomolecules (*e.g.*, DNA) separation with sub-micro-size resolution. A diluted concentration of the sample of interest (*e.g.*,  $<10^6$  cells  $\text{ml}^{-1}$ ) needs to be used to prevent clogging of the networks.<sup>241</sup>

Most pressure-driven flow fraction networks were used with particles suspended in the fluid stream. Careful design of channel routes will allow precise control of the flow fraction of the streamlines containing different-sized particles. These flow fraction networks can be integrated with hydrodynamic focusing,<sup>242</sup> spreading,<sup>243</sup> or filtering functions (this section) for continuous-flow particle alignment, concentration, extraction, filtration, patterning, or separation. For example, the use of the hydrodynamic filtering networks is a proven technique for the concentration, alignment, and enrichment procedures of (biological) particles.

#### 6.4 Dynamic flow change network: hydrodynamic trapping

The use of dynamic change of hydraulic resistance enables hydrodynamic trapping of particles in microfluidic networks.

When fluids flow with suspended particles, whose size is comparable to the channel dimension, hydraulic resistance of the channels is sensitive to the distribution and blockage of particles. Fig. 17a shows a typical example of hydrodynamic particle trapping.<sup>244</sup> In this design, the hydraulic resistance of path 1 was smaller than that of path 2. When a main channel (path 1) was blocked by a trapped bead, its resistance was substantially amplified. This hydrodynamic trapping made subsequent particles detour to a bypass channel (path 2). This device was used to transport and immobilize the beads, infuse reagents, observe the reaction, and retrieve selected beads for one-bead-one-compound-based combinatorial screening. A similar design was used to trap single cells and demonstrate cell division.<sup>245</sup>

A similar approach has also been reported to trap droplets.<sup>246–248</sup> Fig. 17b shows a typical design for such droplet trapping.<sup>248</sup> In this design, the hydraulic resistance of path 1 was larger than that of path 2, which was different from the principle of capturing the rigid beads. So the droplet 1 preferred to flow through the path 2, resulting in increase of its hydraulic resistance. Then the subsequent droplet 2 flowed through the path 1 and was tapped in a trap structure.

Paring of two different types of microbeads was demonstrated in a symmetric, meander-shaped, dynamic microfluidic network (Fig. 17c).<sup>249</sup> In contrast to the microfluidic network-based dynamic trapping, pocket-shaped array structures placed in the middle of channels were used to hydrodynamically trap single

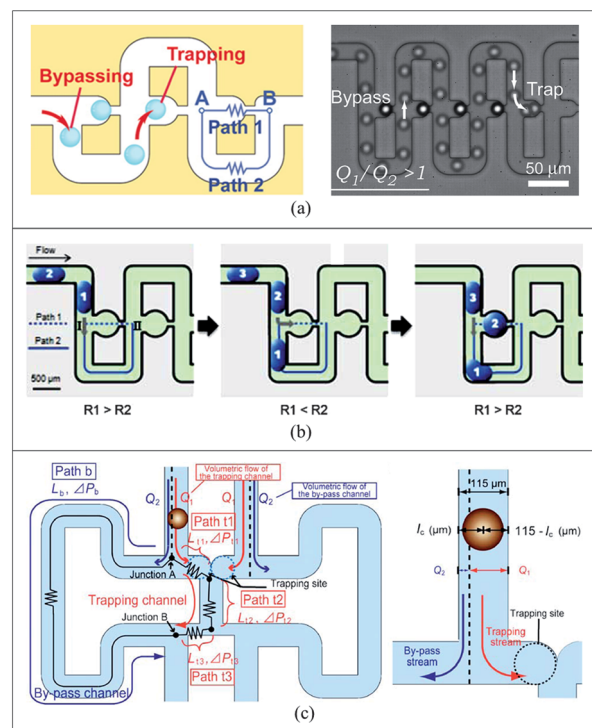


**Fig. 17** Selected examples of dynamic change of hydraulic resistance in flow-dependent microfluidic networks for hydrodynamic tapping. (a) Hydrodynamic bead trapping using trapping and by-pass channels (reprinted with permission from ref. 244, copyright 2007 National Academy of Sciences). (b) Hydrodynamic droplet trapping (from ref. 248, copyright 2008 Royal Society of Chemistry). (c) Hydrodynamic bead pairing using a symmetric, meander-shaped channel network (from ref. 249, copyright 2010 Royal Society of Chemistry).

cells<sup>250,251</sup> or droplets.<sup>252</sup> In addition, paring of cells<sup>253</sup> or droplets<sup>254</sup> was performed in array structures by manipulating flow directions (*e.g.*, forward and backward flows). Advantage of particle manipulation by the dynamic change of hydraulic resistance in flow-dependent microfluidic networks is in that the method is autonomous and passive without using any extra force.

## 7. Limitations and outlook

### 7.1 Summary

The use of the electric circuit analogy is a straightforward strategy to design pressure-driven microfluidic networks. The analogy describes the relationship between hydraulic properties (*e.g.*, flow rate, hydraulic resistance, pressure drop, and viscosity) and channel dimensions and geometry (*e.g.*, width, height, length, and shape of cross-section) in pressure-driven laminar flow. Thus, the behaviour of the pressure-driven laminar flow can be precisely engineered by defining only the channel dimensions and geometry, which is the major advantage of the analogy. Systematic divide-and/or-conquer of fluids through microfluidic networks has accelerated numerous concentration- and shear stress-dependent applications. A number of microfluidic network-based concentration gradient generators have been developed to investigate various chemical and biological questions. In addition, flow-dependent manipulation of fluids suspended with particles has been applied for distribution, filtering, focusing, sorting, spreading, and trapping of the particles (*e.g.*, bead, cell, and droplet).

### 7.2 Advanced aspects and outlook

In this section, we briefly overview selected advanced topics and the outlook in using the electric circuit analogy: limitations, viscosity, time-variant flow, dynamic flow change, dynamic hydraulic resistance change, modular assembly, non-channel-based network, capillary-driven flow, droplet-based microfluidics, electrokinetic flow, inertial microfluidics, non-traditional application, and miniaturization and commercialization.

**Limitations.** If taken too far, the electric circuit analogy can create misconceptions when analysing a microfluidic system. Recall that Ohm's law cannot explain the details of the microscopic transport of electrons in electrical systems. Rather, it describes an average effect (*e.g.*, current flow) that is consistent with the net flux of electrons in a conductor. In the similar manner, Hagen–Poiseuille's law, analogous to Ohm's law, describes the average volumetric flow in a microchannel. The application of electric circuit methods to microfluidics does not provide detailed information about the flow field itself (*e.g.*, the spatial distribution of the velocity field within a channel). Numerically based CFD simulations are recommended to investigate the details of such behaviour, especially in 2D and 3D systems. The flow fraction networks (see Section 6.3) are examples where the breakdown of the electric circuit analogy is interesting in that there are multiple types of fluids, but only one type of electron. Although we can approximate the boundary width between multiple types of fluids by the ratio of the

incoming or outgoing flow rates with the 1D model (see Section 4.3), we must consider the detailed information of the actual 3D flow field in order to precisely determine the fractioned boundary width.

**Viscosity.** To date microfluidic applications have been mostly limited to systems where the fluid viscosities are homogeneous across the channels and similar to that of water. The distribution of both the concentration and flow rate in the networks is strongly subject to the viscosity distribution, which affects the hydrodynamic resistance distribution (see eqn (11)). If two incoming fluids with different viscosities are supplied as the buffer and the sample solutions, the design of concentration-dependent microfluidic networks will not be simple as discussed in **Box 1**. The resulting profiles of both concentrations and flow rates will differ from the case with homogeneous fluids: deviated concentrations and unequal outlet flow rates.<sup>255</sup> Often, this fact enables us to measure viscosity of an unknown sample using microfluidic devices.<sup>256–260</sup>

**Time-variant flow.** In this review, we have largely focused on steady-state laminar flow in purely resistive networks. However, for time-variant (or frequency-dependent) flow, we need to analyse resonant microfluidic networks that can have resistive, capacitive, and inductive like components, analogous to RLC circuits. This requires the application of the concepts of hydraulic compliance and inertia. Time-variant analysis has proven useful in applications such as frequency-dependent chemical concentration generation,<sup>117,118</sup> flow-encoded switching,<sup>119</sup> and valving.<sup>261,262</sup>

**Dynamic flow change.** In some applications, we need to change flow dynamically and temporarily. The direct control of flow from external pumping sources<sup>50,98,260,263</sup> is an obvious approach, although it will be difficult to control complex networks due to increased number of interfaces to external flow sources (*e.g.*, syringe pumps). Since the introduction of pneumatic valves from the Quake group<sup>82,264</sup> indirect control of flow has been popular for pinching off individual channels.<sup>46</sup> This allows on/off switching, flow regulation, and even pumping in a large-scale integrated format. However, this also needs a large number of external macrovalves to control pneumatic pressures (*e.g.*, vacuum, pressure).

**Dynamic hydraulic resistance change.** Output performance of passive-type pressure-driven microfluidic networks strongly depends on the defined input conditions and device design. One of the desirable features in pressure-driven microfluidic networks (of course not necessary for certain applications) is on-demand programmable capability that allows active tuning of the hydraulic resistance of each channel to generate different but precisely predictable profiles of concentration or flow rate in the same network configuration. This may be realized by incorporating currently available actuation mechanisms (*e.g.*, electric, hydraulic, magnetic, manual, optical, piezo, pneumatic, thermal, ultrasonic, and other physical forces).<sup>265</sup> For example, the Folch group has demonstrated a microfluidic perfusion network with combinatorial choice of inputs, mixtures, gradient patterns, and flow rates by the pneumatic mechanism.<sup>182</sup>

**Modular assembly.** Complex microfluidic networks can be arbitrarily customized by assembling individual modules that function different unit operations (*e.g.*, mixer, combiner, distributor, multiplexer, variable resistive channel, pyramidal network, chamber, reactor, valve, pump).<sup>266–269</sup> Each module can be interconnected through a microfluidic motherboard or each other to form modular-based microfluidic networks. Leak-free and standardized interfacing is critical to such plug-and-play<sup>269</sup> or fit-to-flow<sup>267</sup> capability.

**Non-channel-based network.** Array structures embedded within channels may be difficult to analyse using the electric circuit analogy because it is not easy to form a simple equivalent electric circuit. CFD-based simulation will be an ideal approach to design such array-type networks. However, in general quasi-equivalent electric circuits can be constructed, if we can dissect array structures into small pieces of electric components that can be connected in parallel and/or series. Although this will not provide exact analytical solutions, it will be useful to understand behaviour of the pressure-driven flow in array-based networks.

**Capillary-driven flow.** Capillarity in channels has been harnessed to drive liquid (*e.g.*, capillary-driven pumping) as well as control flow (*e.g.*, capillary-based passive valving). Liquid filling in channels is a complex process that depends on channel geometry, flow rate, pressure, liquid surface tension, and contact angle of channel surface. For example, valving or switching using the passive capillary effect can be done by abrupt changes in the wettability of channels or in the cross-sectional area of channels. A hydrophobic patch in a hydrophilic channel or a step-wise cross-section change in a hydrophobic channel will cause a liquid–air meniscus to stop at the patch or valve. If a certain pressure that can overcome the capillary pressure drop across the liquid–air interface at the patch or valve is applied at the inlet, the liquid column will move again across the passive valving structure.<sup>91</sup> A simple analytical approach to model such liquid filling in capillary-driven microfluidic networks was suggested by using the similar electric circuit analogy.<sup>270</sup>

**Electrokinetic flow.** Microfluidic flow can be driven by either an applied electric field or a combined electric field and pressure gradient.<sup>271</sup> At steady state, the electrokinetic or electroosmotic flow (EOF) is described by the Navier–Stokes equation (eqn (1)) with an addition of an electrical body force. The EOF is known to generate a flat velocity profile, unlike the parabolic profile for the pressure-driven flow. Numerous methods of using the similar electric circuit analogy have been reported to analyse the EOF-based microfluidic networks.<sup>272–278</sup> They can be analysed in equivalent electric circuits in a superposed form of the electrical and hydraulic effects.

**Droplet-based microfluidics.** The use of two-phase (pressure-driven and droplet-based) flow has been recently widespread. The inhomogeneous and time-dependent nature of two-phase flow gives rise to interesting behaviours of trains of droplets in droplet-based microfluidic networks. In general, droplets packed in channels (*e.g.*, flattened or plug-shaped droplets) significantly increase the hydraulic resistance of the channel, which enables fluid mediated interaction between droplets moving at different

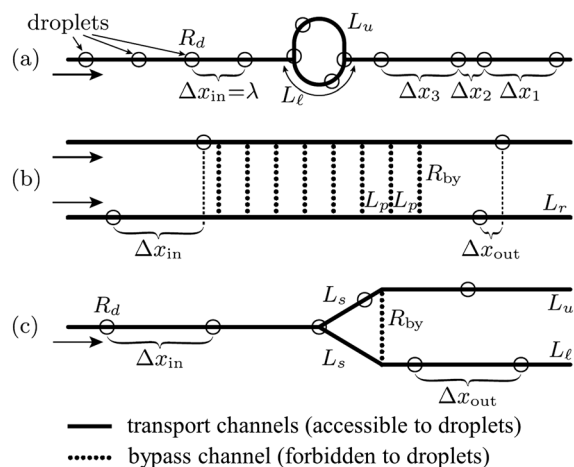


**Fig. 18** Schematic representations of three droplet-based microfluidic networks: (a) a loop; (b) a ladder; and (c) a bypassed T junction (reprinted with permission from ref. 287, copyright 2008 American Physical Society).

points in a network. Coding and decoding through a loop (Fig. 18a),<sup>279–282</sup> synchronization through a ladder (Fig. 18b),<sup>283,284</sup> and passive regulation of droplet traffic at a junction (Fig. 18c)<sup>285</sup> have been demonstrated. Understanding of such droplet traffic in microfluidic networks has also been practical by the use of the electric circuit analogy.<sup>286–288</sup>

**Inertial microfluidics.** Despite the common negligence of inertial effects in most pressure-driven laminar flow, recent studies have shown a variety of useful applications that depend on fluid inertia, such as secondary flows (*e.g.*, Dean flows) in curved channels<sup>289,290</sup> and inertial migration of particles.<sup>36</sup> The inertial effects are often dominant at relatively high flow rates. Thus, inertial microfluidics has gained increasing interest in the LOC and microfluidics community for potential use in high-throughput flow cytometry and separation applications.<sup>34</sup>

**Non-traditional application.** While pressure-driven microfluidic networks are most commonly used for conventional high-throughput or hand-held applications (*e.g.*, biological, chemical, and pharmaceutical), they are also useful for many other non-traditional applications. These include energy harvesting (*e.g.*, fuel cell,<sup>291,292</sup> streaming energy<sup>293</sup>), material synthesis (*e.g.*, particle, fiber),<sup>294</sup> microfluidic actuation (*e.g.*, hydraulic, pneumatic),<sup>295</sup> microfluidic cooling,<sup>296</sup> microfluidic display,<sup>297</sup> microfluidic logics,<sup>283,298</sup> microfluidic metamaterials,<sup>299,300</sup> microfluidic sensing (*e.g.*, temperature, viscosity, pressure),<sup>260</sup> optofluidics,<sup>301–303</sup> and even microfluidic mazes.<sup>37</sup> Indeed, pressure-driven microfluidic networks facilitate a wide range of applications covering both the conventional and non-traditional areas.

**Miniaturization and commercialization.** Another practical issue encountered in applications of microfluidic networks involves the miniaturization of external pressure or flow sources. For high-throughput applications, this may not be a big concern because microfluidic systems will be used in a laboratory setting equipped with syringe pumps, microscopes, and computer-based controllers. We anticipate that more high-throughput applications will

be appreciated in the pressure-driven continuous-flow microfluidic networks (*e.g.*, traditional single-phase, droplet-based, and inertial microfluidics). However, for hand-held applications, this has been troublesome for many years. A variety of smart platforms, *e.g.*, acoustic-driven,<sup>304</sup> Braille-based,<sup>305</sup> capillary-driven,<sup>306</sup> centrifugal-driven,<sup>307</sup> electrokinetic-driven,<sup>308</sup> electrowetting-driven,<sup>309,310</sup> evaporation-driven,<sup>311</sup> optoelectric-driven,<sup>312</sup> paper-based,<sup>313</sup> pressurized-gas-driven,<sup>314</sup> thermocapillary-driven,<sup>315</sup> and vacuum-assisted platforms,<sup>114,316,317</sup> and even fully integrated platforms with pumps and valves,<sup>265</sup> have been suggested to replace the bulky external sources for hand-held applications.<sup>318,319</sup> Despite this progress, there is still substantial opportunity to advance pressure-driven microfluidic networks, develop new platform technologies, and improve cost-effectiveness for commercialization.

Applications of microfluidic networks are proliferating and the whole field is advancing rapidly towards more comprehensive systems having more functionality and a higher degree of integration either in single-platform or hybrid-platform formats. The use of the electric circuit analogy will be especially useful in the advancement of microfluidic network applications. It provides intuitive understanding of such systems and enables the practical design of small-scale and complex large-scale microfluidic networks. We expect that the LOC and microfluidics community will gain insightful ideas and practical design strategies to develop unique microfluidic networks to advance many biological, chemical, pharmaceutical, and other scientific and technical challenges.

## Acknowledgements

This work was supported by grants to K. W. Oh from NSF (ECCS-1002255 and ECCS-0736501) and the Intelligent Microsystems Center at Korea Institute of Science and Technology (KIST).

## Notes and references

- 1 J. West, M. Becker, S. Tombrink and A. Manz, Micro total analysis systems: latest achievements, *Anal. Chem.*, 2008, **80**, 4403–4419.
- 2 P. A. Auroux, D. Iossifidis, D. R. Reyes and A. Manz, Micro total analysis systems. 2. Analytical standard operations and applications, *Anal. Chem.*, 2002, **74**, 2637–2652.
- 3 D. R. Reyes, D. Iossifidis, P. A. Auroux and A. Manz, Micro total analysis systems. 1. Introduction, theory, and technology, *Anal. Chem.*, 2002, **74**, 2623–2636.
- 4 T. Vilkner, D. Janasek and A. Manz, Micro total analysis systems. Recent developments, *Anal. Chem.*, 2004, **76**, 3373–3385.
- 5 P. S. Dittrich, K. Tachikawa and A. Manz, Micro total analysis systems. Latest advancements and trends, *Anal. Chem.*, 2006, **78**, 3887–3907.
- 6 A. Arora, G. Simone, G. B. Salieb-Beugelaar, J. T. Kim and A. Manz, Latest developments in micro total analysis systems, *Anal. Chem.*, 2010, **82**, 4830–4847.
- 7 A. Manz, N. Gruber and H. M. Widmer, Miniaturized total chemical-analysis systems—a novel concept for chemical sensing, *Sens. Actuators, B*, 1990, **1**, 244–248.
- 8 G. B. Salieb-Beugelaar, G. Simone, A. Arora, A. Philippi and A. Manz, Latest developments in microfluidic cell biology and analysis systems, *Anal. Chem.*, 2010, **82**, 4848–4864.
- 9 G. M. Whitesides, The origins and the future of microfluidics, *Nature*, 2006, **442**, 368–373.
- 10 D. Rothbart, *Explaining the Growth of Scientific Knowledge: Metaphors, Models, and Meanings*, E. Mellen Press, Lewiston, NY, 1997.
- 11 J. Turner, Maxwell on the method of physical analogy, *Br. J. Philos. Sci.*, 1955, **6**, 226–238.
- 12 P. A. Fishwick and P. A. Luker, *Qualitative Simulation Modeling and Analysis*, Springer-Verlag, 1991.
- 13 B. R. Munson and T. H. Okiishi, *Fundamentals of Fluid Mechanics*, J. Wiley & Sons, Hoboken, NJ, 6th edn, 2009.
- 14 W. H. Hayt, J. E. Kemmerly and S. M. Durbin, *Engineering Circuit Analysis*, McGraw-Hill, New York, 8th edn, 2012.
- 15 A. J. Henry, *Recent Practice in the Erection of Lightning Conductors*, Weather bureau, 1906.
- 16 O. Lodge, Lightning conductors from a modern point of view, *Electr. Eng.*, 1890, **10**, 21–22.
- 17 C. C. Haskins, *Electricity Made Simple and Treated Non-Technically*, C. Macdonald, 1900.
- 18 E. Club and W. Club, *The Electric Journal*, The Club, 1911.
- 19 A. Esposito, A simplified method for analyzing hydraulic circuits by analogy, *Mach. Des.*, 1969, **41**, 173–177.
- 20 T. Croft, *Practical Electricity*, McGraw-Hill book company, inc, 1917.
- 21 E. Meng, *Biomedical Microsystems*, Taylor and Francis, 2010.
- 22 B. Kirby, *Micro- and Nanoscale Fluid Mechanics: Transport in Microfluidic Devices*, Cambridge University Press, New York, 2010.
- 23 M. Gad-el-Hak, *The MEMS Handbook*, CRC Press, 2002.
- 24 M. Gad-el-Hak, *MEMS: Introduction and Fundamentals*, Taylor and Francis, 2005.
- 25 J. Berthier and P. Silberzan, *Microfluidics for Biotechnology*, Artech House, 2009.
- 26 W. B. J. Zimmerman and International Centre for Mechanical Sciences, *Microfluidics: History, Theory and Applications*, Springer, Wien, New York, 2006.
- 27 K. Lee, C. Kim, B. Ahn, R. Panchapakesan, A. R. Full, L. Nordee, J. Y. Kang and K. W. Oh, Generalized serial dilution module for monotonic and arbitrary microfluidic gradient generators, *Lab Chip*, 2009, **9**, 709–717.
- 28 D. J. Beebe, G. A. Mensing and G. M. Walker, Physics and applications of microfluidics in biology, *Annu. Rev. Biomed. Eng.*, 2002, **4**, 261–286.
- 29 H. A. Stone, A. D. Stroock and A. Ajdari, Engineering flows in small devices: microfluidics toward a lab-on-a-chip, *Annu. Rev. Fluid Mech.*, 2004, **36**, 381–411.
- 30 T. M. Squires and S. R. Quake, Microfluidics: fluid physics at the nanoliter scale, *Rev. Mod. Phys.*, 2005, **77**, 977–1026.
- 31 G. M. Whitesides and A. D. Stroock, Flexible methods for microfluidics, *Phys. Today*, 2001, **54**, 42–48.
- 32 G. L. Lettieri, A. Dodge, G. Boer, N. F. de Rooij and E. Verpoorte, A novel microfluidic concept for bioanalysis using freely moving beads trapped in recirculating flows, *Lab Chip*, 2003, **3**, 34–39.
- 33 J. M. Koo and C. Kleinstreuer, Liquid flow in microchannels: experimental observations and computational analyses of microfluidics effects, *J. Micromech. Microeng.*, 2003, **13**, 568–579.
- 34 D. Di Carlo, Inertial microfluidics, *Lab Chip*, 2009, **9**, 3038–3046.
- 35 D. Huh, J. H. Bahng, Y. B. Ling, H. H. Wei, O. D. Kripfgans, J. B. Fowlkes, J. B. Grotberg and S. Takayama, Gravity-driven microfluidic particle sorting device with hydrodynamic separation amplification, *Anal. Chem.*, 2007, **79**, 1369–1376.
- 36 D. Di Carlo, D. Irimia, R. G. Tompkins and M. Toner, Continuous inertial focusing, ordering, and separation of particles in microchannels, *Proc. Natl. Acad. Sci. U. S. A.*, 2007, **104**, 18892–18897.
- 37 M. J. Fuerstman, P. Deschatelets, R. Kane, A. Schwartz, P. J. A. Kenis, J. M. Deutch and G. M. Whitesides, Solving mazes using microfluidic networks, *Langmuir*, 2003, **19**, 4714–4722.
- 38 D. E. Angelescu, *Highly Integrated Microfluidics Design*, Artech House, 2011.
- 39 R. J. Cornish, Flow in a pipe of rectangular cross-section, *Proc. R. Soc. London, Ser. A*, 1928, **120**, 691–700.
- 40 G. T. A. Kovacs, *Micromachined Transducers Sourcebook*, WCB/McGraw-Hill, Boston, 1998.
- 41 N. A. Mortensen, F. Okkels and H. Bruus, Reexamination of Hagen–Poiseuille flow: shape dependence of the hydraulic resistance in microchannels, *Phys. Rev. E: Stat., Nonlinear, Soft Matter Phys.*, 2005, **71**, 057301.
- 42 J. B. Bao and D. J. Harrison, Measurement of flow in microfluidic networks with micrometer-sized flow restrictors, *AIChE J.*, 2006, **52**, 75–85.

- 43 R. M. Benrey, Fludics: how they've taught a stream of air to think, *Pop. Sci.*, 1967, **190**, 118–121, 196–197.
- 44 D. J. Laser and J. G. Santiago, A review of micropumps, *J. Micromech. Microeng.*, 2004, **14**, R35–R64.
- 45 X. Zhu, L. Y. Chu, B. H. Chueh, M. Shen, B. Hazarika, N. Phadke and S. Takayama, Arrays of horizontally-oriented mini-reservoirs generate steady microfluidic flows for continuous perfusion cell culture and gradient generation, *Analyst*, 2004, **129**, 1026–1031.
- 46 K. W. Oh, R. Rong and C. H. Ahn, Miniaturization of pinch-type valves and pumps for practical micro total analysis system integration, *J. Micromech. Microeng.*, 2005, **15**, 2449–2455.
- 47 T. Kim and Y. H. Cho, A pumpless cell culture chip with the constant medium perfusion-rate maintained by balanced droplet dispensing, *Lab Chip*, 2011, **11**, 1825–1830.
- 48 N. S. Lynn and D. S. Dandy, Passive microfluidic pumping using coupled capillary/evaporation effects, *Lab Chip*, 2009, **9**, 3422–3429.
- 49 C. Futterer, N. Minc, V. Bormuth, J. H. Codarbox, P. Laval, J. Rossier and J. L. Viovy, Injection and flow control system for microchannels, *Lab Chip*, 2004, **4**, 351–356.
- 50 T. Braschler, L. Metref, R. Zvitov-Marabi, H. van Lintel, N. Demierre, J. Theytaz and P. Renaud, A simple pneumatic setup for driving microfluidics, *Lab Chip*, 2007, **7**, 420–422.
- 51 S. Sugiura, J. Edahiro, K. Kikuchi, K. Sumaru and T. Kanamori, Pressure-driven perfusion culture microchamber array for a parallel drug cytotoxicity assay, *Biotechnol. Bioeng.*, 2008, **100**, 1156–1165.
- 52 S. Yang, A. Undar and J. D. Zahn, A microfluidic device for continuous, real time blood plasma separation, *Lab Chip*, 2006, **6**, 871–880.
- 53 M. Kim, S. M. Jung, K. H. Lee, Y. J. Kang and S. Yang, A microfluidic device for continuous white blood cell separation and lysis from whole blood, *Artif. Organs*, 2010, **34**, 996–1002.
- 54 C. van Berkel, J. D. Gwyer, S. Deane, N. Green, J. Holloway, V. Hollis and H. Morgan, Integrated systems for rapid point of care (PoC) blood cell analysis, *Lab Chip*, 2011, **11**, 1249–1255.
- 55 K. Lee, C. Kim, G. Jung, T. S. Kim, J. Y. Kang and K. W. Oh, Microfluidic network-based combinatorial dilution device for high throughput screening and optimization, *Microfluid. Nanofluid.*, 2010, **8**, 677–685.
- 56 K. Lee, C. Kim, Y. Kim, K. Jung, B. Ahn, J. Y. Kang and K. W. Oh, 2-layer based microfluidic concentration generator by hybrid serial and volumetric dilutions, *Biomed. Microdevices*, 2010, **12**, 297–309.
- 57 K. Lee, C. Kim, Y. Kim, B. Ahn, J. Bang, J. Kim, R. Panchapakesan, Y. K. Yoon, J. Y. Kang and K. W. Oh, Microfluidic concentration-on-demand combinatorial dilutions, *Microfluid. Nanofluid.*, 2011, **11**, 75–86.
- 58 C. Kim, K. Lee, J. H. Kim, K. S. Shin, K. J. Lee, T. S. Kim and J. Y. Kang, A serial dilution microfluidic device using a ladder network generating logarithmic or linear concentrations, *Lab Chip*, 2008, **8**, 473–479.
- 59 D. Kim, N. C. Chesler and D. J. Beebe, A method for dynamic system characterization using hydraulic series resistance, *Lab Chip*, 2006, **6**, 639–644.
- 60 K. E. Herold and A. Rasooly, *Lab on a Chip Technology*, Caister Academic Press, Norfolk, UK, 2009.
- 61 W. P. Bula, W. Verboom, D. N. Reinoudt and H. J. Gardeniers, Multichannel quench-flow microreactor chip for parallel reaction monitoring, *Lab Chip*, 2007, **7**, 1717–1722.
- 62 K. Campbell and A. Groisman, Generation of complex concentration profiles in microchannels in a logarithmically small number of steps, *Lab Chip*, 2007, **7**, 264–272.
- 63 D. Titmarsh and J. Cooper-White, Microbioreactor array for full-factorial analysis of provision of multiple soluble factors in cellular microenvironments, *Biotechnol. Bioeng.*, 2009, **104**, 1240–1244.
- 64 P. J. Hung, P. J. Lee, P. Sabourchi, N. Aghdam, R. Lin and L. P. Lee, A novel high aspect ratio microfluidic design to provide a stable and uniform microenvironment for cell growth in a high throughput mammalian cell culture array, *Lab Chip*, 2005, **5**, 44–48.
- 65 N. T. Nguyen and Z. G. Wu, Micromixers—a review, *J. Micromech. Microeng.*, 2005, **15**, R1–R16.
- 66 K. Hattori, S. Sugiura and T. Kanamori, Generation of arbitrary monotonic concentration profiles by a serial dilution microfluidic network composed of microchannels with a high fluidic-resistance ratio, *Lab Chip*, 2009, **9**, 1763–1772.
- 67 C. H. Yeh, C. H. Chen and Y. C. Lin, Use of a gradient-generating microfluidic device to rapidly determine a suitable glucose concentration for cell viability test, *Microfluid. Nanofluid.*, 2011, **10**, 1011–1018.
- 68 N. Damean, L. F. Olgun, F. Hollfelder, C. Abell and W. T. Huck, Simultaneous measurement of reactions in microdroplets filled by concentration gradients, *Lab Chip*, 2009, **9**, 1707–1713.
- 69 J. Atencia and D. J. Beebe, Controlled microfluidic interfaces, *Nature*, 2005, **437**, 648–655.
- 70 K. Lee, C. Kim, B. Ahn, J. Y. Kang and K. W. Oh, Hydrodynamically focused particle filtration using an island structure, *BioChip J.*, 2009, **3**, 275–280.
- 71 M. Yamada and M. Seki, Hydrodynamic filtration for on-chip particle concentration and classification utilizing microfluidics, *Lab Chip*, 2005, **5**, 1233–1239.
- 72 T. Stiles, R. Fallon, T. Vestad, J. Oakey, D. W. M. Marr, J. Squier and R. Jimenez, Hydrodynamic focusing for vacuum-pumped microfluidics, *Microfluid. Nanofluid.*, 2005, **1**, 280–283.
- 73 M. Liu, Y. Chen, Q. Q. Guo, R. Y. Li, X. L. Sun and J. Yang, Controllable positioning and alignment of silver nanowires by tunable hydrodynamic focusing, *Nanotechnology*, 2011, **22**, 125302.
- 74 J. Takagi, M. Yamada, M. Yasuda and M. Seki, Continuous particle separation in a microchannel having asymmetrically arranged multiple branches, *Lab Chip*, 2005, **5**, 778–784.
- 75 G. B. Lee, C. C. Chang, S. B. Huang and R. J. Yang, The hydrodynamic focusing effect inside rectangular microchannels, *J. Micromech. Microeng.*, 2006, **16**, 1024–1032.
- 76 K. B. Andersen, S. Levinsen, W. E. Svendsen and F. Okkels, A generalized theoretical model for “continuous particle separation in a microchannel having asymmetrically arranged multiple branches”, *Lab Chip*, 2009, **9**, 1638–1639.
- 77 E. W. Young and C. A. Simmons, Macro- and microscale fluid flow systems for endothelial cell biology, *Lab Chip*, 2010, **10**, 143–160.
- 78 R. K. Shah and A. L. London, *Laminar Flow Forced Convection in Ducts: a Source Book for Compact Heat Exchanger Analytical Data*, Academic Press, 1978.
- 79 E. Gutierrez, B. G. Petrich, S. J. Shattil, M. H. Ginsberg, A. Groisman and A. Kasirer-Friede, Microfluidic devices for studies of shear-dependent platelet adhesion, *Lab Chip*, 2008, **8**, 1486–1495.
- 80 G. M. Walker, J. Q. Sai, A. Richmond, M. Stremler, C. Y. Chung and J. P. Wikswo, Effects of flow and diffusion on chemotaxis studies in a microfabricated gradient generator, *Lab Chip*, 2005, **5**, 611–618.
- 81 M. Abdalgawad, M. W. L. Watson, E. W. K. Young, J. M. Mudrik, M. D. Ungrin and A. R. Wheeler, Soft lithography: masters on demand, *Lab Chip*, 2008, **8**, 1379–1385.
- 82 M. A. Unger, H. P. Chou, T. Thorsen, A. Scherer and S. R. Quake, Monolithic microfabricated valves and pumps by multilayer soft lithography, *Science*, 2000, **288**, 113–116.
- 83 D. C. Duffy, J. C. McDonald, O. J. A. Schueller and G. M. Whitesides, Rapid prototyping of microfluidic systems in poly(dimethylsiloxane), *Anal. Chem.*, 1998, **70**, 4974–4984.
- 84 J. Friend and L. Yeo, Fabrication of microfluidic devices using polydimethylsiloxane, *Biomicrofluidics*, 2010, **4**, 026502.
- 85 D. A. Bartholomeusz, R. W. Boutte and J. D. Andrade, Xurography: rapid prototyping of microstructures using a cutting plotter, *J. Microelectromech. Syst.*, 2005, **14**, 1364–1374.
- 86 M. Focke, D. Kosse, C. Muller, H. Reinecke, R. Zengerle and F. von Stetten, Lab-on-a-foil: microfluidics on thin and flexible films, *Lab Chip*, 2010, **10**, 1365–1386.
- 87 J. Do, J. Y. Zhang and C. M. Klapperich, Maskless writing of microfluidics: rapid prototyping of 3D microfluidics using scratch on a polymer substrate, *Robotics and Computer-Integrated Manufacturing*, 2011, **27**, 245–248.
- 88 S. H. Chao, R. Carlson and D. R. Meldrum, Rapid fabrication of microchannels using microscale plasma activated templating (mu PLAT) generated water molds, *Lab Chip*, 2007, **7**, 641–643.
- 89 H. Becker and L. E. Locascio, Polymer microfluidic devices, *Talanta*, 2002, **56**, 267–287.
- 90 H. Becker and C. Gartner, Polymer microfabrication methods for microfluidic analytical applications, *Electrophoresis*, 2000, **21**, 12–26.
- 91 C. H. Ahn, J. W. Choi, G. Beauchage, J. H. Nevin, J. B. Lee, A. Puntambekar and J. Y. Lee, Disposable Smart lab on a chip for point-of-care clinical diagnostics, *Proc. IEEE*, 2004, **92**, 154–173.

- Published on 16 December 2011. Downloaded by University of California - Riverside on 14/09/2015 19:19:59.
- 92 K. W. Oh, C. S. Park, K. Namkoong, J. Kim, K. S. Ock, S. Kim, Y. A. Kim, Y. K. Cho and C. Ko, World-to-chip microfluidic interface with built-in valves for multichamber chip-based PCR assays, *Lab Chip*, 2005, **5**, 845–850.
  - 93 C. H. Lin, G. B. Lee, Y. H. Lin and G. L. Chang, A fast prototyping process for fabrication of microfluidic systems on soda-lime glass, *J. Micromech. Microeng.*, 2001, **11**, 726–732.
  - 94 S. Sugiura, K. Hattori and T. Kanamori, Microfluidic serial dilution cell-based assay for analyzing drug dose response over a wide concentration range, *Anal. Chem.*, 2010, **82**, 8278–8282.
  - 95 T. Gervais, J. El-Ali, A. Gunther and K. F. Jensen, Flow-induced deformation of shallow microfluidic channels, *Lab Chip*, 2006, **6**, 500–507.
  - 96 D. W. Inglis, A method for reducing pressure-induced deformation in silicone microfluidics, *Biomicrofluidics*, 2010, **4**, 026504.
  - 97 L. F. Hong and T. R. Pan, Three-dimensional surface microfluidics enabled by spatiotemporal control of elastic fluidic interface, *Lab Chip*, 2010, **10**, 3271–3276.
  - 98 Y. Kim, B. Kuczenski, P. R. LeDuc and W. C. Messner, Modulation of fluidic resistance and capacitance for long-term, high-speed feedback control of a microfluidic interface, *Lab Chip*, 2009, **9**, 2603–2609.
  - 99 D. Armani, C. Liu and N. Aluru, Re-configurable fluid circuits by PDMS elastomer micromachining, *Proc. IEEE Micr. Elect.*, 1999, 222–227.
  - 100 H. Schmid and B. Michel, Siloxane polymers for high-resolution, high-accuracy soft lithography, *Macromolecules*, 2000, **33**, 3042–3049.
  - 101 A. Plecis and Y. Chen, Fabrication of microfluidic devices based on glass–PDMS–glass technology, *Microelectron. Eng.*, 2007, **84**, 1265–1269.
  - 102 J. M. K. Ng, I. Gitlin, A. D. Stroock and G. M. Whitesides, Components for integrated poly(dimethylsiloxane) microfluidic systems, *Electrophoresis*, 2002, **23**, 3461–3473.
  - 103 C. K. Fredrickson and Z. H. Fan, Macro-to-micro interfaces for microfluidic devices, *Lab Chip*, 2004, **4**, 526–533.
  - 104 P. Li, Y. T'ian and D. Pappas, Comparison of inlet geometry in microfluidic cell affinity chromatography, *Anal. Chem.*, 2011, **83**, 774–781.
  - 105 B. K. Lee and T. H. Kwon, A novel monolithic fabrication method for a plastic microfluidic chip with liquid interconnecting ports, *J. Micromech. Microeng.*, 2010, **20**, 105004.
  - 106 H. Kortmann, L. M. Blank and A. Schmid, A rapid, reliable, and automatable lab-on-a-chip interfaced, *Lab Chip*, 2009, **9**, 1455–1460.
  - 107 G. A. Cooksey, A. L. Plant and J. Atencia, A vacuum manifold for rapid world-to-chip connectivity of complex PDMS microdevices, *Lab Chip*, 2009, **9**, 1298–1300.
  - 108 C. F. Chen, J. Liu, L. P. Hromada, C. W. Tsao, C. C. Chang and D. L. DeVoe, High-pressure needle interface for thermoplastic microfluidics, *Lab Chip*, 2009, **9**, 50–55.
  - 109 E. R. Murphy, T. Inoue, H. R. Sahoo, N. Zaborenko and K. F. Jensen, Solder-based chip-to-tube and chip-to-chip packaging for microfluidic devices, *Lab Chip*, 2007, **7**, 1309–1314.
  - 110 K. H. Han and A. B. Frazier, Reliability aspects of packaging and integration technology for microfluidic systems, *IEEE Trans. Device Mater. Reliab.*, 2005, **5**, 452–457.
  - 111 <http://www.rsc.org/loc/chips&tips>.
  - 112 W. L. Ong, K. C. Tang, A. Agarwal, R. Nagarajan, L. W. Luo and L. Yobas, Microfluidic integration of substantially round glass capillaries for lateral patch clamping on chip, *Lab Chip*, 2007, **7**, 1357–1366.
  - 113 J. H. Kang, Y. C. Kim and J. K. Park, Analysis of pressure-driven air bubble elimination in a microfluidic device, *Lab Chip*, 2008, **8**, 176–178.
  - 114 K. Hosokawa, K. Sato, N. Ichikawa and M. Maeda, Power-free poly (dimethylsiloxane) microfluidic devices for gold nanoparticle-based DNA analysis, *Lab Chip*, 2004, **4**, 181–185.
  - 115 J. Monahan, A. A. Gewirth and R. G. Nuzzo, A method for filling complex polymeric microfluidic devices and arrays, *Anal. Chem.*, 2001, **73**, 3193–3197.
  - 116 P. Vulto, S. Podszun, P. Meyer, C. Hermann, A. Manz and G. A. Urban, Phageguides: a paradigm shift in microfluidic priming and emptying, *Lab Chip*, 2011, **11**, 1596–1602.
  - 117 L. Chen, F. Azizi and C. H. Mastrangelo, Generation of dynamic chemical signals with microfluidic C-DACs, *Lab Chip*, 2007, **7**, 850–855.
  - 118 Y. Xie, Y. Wang, L. Chen and C. H. Mastrangelo, Fourier microfluidics, *Lab Chip*, 2008, **8**, 779–785.
  - 119 K. R. King, S. Wang, A. Jayaraman, M. L. Yarmush and M. Toner, Microfluidic flow-encoded switching for parallel control of dynamic cellular microenvironments, *Lab Chip*, 2008, **8**, 107–116.
  - 120 K. K. Coti, Y. Wang, W. Y. Lin, C. C. Chen, Z. T. F. Yu, K. Liu, C. K. F. Shen, M. Selke, A. Yeh, W. X. Lu and H. R. Tseng, A dynamic micromixer for arbitrary control of disguised chemical selectivity, *Chem. Commun.*, 2008, 3426–3428.
  - 121 N. L. Jeon, S. K. W. Dertinger, D. T. Chiu, I. S. Choi, A. D. Stroock and G. M. Whitesides, Generation of solution and surface gradients using microfluidic systems, *Langmuir*, 2000, **16**, 8311–8316.
  - 122 E. Yakhshi-Tafti, H. J. Cho and R. Kumar, Diffusive mixing through velocity profile variation in microchannels, *Exp. Fluids*, 2011, **50**, 535–545.
  - 123 W. F. Fang, M. H. Hsu, Y. T. Chen and J. T. Yang, Characterization of microfluidic mixing and reaction in microchannels via analysis of cross-sectional patterns, *Biomicrofluidics*, 2011, **5**, 014111.
  - 124 C. Yu, S. Mutlu, P. Selvaganapathy, C. H. Mastrangelo, F. Svec and J. M. J. Frechett, Flow control valves for analytical microfluidic chips without mechanical parts based on thermally responsive monolithic polymers, *Anal. Chem.*, 2003, **75**, 1958–1961.
  - 125 M. Yamada, T. Hirano, M. Yasuda and M. Seki, A microfluidic flow distributor generating stepwise concentrations for high-throughput biochemical processing, *Lab Chip*, 2006, **6**, 179–184.
  - 126 J. K. Chang, H. Bang, S. J. Park, S. Chung, C. Chung and D. C. Han, Fabrication of the PDMS microchip for serially diluting sample with buffer, *Microsyst. Technol.*, 2003, **9**, 555–558.
  - 127 H. Bang, S. H. Lim, Y. K. Lee, S. Chung, C. Chung, D. C. Han and J. K. Chang, Serial dilution microchip for cytotoxicity test, *J. Micromech. Microeng.*, 2004, **14**, 1165–1170.
  - 128 C. W. Li, R. S. Chen and M. S. Yang, Generation of linear and non-linear concentration gradients along microfluidic channel by microtunnel controlled stepwise addition of sample solution, *Lab Chip*, 2007, **7**, 1371–1373.
  - 129 G. M. Walker, N. Monteiro-Riviere, J. Rouse and A. T. O'Neill, A linear dilution microfluidic device for cytotoxicity assays, *Lab Chip*, 2007, **7**, 226–232.
  - 130 S. K. W. Dertinger, D. T. Chiu, N. L. Jeon and G. M. Whitesides, Generation of gradients having complex shapes using microfluidic networks, *Anal. Chem.*, 2001, **73**, 1240–1246.
  - 131 X. Y. Jiang, Q. B. Xu, S. K. W. Dertinger, A. D. Stroock, T. M. Fu and G. M. Whitesides, A general method for patterning gradients of biomolecules on surfaces using microfluidic networks, *Anal. Chem.*, 2005, **77**, 2338–2347.
  - 132 S. Kim, H. J. Kim and N. L. Jeon, Biological applications of microfluidic gradient devices, *Integr. Biol.*, 2010, **2**, 584–603.
  - 133 F. Lin, W. Saadi, S. W. Rhee, S. J. Wang, S. Mittal and N. L. Jeon, Generation of dynamic temporal and spatial concentration gradients using microfluidic devices, *Lab Chip*, 2004, **4**, 164–167.
  - 134 J. Sager, M. Young and D. Stefanovic, Characterization of transverse channel concentration profiles obtainable with a class of microfluidic networks, *Langmuir*, 2006, **22**, 4452–4455.
  - 135 Y. Wang, T. Mukherjee and Q. Lin, Systematic modeling of microfluidic concentration gradient generators, *J. Micromech. Microeng.*, 2006, **16**, 2128–2137.
  - 136 B. R. Gorman and J. P. Wikswo, Characterization of transport in microfluidic gradient generators, *Microfluid. Nanofluid.*, 2008, **4**, 273–285.
  - 137 Y. Wang, A. S. Bedekar, S. Krishnamoorthy, S. S. Siddhaye and S. Sundaram, System-level modeling and simulation of biochemical assays in lab-on-a-chip devices, *Microfluid. Nanofluid.*, 2007, **3**, 307–322.
  - 138 H. A. Yusuf, S. J. Baldock, R. W. Barber, P. R. Fielden, N. J. Goddard, S. Mohr and B. J. T. Brown, Optimisation and analysis of microreactor designs for microfluidic gradient generation using a purpose built optical detection system for entire chip imaging, *Lab Chip*, 2009, **9**, 1882–1889.
  - 139 P. Herzmark, K. Campbell, F. Wang, K. Wong, H. El-Samad, A. Groisman and H. R. Bourne, Bound attractant at the leading vs. the trailing edge determines chemotactic prowess, *Proc. Natl. Acad. Sci. U. S. A.*, 2007, **104**, 13349–13354.
  - 140 H. A. Yusuf, S. J. Baldock, R. W. Barber, P. R. Fielden, N. J. Goddard and B. J. T. Brown, Novel microsystems for

- concentration gradient generation through computer optimization with validation using optical instrumentation, *Microelectron. Eng.*, 2008, **85**, 1265–1268.
- 141 D. Irimia, D. A. Geba and M. Toner, Universal microfluidic gradient generator, *Anal. Chem.*, 2006, **78**, 3472–3477.
- 142 D. Stroompoulis, H. N. Zhang, L. Rubalcava, J. Glem and M. Tirrell, Cell adhesion and growth to peptide-patterned supported lipid membranes, *Langmuir*, 2007, **23**, 3849–3856.
- 143 S. K. W. Dertinger, X. Y. Jiang, Z. Y. Li, V. N. Murthy and G. M. Whitesides, Gradients of substrate-bound laminin orient axonal specification of neurons, *Proc. Natl. Acad. Sci. U. S. A.*, 2002, **99**, 12542–12547.
- 144 G. Vozzi, D. Mazzei, A. Tirella, F. Vozzi and A. Ahluwalia, Finite element modelling and design of a concentration gradient generating bioreactor: application to biological pattern formation and toxicology, *Toxicol. in Vitro*, 2010, **24**, 1828–1837.
- 145 W. Saadi, S. J. Wang, F. Lin and N. L. Jeon, A parallel-gradient microfluidic chamber for quantitative analysis of breast cancer cell chemotaxis, *Biomed. Microdevices*, 2006, **8**, 109–118.
- 146 A. Tirella, M. Marano, F. Vozzi and A. Ahluwalia, A microfluidic gradient maker for toxicity testing of bupivacaine and lidocaine, *Toxicol. in Vitro*, 2008, **22**, 1957–1964.
- 147 B. G. Chung, L. A. Flanagan, S. W. Rhee, P. H. Schwartz, A. P. Lee, E. S. Monuki and N. L. Jeon, Human neural stem cell growth and differentiation in a gradient-generating microfluidic device, *Lab Chip*, 2005, **5**, 401–406.
- 148 D. Liu, L. Wang, R. Zhong, B. Li, N. Ye, X. Liu and B. Lin, Parallel microfluidic networks for studying cellular response to chemical modulation, *J. Biotechnol.*, 2007, **131**, 286–292.
- 149 N. N. Ye, J. H. Qin, W. W. Shi, X. Liu and B. C. Lin, Cell-based high content screening using an integrated microfluidic device, *Lab Chip*, 2007, **7**, 1696–1704.
- 150 D. M. Thompson, K. R. King, K. J. Wieder, M. Toner, M. L. Yarmush and A. Jayaraman, Dynamic gene expression profiling using a microfabricated living cell array, *Anal. Chem.*, 2004, **76**, 4098–4103.
- 151 R. C. Gunawan, J. Silvestre, H. R. Gaskins, P. J. A. Kenis and D. E. Leckband, Cell migration and polarity on microfabricated gradients of extracellular matrix proteins, *Langmuir*, 2006, **22**, 4250–4258.
- 152 M. Polinkovsky, E. Gutierrez, A. Levchenko and A. Groisman, Fine temporal control of the medium gas content and acidity and on-chip generation of series of oxygen concentrations for cell cultures, *Lab Chip*, 2009, **9**, 1073–1084.
- 153 R. H. W. Lam, M. C. Kim and T. Thorsen, Culturing aerobic and anaerobic bacteria and mammalian cells with a microfluidic differential oxygenator, *Anal. Chem.*, 2009, **81**, 5918–5924.
- 154 A. T. O'Neill, N. A. Monteiro-Riviere and G. M. Walker, Microfabricated curtains for controlled cell seeding in high throughput microfluidic systems, *Lab Chip*, 2009, **9**, 1756–1762.
- 155 K. Stephan, P. Pittet, M. Sigaud, L. Renaud, O. Vittori, P. Morin, N. Ouaini and R. Ferrigno, Amperometric quantification based on serial dilution microfluidic systems, *Analyst*, 2009, **134**, 472–477.
- 156 H. Chon, C. Lim, S. M. Ha, Y. Ahn, E. K. Lee, S. I. Chang, G. H. Seong and J. Choo, On-chip immunoassay using surface-enhanced Raman scattering of hollow gold nanospheres, *Anal. Chem.*, 2010, **82**, 5290–5295.
- 157 U. Levy, K. Campbell, A. Groisman, S. Mookherjea and Y. Fainman, On-chip microfluidic tuning of an optical microring resonator, *Appl. Phys. Lett.*, 2006, **88**, 111107.
- 158 D. Baah, D. VickerS, A. Hollinger and T. Floyd-Smith, Patterned dispersion of nanoparticles in hydrogels using microfluidics, *Mater. Lett.*, 2008, **62**, 3833–3835.
- 159 M. Hosokawa, T. Hayashi, T. Mori, T. Yoshino, S. Nakasono and T. Matsunaga, Microfluidic device with chemical gradient for single-cell cytotoxicity assays, *Anal. Chem.*, 2011, **83**, 3648–3654.
- 160 F. Greve, L. Seemann, A. Hierlemann and J. Lichtenberg, A hybrid microsystem for parallel perfusion experiments on living cells, *J. Micromech. Microeng.*, 2007, **17**, 1721–1730.
- 161 X. Y. Jiang, J. M. K. Ng, A. D. Stroock, S. K. W. Dertinger and G. M. Whitesides, A miniaturized, parallel, serially diluted immunoassay for analyzing multiple antigens, *J. Am. Chem. Soc.*, 2003, **125**, 5294–5295.
- 162 L. Kim, M. D. Vahey, H. Y. Lee and J. Voldman, Microfluidic arrays for logarithmically perfused embryonic stem cell culture, *Lab Chip*, 2006, **6**, 394–406.
- 163 D. C. Webster, Combinatorial and high-throughput methods in macromolecular materials research and development, *Macromol. Chem. Phys.*, 2008, **209**, 237–246.
- 164 R. A. Potyrailo and I. Takeuchi, Role of high-throughput characterization tools in combinatorial materials science, *Meas. Sci. Technol.*, 2005, **16**, 1–4.
- 165 W. F. Maier, K. Stowe and S. Sieg, Combinatorial and high-throughput materials science, *Angew. Chem., Int. Ed.*, 2007, **46**, 6016–6067.
- 166 J. Lehar, A. S. Krueger, W. Avery, A. M. Heilbut, L. M. Johansen, E. R. Price, R. J. Rickles, G. F. Short, 3rd, J. E. Staunton, X. Jin, M. S. Lee, G. R. Zimmermann and A. A. Borisy, Synergistic drug combinations tend to improve therapeutically relevant selectivity, *Nat. Biotechnol.*, 2009, **27**, 659–666.
- 167 N. Agrawal, J. Pallos, N. Slepko, B. L. Apostol, L. Bodai, L. W. Chang, A. S. Chiang, L. M. Thompson and J. L. Marsh, Identification of combinatorial drug regimens for treatment of Huntington's disease using *Drosophila*, *Proc. Natl. Acad. Sci. U. S. A.*, 2005, **102**, 3777–3781.
- 168 C. J. Flaim, S. Chien and S. N. Bhatia, An extracellular matrix microarray for probing cellular differentiation, *Nat. Methods*, 2005, **2**, 119–125.
- 169 F. Yang, S. W. Cho, S. M. Son, S. P. Hudson, S. Bogatyrev, L. Keung, D. S. Kohane, R. Langer and D. G. Anderson, Combinatorial extracellular matrices for human embryonic stem cell differentiation in 3D, *Biomacromolecules*, 2010, **11**, 1909–1914.
- 170 M. Nakajima, T. Ishimuro, K. Kato, I. K. Ko, I. Hirata, Y. Arima and H. Iwata, Combinatorial protein display for the cell-based screening of biomaterials that direct neural stem cell differentiation, *Biomaterials*, 2007, **28**, 1048–1060.
- 171 R. F. Ismagilov, J. M. K. Ng, P. J. A. Kenis and G. M. Whitesides, Microfluidic arrays of fluid–fluid diffusional contacts as detection elements and combinatorial tools, *Anal. Chem.*, 2001, **73**, 5207–5213.
- 172 A. Tourovskaya, X. Figueira-Masot and A. Folch, Differentiation-on-a-chip: a microfluidic platform for long-term cell culture studies, *Lab Chip*, 2005, **5**, 14–19.
- 173 A. Folch, B. H. Jo, O. Hurtado, D. J. Beebe and M. Toner, Microfabricated elastomeric stencils for micropatterning cell cultures, *J. Biomed. Mater. Res.*, 2000, **52**, 346–353.
- 174 K. Hattori, S. Sugiura and T. Kanamori, Microenvironment array chip for cell culture environment screening, *Lab Chip*, 2011, **11**, 212–214.
- 175 E. Kim, Y. N. Xia and G. M. Whitesides, Polymer microstructures formed by molding in capillaries, *Nature*, 1995, **376**, 581–584.
- 176 B. R. Schudel, C. J. Choi, B. T. Cunningham and P. J. A. Kenis, Microfluidic chip for combinatorial mixing and screening of assays, *Lab Chip*, 2009, **9**, 1676–1680.
- 177 Z. T. F. Yu, K. I. Kamei, H. Takahashi, C. J. Shu, X. P. Wang, G. W. He, R. Silverman, C. G. Radu, O. N. Witte, K. B. Lee and H. R. Tseng, Integrated microfluidic devices for combinatorial cell-based assays, *Biomed. Microdevices*, 2009, **11**, 547–555.
- 178 Y. Kikutani, T. Horiuchi, K. Uchiyama, H. Hisamoto, M. Tokeshi and T. Kitamori, Glass microchip with three-dimensional microchannel network for 2 × 2 parallel synthesis, *Lab Chip*, 2002, **2**, 188–192.
- 179 Y. Kikutani, M. Ueno, H. Hisamoto, M. Tokeshi and T. Kitamori, Continuous-flow chemical processing in three-dimensional microchannel network for on-chip integration of multiple reactions in a combinatorial mode, *QSAR Comb. Sci.*, 2005, **24**, 742–757.
- 180 M. C. Liu, D. Ho and Y. C. Tai, Monolithic fabrication of three-dimensional microfluidic networks for constructing cell culture array with an integrated combinatorial mixer, *Sens. Actuators, B*, 2008, **129**, 826–833.
- 181 M. C. Liu and Y. C. Tai, A 3-D microfluidic combinatorial cell array, *Biomed. Microdevices*, 2011, **13**, 191–201.
- 182 G. A. Cooksey, C. G. Sip and A. Folch, A multi-purpose microfluidic perfusion system with combinatorial choice of inputs, mixtures, gradient patterns, and flow rates, *Lab Chip*, 2009, **9**, 417–426.
- 183 G. Kirsten and W. F. Maier, Strategies for the discovery of new catalysts with combinatorial chemistry, *Appl. Surf. Sci.*, 2004, **223**, 87–101.
- 184 H. Tye, Application of statistical ‘design of experiments’ methods in drug discovery, *Drug Discovery Today*, 2004, **9**, 485–491.

- 185 R. S. Islam, D. Tisi, M. S. Levy and G. J. Lye, Framework for the rapid optimization of soluble protein expression in *Escherichia coli* combining microscale experiments and statistical experimental design, *Biotechnol. Prog.*, 2007, **23**, 785–793.
- 186 S. R. M. Pereira, F. Clerc, D. Farrusseng, J. C. van der Waal and T. Maschmeyer, Optimisation methodologies and algorithms for research on catalysis employing high-throughput methods: comparison using the selox benchmark, *Comb. Chem. High Throughput Screening*, 2007, **10**, 149–159.
- 187 B. Singh, R. Kumar and N. Ahuja, Optimizing drug delivery systems using systematic “design of experiments.” Part I: fundamental aspects, *Crit. Rev. Ther. Drug Carrier Syst.*, 2005, **22**, 27–105.
- 188 K. Muteki, J. F. MacGregor and T. Ueda, Mixture designs and models for the simultaneous selection of ingredients and their ratios, *Chemom. Intell. Lab. Syst.*, 2007, **86**, 17–25.
- 189 D. T. Chiu, E. Pezzoli, H. K. Wu, A. D. Stroock and G. M. Whitesides, Using three-dimensional microfluidic networks for solving computationally hard problems, *Proc. Natl. Acad. Sci. U. S. A.*, 2001, **98**, 2961–2966.
- 190 C. Neils, Z. Tyree, B. Finlayson and A. Folch, Combinatorial mixing of microfluidic streams, *Lab Chip*, 2004, **4**, 342–350.
- 191 M. A. Holden, S. Kumar, E. T. Castellana, A. Beskok and P. S. Cremer, Generating fixed concentration arrays in a microfluidic device, *Sens. Actuators, B*, 2003, **92**, 199–207.
- 192 A. Hatch, A. E. Kamholz, K. R. Hawkins, M. S. Munson, E. A. Schilling, B. H. Weigl and P. Yager, A rapid diffusion immunoassay in a T-sensor, *Nat. Biotechnol.*, 2001, **19**, 461–465.
- 193 E. A. Schilling, A. E. Kamholz and P. Yager, Cell lysis and protein extraction in a microfluidic device with detection by a fluorogenic enzyme assay, *Anal. Chem.*, 2002, **74**, 1798–1804.
- 194 J. Pihl, J. Sinclair, E. Sahlin, M. Karlsson, F. Petterson, J. Olofsson and O. Orwar, Microfluidic gradient-generating device for pharmacological profiling, *Anal. Chem.*, 2005, **77**, 3897–3903.
- 195 H. B. Mao, P. S. Cremer and M. D. Manson, A sensitive, versatile microfluidic assay for bacterial chemotaxis, *Proc. Natl. Acad. Sci. U. S. A.*, 2003, **100**, 5449–5454.
- 196 G. M. Walker, M. S. Ozers and D. J. Beebe, Cell infection within a microfluidic device using virus gradients, *Sens. Actuators, B*, 2004, **98**, 347–355.
- 197 S. E. Hulme, S. S. Shevkoplyas, J. Apfeld, W. Fontana and G. M. Whitesides, A microfabricated array of clamps for immobilizing and imaging *C. elegans*, *Lab Chip*, 2007, **7**, 1515–1523.
- 198 E. W. Young, A. R. Wheeler and C. A. Simmons, Matrix-dependent adhesion of vascular and valvular endothelial cells in microfluidic channels, *Lab Chip*, 2007, **7**, 1759–1766.
- 199 G. Tomaiuolo, M. Barra, V. Preziosi, A. Cassinelli, B. Rotoli and S. Guido, Microfluidics analysis of red blood cell membrane viscoelasticity, *Lab Chip*, 2011, **11**, 449–454.
- 200 Y. Zhang, V. Bailey, C. M. Puleo, H. Easwaran, E. Griffiths, J. G. Herman, S. B. Baylin and T. H. Wang, DNA methylation analysis on a droplet-in-oil PCR array, *Lab Chip*, 2009, **9**, 1059–1064.
- 201 C. Kim, K. S. Lee, J. H. Bang, Y. E. Kim, M. C. Kim, K. W. Oh, S. H. Lee and J. Y. Kang, 3-Dimensional cell culture for on-chip differentiation of stem cells in embryoid body, *Lab Chip*, 2011, **11**, 874–882.
- 202 L. Kim, Y. C. Toh, J. Voldman and H. Yu, A practical guide to microfluidic perfusion culture of adherent mammalian cells, *Lab Chip*, 2007, **7**, 681–694.
- 203 L. Sajas, J. Autebert, L. Malaquin and J. L. Viovy, Design, modeling and characterization of microfluidic architectures for high flow rate, small footprint microfluidic systems, *Lab Chip*, 2011, **11**, 822–832.
- 204 R. D. Lovchik, F. Bianco, M. Matteoli and E. Delamarche, Controlled deposition of cells in sealed microfluidics using flow velocity boundaries, *Lab Chip*, 2009, **9**, 1395–1402.
- 205 P. J. Hung, P. J. Lee, P. Sabourchi, R. Lin and L. P. Lee, Continuous perfusion microfluidic cell culture array for high-throughput cell-based assays, *Biotechnol. Bioeng.*, 2005, **89**, 1–8.
- 206 C. J. Wang, X. Li, B. Lin, S. Shim, G. L. Ming and A. Levchenko, A microfluidics-based turning assay reveals complex growth cone responses to integrated gradients of substrate-bound ECM molecules and diffusible guidance cues, *Lab Chip*, 2008, **8**, 227–237.
- 207 R. Gomez-Sjoberg, A. A. Leyrat, D. M. Pirone, C. S. Chen and S. R. Quake, Versatile, fully automated, microfluidic cell culture system, *Anal. Chem.*, 2007, **79**, 8557–8563.
- 208 D. H. Kim, P. K. Wong, J. Park, A. Levchenko and Y. Sun, Microengineered platforms for cell mechanobiology, *Annu. Rev. Biomed. Eng.*, 2009, **11**, 203–233.
- 209 H. Lu, L. Y. Koo, W. M. Wang, D. A. Lauffenburger, L. G. Griffith and K. F. Jensen, Microfluidic shear devices for quantitative analysis of cell adhesion, *Anal. Chem.*, 2004, **76**, 5257–5264.
- 210 R. D. Lovchik, N. Tonna, F. Bianco, M. Matteoli and E. Delamarche, A microfluidic device for depositing and addressing two cell populations with intercellular population communication capability, *Biomed. Microdevices*, 2010, **12**, 275–282.
- 211 S. Kou, L. Pan, D. van Noort, G. Meng, X. Wu, H. Sun, J. Xu and I. Lee, A multishear microfluidic device for quantitative analysis of calcium dynamics in osteoblasts, *Biochem. Biophys. Res. Commun.*, 2011, **408**, 350–355.
- 212 E. Gutierrez and A. Groisman, Quantitative measurements of the strength of adhesion of human neutrophils to a substratum in a microfluidic device, *Anal. Chem.*, 2007, **79**, 2249–2258.
- 213 E. Tkachenko, E. Gutierrez, M. H. Ginsberg and A. Groisman, An easy to assemble microfluidic perfusion device with a magnetic clamp, *Lab Chip*, 2009, **9**, 1085–1095.
- 214 D. R. Emerson, K. Cieslicki, X. Gu and R. W. Barber, Biomimetic design of microfluidic manifolds based on a generalised Murray's law, *Lab Chip*, 2006, **6**, 447–454.
- 215 W. Wu, C. J. Hansen, A. M. Aragon, P. H. Geubelle, S. R. White and J. A. Lewis, Direct-write assembly of biomimetic microvascular networks for efficient fluid transport, *Soft Matter*, 2010, **6**, 739–742.
- 216 R. W. Barber and D. R. Emerson, Optimal design of microfluidic networks using biologically inspired principles, *Microfluid. Nanofluid.*, 2008, **4**, 179–191.
- 217 D. Lim, Y. Kamotani, B. Cho, J. Mazumder and S. Takayama, Fabrication of microfluidic mixers and artificial vasculatures using a high-brightness diode-pumped Nd:YAG laser direct write method, *Lab Chip*, 2003, **3**, 318–323.
- 218 J. T. Borenstein, M. M. Tupper, P. J. Mack, E. J. Weinberg, A. S. Khalil, J. Hsiao and G. Garcia-Cardena, Functional endothelialized microvascular networks with circular cross-sections in a tissue culture substrate, *Biomed. Microdevices*, 2010, **12**, 71–79.
- 219 D. M. Hoganson, H. I. Pryor, 2nd, E. K. Bassett, I. D. Spool and J. P. Vacanti, Lung assist device technology with physiologic blood flow developed on a tissue engineered scaffold platform, *Lab Chip*, 2011, **11**, 700–707.
- 220 D. M. Hoganson, J. L. Anderson, E. F. Weinberg, E. J. Swart, B. K. Orrick, J. T. Borenstein and J. P. Vacanti, Branched vascular network architecture: a new approach to lung assist device technology, *J. Thorac. Cardiovasc. Surg.*, 2010, **140**, 990–995.
- 221 A. Carraro, W. M. Hsu, K. M. Kulig, W. S. Cheung, M. L. Miller, E. J. Weinberg, E. F. Swart, M. Kaazempur-Mofrad, J. T. Borenstein, J. P. Vacanti and C. Neville, *In vitro* analysis of a hepatic device with intrinsic microvascular-based channels, *Biomed. Microdevices*, 2008, **10**, 795–805.
- 222 P. Wilding, L. J. Kricka, J. Cheng, G. Hvichia, M. A. Shoffner and P. Fortina, Integrated cell isolation and polymerase chain reaction analysis using silicon microfilter chambers, *Anal. Biochem.*, 1998, **257**, 95–100.
- 223 M. Yamada and M. Seki, Microfluidic particle sorter employing flow splitting and recombining, *Anal. Chem.*, 2006, **78**, 1357–1362.
- 224 M. Yamada, K. Kano, Y. Tsuda, J. Kobayashi, M. Yamato, M. Seki and T. Okano, Microfluidic devices for size-dependent separation of liver cells, *Biomed. Microdevices*, 2007, **9**, 637–645.
- 225 R. Aoki, M. Yamada, M. Yasuda and M. Seki, In-channel focusing of flowing microparticles utilizing hydrodynamic filtration, *Microfluid. Nanofluid.*, 2009, **6**, 571–576.
- 226 R. Fan, O. Vermesh, A. Srivastava, B. K. H. Yen, L. D. Qin, H. Ahmad, G. A. Kwong, C. C. Liu, J. Gould, L. Hood and J. R. Heath, Integrated barcode chips for rapid, multiplexed analysis of proteins in microliter quantities of blood, *Nat. Biotechnol.*, 2008, **26**, 1373–1378.
- 227 M. Kersaudy-Kerhoas, R. Dhariwal, M. P. Y. Desmulliez and L. Jouvet, Hydrodynamic blood plasma separation in microfluidic channels, *Microfluid. Nanofluid.*, 2010, **8**, 105–114.
- 228 S. Yang, A. Undar and J. D. Zahn, Blood plasma separation in microfluidic channels using flow rate control, *ASAIO J.*, 2005, **51**, 585–590.

- 229 L. D. Qin, O. Vermesh, Q. H. Shi and J. R. Heath, Self-powered microfluidic chips for multiplexed protein assays from whole blood, *Lab Chip*, 2009, **9**, 2016–2020.
- 230 S. S. Shevkoplyas, T. Yoshida, L. L. Munn and M. W. Bitensky, Biomimetic autoseparation of leukocytes from whole blood in a microfluidic device, *Anal. Chem.*, 2005, **77**, 933–937.
- 231 S. S. Shevkoplyas, T. Yoshida, S. C. Gifford and M. W. Bitensky, Direct measurement of the impact of impaired erythrocyte deformability on microvascular network perfusion in a microfluidic device, *Lab Chip*, 2006, **6**, 914–920.
- 232 S. Yang, A. Undar and J. D. Zahn, Continuous cytometric bead processing within a microfluidic device for bead based sensing platforms, *Lab Chip*, 2007, **7**, 588–595.
- 233 M. Yamada, J. Kobayashi, M. Yamato, M. Seki and T. Okano, Millisecond treatment of cells using microfluidic devices via two-step carrier-medium exchange, *Lab Chip*, 2008, **8**, 772–778.
- 234 P. Augustsson, L. B. Aberg, A. M. K. Sward-Nilsson and T. Laurell, Buffer medium exchange in continuous cell and particle streams using ultrasonic standing wave focusing, *Microchim. Acta*, 2009, **164**, 269–277.
- 235 C. Kim, K. S. Lee, Y. E. Kim, K. J. Lee, S. H. Lee, T. S. Kim and J. Y. Kang, Rapid exchange of oil-phase in microencapsulation chip to enhance cell viability, *Lab Chip*, 2009, **9**, 1294–1297.
- 236 S. K. Yoon, G. W. Fichtl and P. J. A. Kenis, Active control of the depletion boundary layers in microfluidic electrochemical reactors, *Lab Chip*, 2006, **6**, 1516–1524.
- 237 K. J. Morton, K. Loutherback, D. W. Inglis, O. K. Tsui, J. C. Sturm, S. Y. Chou and R. H. Austin, Hydrodynamic metamaterials: microfabricated arrays to steer, refract, and focus streams of biomaterials, *Proc. Natl. Acad. Sci. U. S. A.*, 2008, **105**, 7434–7438.
- 238 L. R. Huang, E. C. Cox, R. H. Austin and J. C. Sturm, Continuous particle separation through deterministic lateral displacement, *Science*, 2004, **304**, 987–990.
- 239 K. Loutherback, K. S. Chou, J. Newman, J. Puchalla, R. H. Austin and J. C. Sturm, Improved performance of deterministic lateral displacement arrays with triangular posts, *Microfluid. Nanofluid.*, 2010, **9**, 1143–1149.
- 240 D. W. Inglis, J. A. Davis, R. H. Austin and J. C. Sturm, Critical particle size for fractionation by deterministic lateral displacement, *Lab Chip*, 2006, **6**, 655–658.
- 241 J. V. Green, M. Radisic and S. K. Murthy, Deterministic lateral displacement as a means to Enrich large cells for tissue engineering, *Anal. Chem.*, 2009, **81**, 9178–9182.
- 242 J. B. Knight, A. Vishwanath, J. P. Brody and R. H. Austin, Hydrodynamic focusing on a silicon chip: mixing nanoliters in microseconds, *Phys. Rev. Lett.*, 1998, **80**, 3863–3866.
- 243 M. Yamada, M. Nakashima and M. Seki, Pinched flow fractionation: continuous size separation of particles utilizing a laminar flow profile in a pinched microchannel, *Anal. Chem.*, 2004, **76**, 5465–5471.
- 244 W. H. Tan and S. Takeuchi, A trap-and-release integrated microfluidic system for dynamic microarray applications, *Proc. Natl. Acad. Sci. U. S. A.*, 2007, **104**, 1146–1151.
- 245 S. Kobel, A. Valero, J. Latt, P. Renaud and M. Lutolf, Optimization of microfluidic single cell trapping for long-term on-chip culture, *Lab Chip*, 2010, **10**, 857–863.
- 246 H. Boukellal, S. Selimovic, Y. Jia, G. Cristobal and S. Fraden, Simple, robust storage of drops and fluids in a microfluidic device, *Lab Chip*, 2009, **9**, 331–338.
- 247 S. S. Bithi and S. A. Vanapalli, Behavior of a train of droplets in a fluidic network with hydrodynamic traps, *Biomicrofluidics*, 2010, **4**, 44110.
- 248 W. Shi, J. Qin, N. Ye and B. Lin, Droplet-based microfluidic system for individual *Caenorhabditis elegans* assay, *Lab Chip*, 2008, **8**, 1432–1435.
- 249 T. Teshima, H. Ishihara, K. Iwai, A. Adachi and S. Takeuchi, A dynamic microarray device for paired bead-based analysis, *Lab Chip*, 2010, **10**, 2443–2448.
- 250 D. Di Carlo, L. Y. Wu and L. P. Lee, Dynamic single cell culture array, *Lab Chip*, 2006, **6**, 1445–1449.
- 251 D. Di Carlo, N. Aghdam and L. P. Lee, Single-cell enzyme concentrations, kinetics, and inhibition analysis using high-density hydrodynamic cell isolation arrays, *Anal. Chem.*, 2006, **78**, 4925–4930.
- 252 A. Huebner, D. Bratton, G. Whyte, M. Yang, A. J. Demello, C. Abell and F. Hollfelder, Static microdroplet arrays: a microfluidic device for droplet trapping, incubation and release for enzymatic and cell-based assays, *Lab Chip*, 2009, **9**, 692–698.
- 253 A. M. Skelley, O. Kirak, H. Suh, R. Jaenisch and J. Voldman, Microfluidic control of cell pairing and fusion, *Nat. Methods*, 2009, **6**, 147–152.
- 254 Y. Bai, X. He, D. Liu, S. N. Patil, D. Bratton, A. Huebner, F. Hollfelder, C. Abell and W. T. Huck, A double droplet trap system for studying mass transport across a droplet–droplet interface, *Lab Chip*, 2010, **10**, 1281–1285.
- 255 H. A. Yusuf, S. J. Baldock, P. R. Fielden, N. J. Goddard, S. Mohr and B. J. T. Brown, Systematic linearisation of a microfluidic gradient network with unequal solution inlet viscosities demonstrated using glycerol, *Microfluid. Nanofluid.*, 2010, **8**, 587–598.
- 256 N. Srivastava and M. A. Burns, Analysis of non-Newtonian liquids using a microfluidic capillary viscometer, *Anal. Chem.*, 2006, **78**, 1690–1696.
- 257 Z. Han, X. Tang and B. Zheng, A PDMS viscometer for microliter Newtonian fluid, *J. Micromech. Microeng.*, 2007, **17**, 1828–1834.
- 258 P. Guillot, P. Panizza, J. B. Salmon, M. Joanicot, A. Colin, C. H. Bruneau and T. Colin, Viscosimeter on a microfluidic chip, *Langmuir*, 2006, **22**, 6438–6445.
- 259 X. Tang and B. Zheng, A PDMS viscometer for assaying endoglycanase activity, *Analyst*, 2011, **136**, 1222–1226.
- 260 S. Choi, M. G. Lee and J. K. Park, Microfluidic parallel circuit for measurement of hydraulic resistance, *Biomicrofluidics*, 2010, **4**, 034110.
- 261 H. A. Stone, Tuned-in flow control, *Nat. Phys.*, 2009, **5**, 178–179.
- 262 D. C. Leslie, C. J. Easley, E. Seker, J. M. Karlinsey, M. Utz, M. R. Begley and J. P. Landers, Frequency-specific flow control in microfluidic circuits with passive elastomeric features, *Nat. Phys.*, 2009, **5**, 231–235.
- 263 B. Kuczenski, P. R. LeDuc and W. C. Messner, Pressure-driven spatiotemporal control of the laminar flow interface in a microfluidic network, *Lab Chip*, 2007, **7**, 647–649.
- 264 J. Melin and S. R. Quake, Microfluidic large-scale integration: the evolution of design rules for biological automation, *Annu. Rev. Biophys. Biomol. Struct.*, 2007, **36**, 213–231.
- 265 K. W. Oh and C. H. Ahn, A review of microvalves, *J. Micromech. Microeng.*, 2006, **16**, R13–R39.
- 266 S. M. Langelier, E. Livak-Dahl, A. J. Manzo, B. N. Johnson, N. G. Walter and M. A. Burns, Flexible casting of modular self-aligning microfluidic assembly blocks, *Lab Chip*, 2011, **11**, 1679–1687.
- 267 A. Chen and T. Pan, Fit-to-Flow (F2F) interconnects: universal reversible adhesive-free microfluidic adaptors for lab-on-a-chip systems, *Lab Chip*, 2011, **11**, 727–732.
- 268 K. Sun, Z. Wang and X. Jiang, Modular microfluidics for gradient generation, *Lab Chip*, 2008, **8**, 1536–1543.
- 269 P. K. Yuen, J. T. Bliss, C. C. Thompson and R. C. Peterson, Multidimensional modular microfluidic system, *Lab Chip*, 2009, **9**, 3303–3305.
- 270 H. J. Song, Y. Wang and K. Pant, System-level simulation of liquid filling in microfluidic chips, *Biomicrofluidics*, 2011, **5**, 024107.
- 271 G. L. Lettieri, A. Dodge, G. Boer, N. F. de Rooij and E. Verpoorte, A novel microfluidic concept for bioanalysis using freely moving beads trapped in recirculating flows, *Lab Chip*, 2003, **3**, 34–39.
- 272 A. Plecic and Y. Chen, Microfluidic analogy of the wheatstone bridge for systematic investigations of electro-osmotic flows, *Anal. Chem.*, 2008, **80**, 3736–3742.
- 273 X. C. Xuan and D. Q. Li, Analysis of electrokinetic flow in microfluidic networks, *J. Micromech. Microeng.*, 2004, **14**, 290–298.
- 274 R. Qiao and N. R. Aluru, A compact model for electroosmotic flows in microfluidic devices, *J. Micromech. Microeng.*, 2002, **12**, 625–635.
- 275 A. N. Chatterjee and N. R. Aluru, Combined circuit/device modeling and simulation of integrated microfluidic systems, *J. Microelectromech. Syst.*, 2005, **14**, 81–95.
- 276 T. Glawdel, C. Elbukten, L. E. J. Lee and C. L. Ren, Microfluidic system with integrated electroosmotic pumps, concentration gradient generator and fish cell line (RTgill-W1)-towards water toxicity testing, *Lab Chip*, 2009, **9**, 3243–3250.
- 277 A. Ajdari, Steady flows in networks of microfluidic channels: building on the analogy with electrical circuits, *C. R. Phys.*, 2004, **5**, 539–546.
- 278 Y. K. Suh and S. Kang, Simple formula for calculation of fluid flows in complex microfluidic networks, *BioChip J.*, 2009, **3**, 37–43.

- 279 M. J. Fuerstman, P. Garstecki and G. M. Whitesides, Coding/decoding and reversibility of droplet trains in microfluidic networks, *Science*, 2007, **315**, 828–832.
- 280 B. J. Smith and D. P. Gaver, 3rd, Agent-based simulations of complex droplet pattern formation in a two-branch microfluidic network, *Lab Chip*, 2010, **10**, 303–312.
- 281 O. Cybulski and P. Garstecki, Dynamic memory in a microfluidic system of droplets traveling through a simple network of microchannels, *Lab Chip*, 2010, **10**, 484–493.
- 282 D. A. Sessoms, M. Belloul, W. Engl, M. Roche, L. Courbin and P. Panizza, Droplet motion in microfluidic networks: hydrodynamic interactions and pressure-drop measurements, *Phys. Rev. E: Stat., Nonlinear, Soft Matter Phys.*, 2009, **80**, 016317.
- 283 M. Prakash and N. Gershenfeld, Microfluidic bubble logic, *Science*, 2007, **315**, 832–835.
- 284 B. Ahn, K. Lee, H. Lee, R. Panchapakesan and K. W. Oh, Parallel synchronization of two trains of droplets using a railroad-like channel network, *Lab Chip*, 2011, **11**, 3965–3962.
- 285 G. Cristobal, J. P. Benoit, M. Joanicot and A. Ajdari, Microfluidic bypass for efficient passive regulation of droplet traffic at a junction, *Appl. Phys. Lett.*, 2006, **89**, 034104.
- 286 F. Jousse, G. Lian, R. Janes and J. Melrose, Compact model for multi-phase liquid–liquid flows in microfluidic devices, *Lab Chip*, 2005, **5**, 646–656.
- 287 M. Schindler and A. Ajdari, Droplet traffic in microfluidic networks: a simple model for understanding and designing, *Phys. Rev. Lett.*, 2008, **100**, 044501.
- 288 M. J. Fuerstman, A. Lai, M. E. Thurlow, S. S. Shevkoplyas, H. A. Stone and G. M. Whitesides, The pressure drop along rectangular microchannels containing bubbles, *Lab Chip*, 2007, **7**, 1479–1489.
- 289 A. A. Bhagat, S. S. Kuntaegowdanahalli and I. Papautsky, Continuous particle separation in spiral microchannels using Dean flows and differential migration, *Lab Chip*, 2008, **8**, 1906–1914.
- 290 S. S. Kuntaegowdanahalli, A. A. Bhagat, G. Kumar and I. Papautsky, Inertial microfluidics for continuous particle separation in spiral microchannels, *Lab Chip*, 2009, **9**, 2973–2980.
- 291 E. R. Choban, L. J. Markoski, A. Wieckowski and P. J. A. Kenis, Microfluidic fuel cell based on laminar flow, *J. Power Sources*, 2004, **128**, 54–60.
- 292 M. H. Sun, G. V. Casquillas, S. S. Guo, J. Shi, H. Ji, Q. Ouyang and Y. Chen, Characterization of microfluidic fuel cell based on multiple laminar flow, *Microelectron. Eng.*, 2007, **84**, 1182–1185.
- 293 S. Pennathur, J. C. Eijkel and A. van den Berg, Energy conversion in microsystems: is there a role for micro/nanofluidics?, *Lab Chip*, 2007, **7**, 1234–1237.
- 294 D. Dendukuri, K. Tsoi, T. A. Hatton and P. S. Doyle, Controlled synthesis of nonspherical microparticles using microfluidics, *Langmuir*, 2005, **21**, 2113–2116.
- 295 S. Z. Hua, F. Sachs, D. X. Yang and H. D. Chopra, Microfluidic actuation using electrochemically generated bubbles, *Anal. Chem.*, 2002, **74**, 6392–6396.
- 296 S. P. Gurum, S. K. Suman, Y. K. Joshi and A. G. Fedorov, Thermal issues in next-generation integrated circuits, *IEEE Trans. Device Mater. Reliab.*, 2004, **4**, 709–714.
- 297 M. Dhindsa, S. Kwon, J. Park, P. D. Rack, I. Papautsky and J. Heikenfeld, Virtual electrowetting channels: electronic liquid transport with continuous channel functionality, *Lab Chip*, 2010, **10**, 832–836.
- 298 M. A. Burns and M. Rhee, Microfluidic pneumatic logic circuits and digital pneumatic microprocessors for integrated microfluidic systems, *Lab Chip*, 2009, **9**, 3131–3143.
- 299 K. J. Morton, K. Loutherback, D. W. Inglis, O. K. Tsui, J. C. Sturm, S. Y. Chou and R. H. Austin, Hydrodynamic metamaterials: microfabricated arrays to steer, refract, and focus streams of biomaterials, *Proc. Natl. Acad. Sci. U. S. A.*, 2008, **105**, 7434–7438.
- 300 T. S. Kasirga, Y. N. Ertas and M. Bayindir, Microfluidics for reconfigurable electromagnetic metamaterials, *Appl. Phys. Lett.*, 2009, **95**, 214102.
- 301 D. B. Wolfe, R. S. Conroy, P. Garstecki, B. T. Mayers, M. A. Fischbach, K. E. Paul, M. Prentiss and G. M. Whitesides, Dynamic control of liquid-core/liquid-cladding optical waveguides, *Proc. Natl. Acad. Sci. U. S. A.*, 2004, **101**, 12434–12438.
- 302 S. K. Tang, C. A. Stan and G. M. Whitesides, Dynamically reconfigurable liquid-core liquid-cladding lens in a microfluidic channel, *Lab Chip*, 2008, **8**, 395–401.
- 303 N. Chronis, G. Liu, K. H. Jeong and L. Lee, Tunable liquid-filled microlens array integrated with microfluidic network, *Opt. Express*, 2003, **11**, 2370–2378.
- 304 S. M. Langelier, D. S. Chang, R. I. Zeitoun and M. A. Burns, Acoustically driven programmable liquid motion using resonance cavities, *Proc. Natl. Acad. Sci. U. S. A.*, 2009, **106**, 12617–12622.
- 305 W. Gu, X. Zhu, N. Futai, B. S. Cho and S. Takayama, Computerized microfluidic cell culture using elastomeric channels and Braille displays, *Proc. Natl. Acad. Sci. U. S. A.*, 2004, **101**, 15861–15866.
- 306 L. Gervais and E. Delamarche, Toward one-step point-of-care immunodiagnostics using capillary-driven microfluidics and PDMS substrates, *Lab Chip*, 2009, **9**, 3330–3337.
- 307 R. Gorkin, J. Park, J. Siegrist, M. Amasia, B. S. Lee, J. M. Park, J. Kim, H. Kim, M. Madou and Y. K. Cho, Centrifugal microfluidics for biomedical applications, *Lab Chip*, 2010, **10**, 1758–1773.
- 308 S. C. Jacobson, T. E. McKnight and J. M. Ramsey, Microfluidic devices for electrokinetically driven parallel and serial mixing, *Anal. Chem.*, 1999, **71**, 4455–4459.
- 309 S. K. Cho, H. J. Moon and C. J. Kim, Creating, transporting, cutting, and merging liquid droplets by electrowetting-based actuation for digital microfluidic circuits, *J. Microelectromech. Syst.*, 2003, **12**, 70–80.
- 310 R. B. Fair, Digital microfluidics: is a true lab-on-a-chip possible?, *Microfluid. Nanofluid.*, 2007, **3**, 245–281.
- 311 N. Goedecke, J. Eijkel and A. Manz, Evaporation driven pumping for chromatography application, *Lab Chip*, 2002, **2**, 219–223.
- 312 P. Y. Chiou, A. T. Ohta and M. C. Wu, Massively parallel manipulation of single cells and microparticles using optical images, *Nature*, 2005, **436**, 370–372.
- 313 A. W. Martinez, S. T. Phillips and G. M. Whitesides, Three-dimensional microfluidic devices fabricated in layered paper and tape, *Proc. Natl. Acad. Sci. U. S. A.*, 2008, **105**, 19606–19611.
- 314 C. C. Hong, J. W. Choi and C. H. Ahn, An on-chip air-bursting detonator for driving fluids on disposable lab-on-a-chip systems, *J. Micromech. Microeng.*, 2007, **17**, 410–417.
- 315 E. Yakhsht-Tafti, H. J. Cho and R. Kumar, Droplet actuation on a liquid layer due to thermocapillary motion: shape effect, *Appl. Phys. Lett.*, 2010, **96**, 264101.
- 316 G. C. Randall and P. S. Doyle, Permeation-driven flow in poly(dimethylsiloxane) microfluidic devices, *Proc. Natl. Acad. Sci. U. S. A.*, 2005, **102**, 10813–10818.
- 317 D. Y. Liang, A. M. Tentori, I. K. Dimov and L. P. Lee, Systematic characterization of degas-driven flow for poly(dimethylsiloxane) microfluidic devices, *Biomicrofluidics*, 2011, **5**, 24108.
- 318 D. Mark, S. Haeberle, G. Roth, F. von Stetten and R. Zengerle, Microfluidic lab-on-a-chip platforms: requirements, characteristics and applications, *Chem. Soc. Rev.*, 2010, **39**, 1153–1182.
- 319 S. Haeberle and R. Zengerle, Microfluidic platforms for lab-on-a-chip applications, *Lab Chip*, 2007, **7**, 1094–1110.